NASA CONTRACTOR REPORT

NASA CR-2328

NASA CR-2328

TOWARD RADSCAT MEASUREMENTS OVER THE SEA AND THEIR INTERPRETATION

by J. P. Claassen, A. K. Fung, S. T. Wu, and H. L. Chan

Prepared by
THE UNIVERSITY OF KANSAS CENTER FOR RESEARCH, INC.
Lawrence, Kans. 66044
for Langley Research Center

NATIONAL AERONAUTICS AND SPACE ADMINISTRATION • WASHINGTON, D. C. • NOVEMBER 1973

1. Report No.	2. Government Accession No.	3. Recipient's Catalog No.
NASA CR-2328		

4. Title and Subtitle	5. Report Date
TOWARD RADSCAT MEASUREMENTS OVER THE SEA AND THEIR INTERPRETATION	November 1973
	6. Performing Organization Code
7. Author(s)	8. Performing Organization Report No.
J. P. Claassen, A. K. Fung, S. T. Wu, H. L. Chan	TR186-6
	10. Work Unit No.
9. Performing Organization Name and Address	11. Contract or Grant No.
University of Kansas Center for Research, Inc. Space Technology Center, 2291 Irving Hill Rd. Campus West Lawrence, Kansas 66044	NAS 1-10048
	13. Type of Report and Period Covered
12. Sponsoring Agency Name and Address	Contractor's Report
National Aeronautics and Space Administration Washington. D.C. 20546	14. Sponsoring Agency Code

15. Supplementary Notes

This is a topical report.

16. Abstract

Investigations into several areas which are essential to the execution and interpretation of sub-orbital observations by a composite radiometer - scatterometer sensor (RADSCAT) are reported. Experiments and theory have been developed to demonstrate the remote anemometric capability of the sensor over the sea through various weather conditions.

RADSCAT aircraft experiments were designed. It is shown that weather situations found in extra-tropical cyclones are useful for demonstrating the "all weather" capability of the composite sensor. The large scale fluctuations of the wind over the sea dictate the observational coverage required to correlate measurements with the mean surface wind speed.

Various theoretical investigations were performed to establish a premise for the joint interpretation of the experiment data. The effects of clouds and rains on downward radiometric observations over the sea were computed. From this study a method of predicting atmospheric attenuation from joint observations is developed. In other theoretical efforts the emission and scattering characteristics of the sea were derived. Composite surface theories with coherent and non-coherent assumptions were employed in these efforts.

17. Key Words (Suggested by Author(s))	18. Distribution Statement
Remote Sensing Sea Winds Microwave Scattering Microwave Emission Oceanography Meteorology	Unclassified - unlimited

19. Security Classif. (of this report)	20. Security Classif. (of this page)	21. No. of Pages	22. Price*
Unclassified	Unclassified	122	Domestic, $4.25 Foreign, $6.75

*For sale by the National Technical Information Service, Springfield, Virginia 22151

FOREWORD

The value of microwave scatterometers and radiometers as remote sea wind sensors has been independently demonstrated by a number of investigators. However, near-simultaneous observations by a composite radiometer and scatterometer (RADSCAT) instrument have been judged to have value in making better estimates of the surface winds beyond the improvement provided by two independent measurements. To demonstrate this potential a joint effort between New York University, General Electric Space Division, the University of Kansas and NASA Langley Research Center was undertaken through the Advanced Applications Flight Experiment program of NASA. This document reports the investigations performed by the University of Kansas during the first year of this joint program.

Specifically, this report was prepared by the Remote Sensing Laboratory of the University of Kansas Center for Research, Inc. under contract NAS 1-10048. The principal investigator under this contract is Dr. R. K. Moore and Project Engineer is Dr. A. K. Fung.

The development of various meterological and oceanographic concepts important to the design of the experiments is largely based on discussions with Dr. V. J. Cardone and Dr. W. J. Pierson, Jr. of the Meteorology and Oceanography Department of New York University. Their assistance is gratefully acknowledged.

TABLE OF CONTENTS

TABLE OF CONTENTS, cont.

LIST OF ILLUSTRATIONS AND TABLES

Illustrations

LIST OF ILLUSTRATIONS AND TABLES
(CONTINUED)

Illustrations — Page

LIST OF ILLUSTRATIONS AND TABLES
(CONTINUED)

Illustrations

LIST OF ILLUSTRATIONS AND TABLES
(CONTINUED)

I. SUMMARY

The wind stress acting at the air-sea interface locally accounts for the wind-wave interaction at the ocean surface. It is generally accepted that the small roughness elements convey the transfer of momentum from wind to sea and that these roughness elements are in equilibrium or near equilibrium with the wind. The fact that scatterometers and radiometers are good roughness sensors has led many to believe that the surface winds can be inferred from remote microwave observations by these sensors. Since this initial recognition, the value of each of these microwave probes as a sea wind sensor has been substantially demonstrated by a number of investigators. The stronger interpretational basis of near simultaneous observations by a composite radiometer-scatterometer instrument for remotely sensing sea winds is currently under investigation.

This stronger interpretational basis for the composite sensor resides in several important factors beyond the innate improvement in making a wind estimate based on observations by two sensors. The primary advantage of the composite sensor lies in its ability to sense when measurements are occurring through cloud covers and potentially to estimate their attenuation. The attenuation estimate could then be used to correct the scatterometric observation to yield a more accurate estimate of wind speed. Since the radiometer tends to lose contact with the surface and to sense atmospheric absorption when clouds intervene, it is evident that the advantage of the composite sensor lies in its ability to operate through more weather situations. This is important because clouds cover so much of the oceans, especially where storm systems are developing. Furthermore, it is known that joint radiometric and scatterometric observations sometimes aid in discriminating surface properties which cannot be realized by the scatterometer or radiometer alone. Since sea foam changes the dielectric constant of the surface this capability of the composite sensor may be quite useful, especially at high wind speeds.

These viewpoints on the composite sensor have been the motivating factors in proposing the composite sensor. Several studies which are essential to the execution and interpretation of sub-orbital observations by this composite sensor are reported herein.

Experiments for the composite sensor have been designed. Important weather situations found in an extra-tropical cyclone formed the basis for designing experiments through clear, cloudy and rainy skies. The performance of the composite sensor is to be evaluated in each of these weather situations for a variety of wind conditions. Although the experiment designs are described in detail in reference [11], certain important aspects are emphasized in this report. Comprehensive sea truth and well-coordinated experiments are shown essential to forming a strong correlative basis for interpreting the microwave observations. Several methods by which this may be achieved are suggested.

The ocean surface is a random process whose geometrical characteristics vary statistically over scales both larger and smaller than the area observed by the RADSCAT sensor; this range of scales affects the measurement technique. Intensive studies were also performed to delineate meteorological and oceanographic situations which form the bases for many of the experiments and to describe sea truth documentation methods.

Theoretical investigations were made into three distinct areas: cloud and rain effects on radiometric observations over the sea, the characteristics of microwave emissions from the sea, and backscatter from the sea.

The effects of clouds and rain on the radiometer observations were computed using horizontally stratified model atmospheres. It is shown that clouds and rains cause the radiometer to lose contact with the surface through the emission and scattering characteristics of cloudy and raining atmospheres. However, it is shown that the atmospheric emission effect may yield the basis by which atmospheric attenuation can be inferred from measurements by the composite instrument. The measure of atmospheric attenuation may be used to make small corrections to the scatterometric observations.

A simple composite surface theory was employed to predict the microwave emission characteristic of the sea. Better agreement with experimental observations is demonstrated than with a previous theory. It is also shown that comparison of both backscatter and emission predictions with measurements forms a stronger basis for evaluating scattering theories.

A new composite surface theory was also developed and applied to predict sea returns. These efforts together with new interpretations of angular behavior of NRL scatterometric observations are converging toward a fuller understanding of the mechanisms and characteristics of sea returns especially at large incident angles.

II. INTRODUCTION

A. Background

The importance of wind measurements over the sea has been recognized by the meteorologist and oceanographer alike. An understanding, although incomplete, of the momentum transfer mechanism from winds to waves has enabled the oceanographer to generate wave development models. With sufficient real time wind information over the sea these models could predict sea state on a global basis.[1] Sea state prediction, in turn, would enable seamen to route their ships with a saving of travel time and under less hazardous conditions. For the meteorologist the same wind information, when properly interpreted in terms of the wind structure in the planetary boundary layer, and augmented with the location of the low pressure centers (from cloud imagery), coastal and island surface pressures, and a few scattered ship reports would permit recovery of the surface atmospheric pressure patterns. Combined knowledge of the pressure field and SIRS data would yield information which can be used for global weather forecasts.[1]

The wind stress acting at the air-sea interface locally accounts for the wind-wave interaction. It has been generally accepted that the momentum is transferred through the small roughness elements of the sea surface. There is good reason to believe that these small roughness elements are in equilibrium or perhaps near equilibrium with the local wind.[2] The fact that microwave scatterometers and radiometers are good roughness sensors has led many to believe that the surface winds can be inferred from these remote microwave observations. This viewpoint is further reinforced by the fact that the scatterometric characteristic and therefore radiometric characteristic are largely responsive to the small surface structure especially at incident angles in excess of roughly 30°.

B. Experimental Verification - Status

Since the initial recognition of this potential, the value of each microwave probe as sea wind sensor has been substantially demonstrated by a number of investigators. A comprehensive study of the wind speed response of scatterometric observations has been conducted by Bradley.[3] His studies of NASA scatterometer data at 13.3 GHz have shown a wind speed dependence w for observations in the upwind direction given by

$$\sigma^{\circ}_{35}/\sigma^{\circ}_{10} = K\, w^{1.49} \qquad (1)$$

where σ°_{35} and σ°_{10} are scattering coefficients at 35° and 10° incident angles, respectively. This dependence together with the data on which it is based is illustrated in Figure 1. Bradley interprets the wind dependence in terms of a ratio of scattering coefficients to assure a measure of wind dependence largely independent of the accuracy and calibration of the scatterometer.

Motivated by Bradley's results and the fact that oceanographers were beginning to report spectral growth of the sea at large wave number (K) over a large range of winds, Claassen and Fung[4] in a rather extensive analysis of NRL upwind scatterometer data* from two missions identified a power law wind dependence in each of the missions. They thereby uncovered systematic biases between missions. When the biases were removed, the wind dependence remained unaltered within computational error. Partial results from these studies are shown in Figures 2 through 5. These graphs indicate power law exponents at 30° of $1.0 \pm .1$ for vertical polarization and $1.1 \pm .1$ for horizontal polarization. Whereas at 60° power law exponents are given as $1.3 \pm .1$ for vertical polarization and $1.5 \pm .1$ for horizontal. The trend in these exponents are believed to be consistent with the wind dependence inferred from the composite surface theory for backscatter when the development of the sea and polarization characteristics are accounted for. These power law relationships were established without recourse to normalization with respect to σ°_{10}, since an accuracy of $\pm$ 2 dB is cited for the NRL scatterometer (discounting the biases). These adjusted responses (except for a point

*See references [46] and [63].

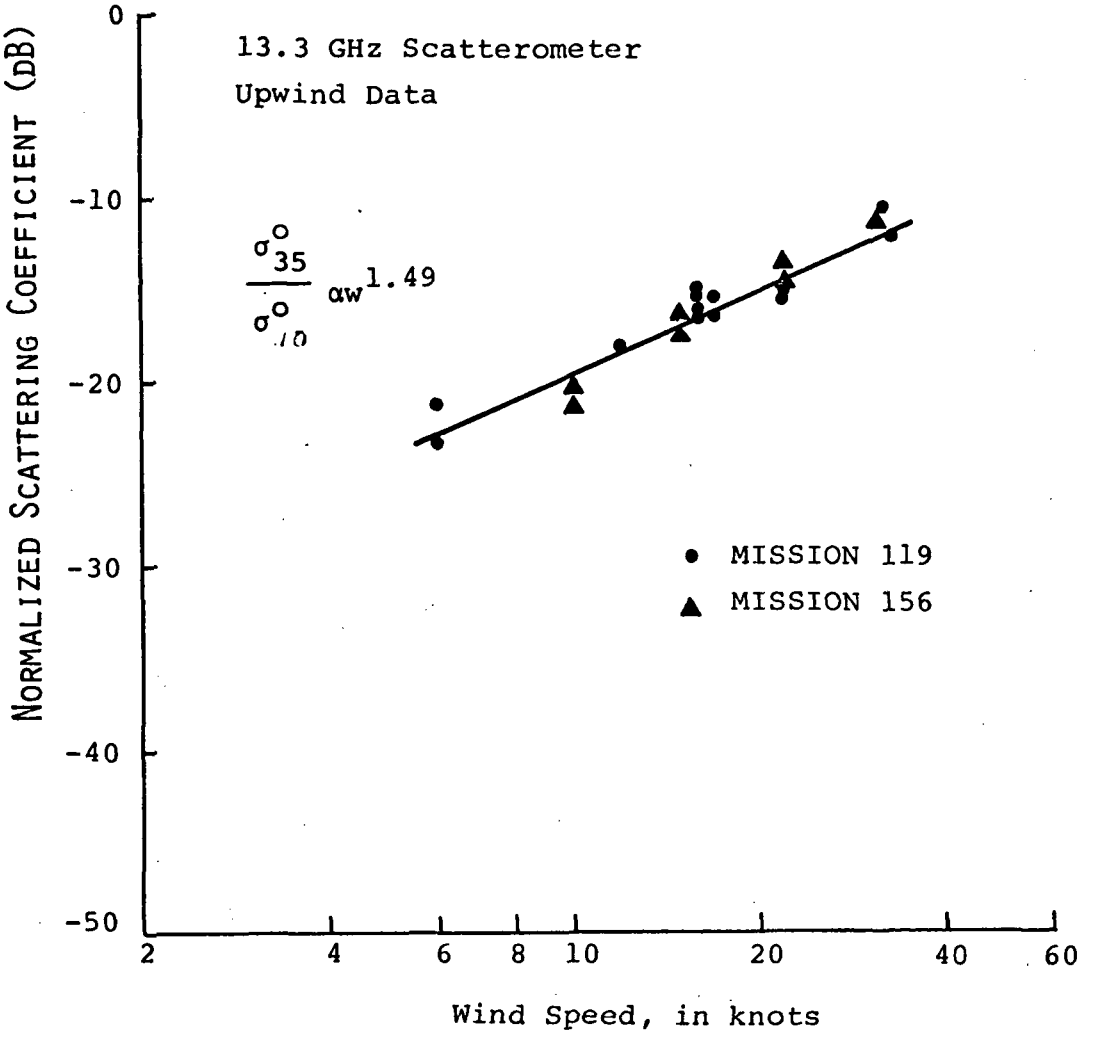

Figure 1. The wind dependence observed at 13.3 GHz by Bradley

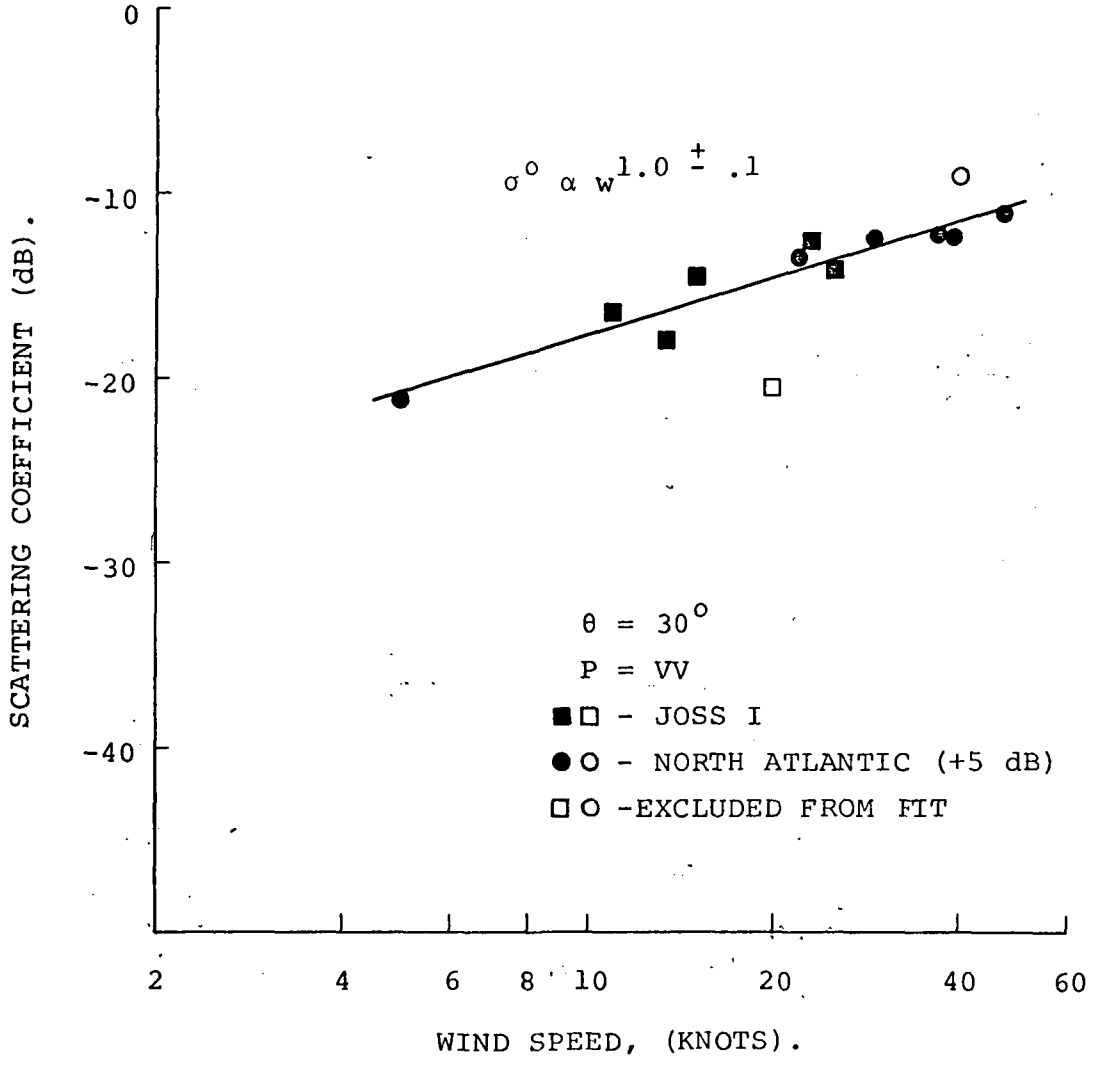

Figure 2. The wind response of NRL scatterometric X-band data with apparent bias removed and under listed conditions.

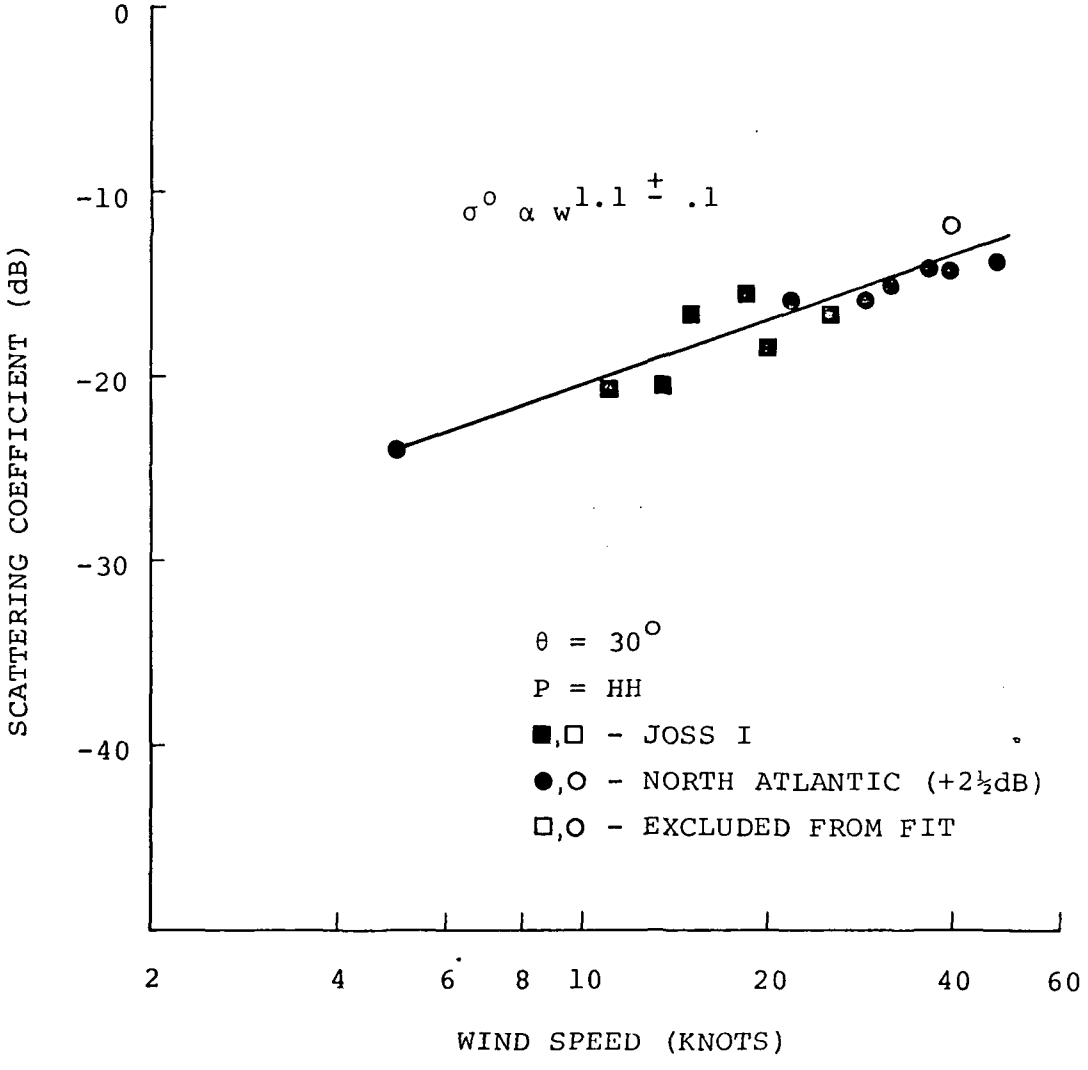

Figure 3. The wind response of NRL scatterometric X-band data with apparent bias removed and under listed conditions.

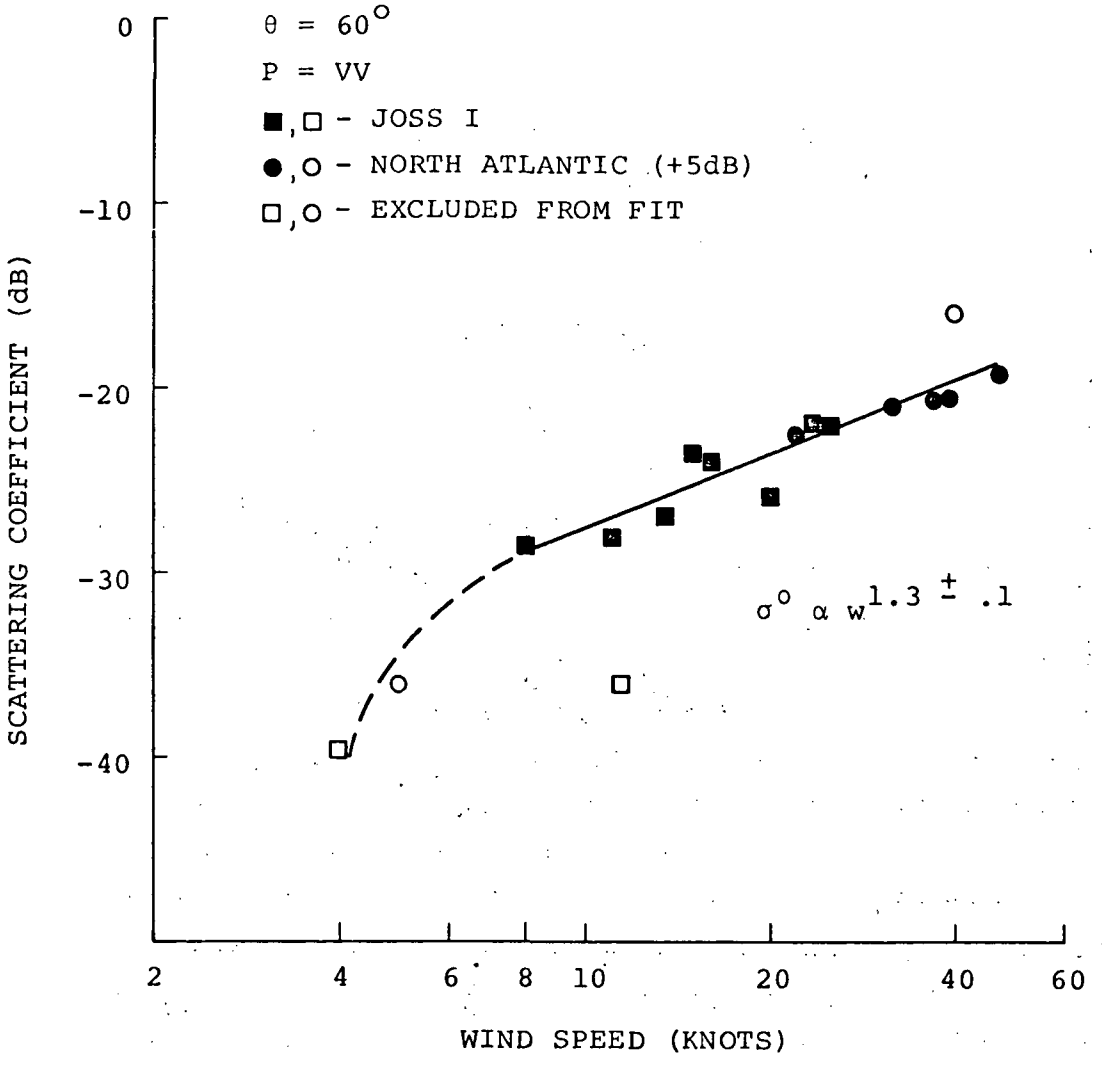

Figure 4. The wind response of NRL scatterometric X-band data with apparent bias removed and under listed conditions.

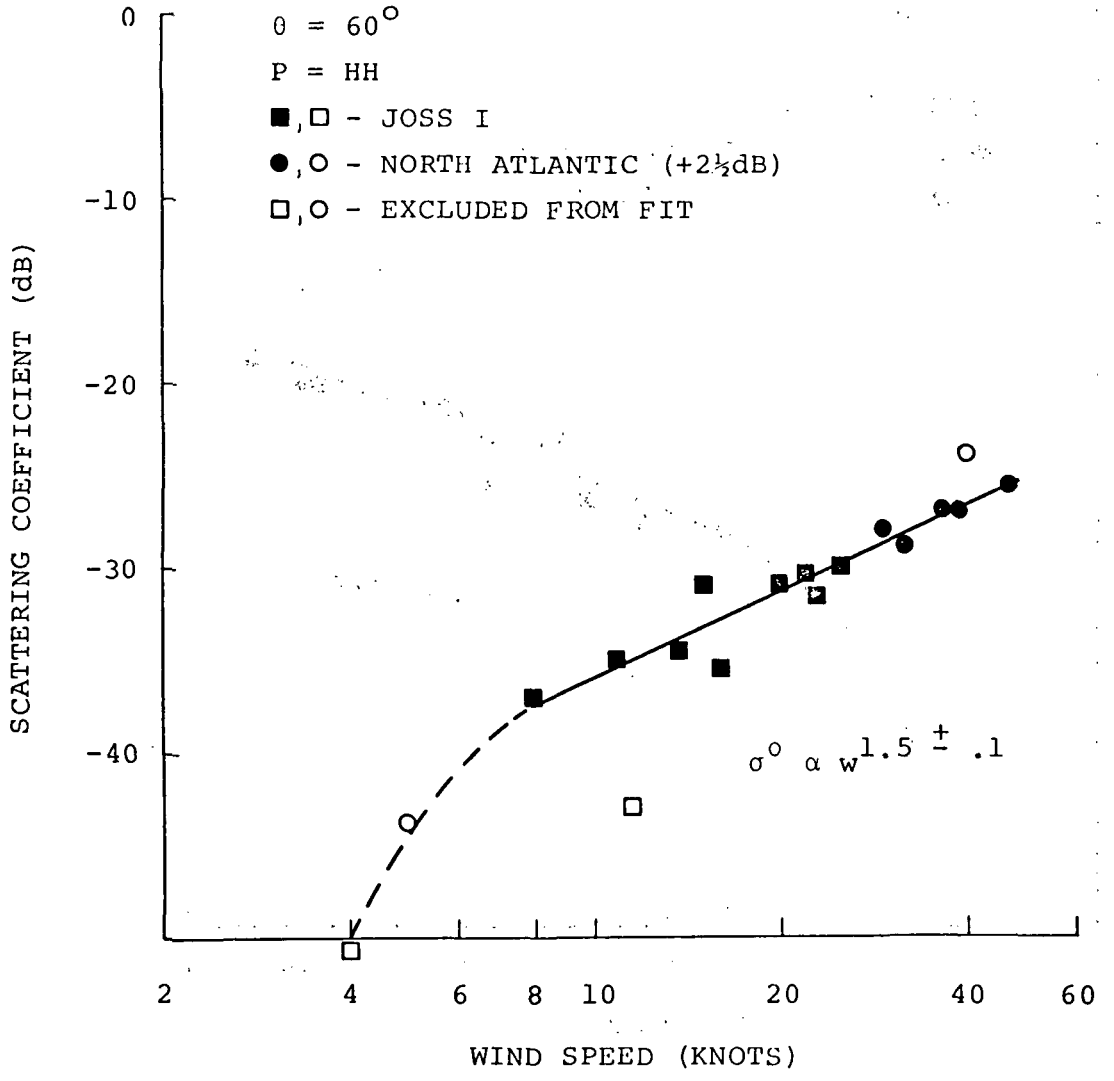

Figure 5. The wind response of NRL scatterometric X-band data with apparent bias removed and under listed conditions.

from each mission not included in the regressional fits) illustrate good correlation with their respective power law fits for winds above 8 knots, i.e., the scatter of data along the curve is small.

Several investigators have reported radiometric observations over wind driven seas. Hollinger of NRL[5,6] has conducted radiometric measurements at three microwave frequencies, 1.41 GHz, 8.36 GHz, and 19.34 GHz, from a tower located in 60 meters of sea. His measurements for horizontally polarized emissions show (1) a linear rising trend with wind speed, (2) an increasing sensitivity to wind speed with frequency, and (3) a small increasing sensitivity to wind speed with incident angle. Vertically polarized emissions exhibited little sensitivity to wind speed except at 19.34 GHz and large nadir angles where a declining trend was observed.

The brightness temperature response to wind speed at an incident view angle of 55° and a frequency of 8.36 GHz is shown in Figure 6. In processing his data Hollinger removed the effects of foam from the apparent temperature (foam causes a rise in brightness temperature[7]). Atmospheric contributions(such as reflected cloud emissions) were also removed from the measurements, so only surface geometry affected the measurements since the water temperature was nearly constant. The reported accuracy in the measurements was $\pm 2^{\circ}K$ ($\pm$ 0.1 dB at $80^{\circ}K$).

Nordberg and his co-investigators[8,9] have also reported the dependence of brightness temperature on wind speed at 19.34 GHz. Their observations were conducted from an aircraft over the North Sea and the North Atlantic Sea. They report selected data which indicated that the brightness temperature at nadir increases with wind speed from 7 m/s to 25 m/s at a rate of about 1.2° K/m/s (see Figure 7). The reported rate at 70° incident angle was $1.8^{\circ}K/m/s$. The brightness temperature dependence was attributed to the increase in white water (foam and sea spray) with wind speed. It is interesting to compare Hollinger's data at the same frequency. The slope dependence at 70° incident angle was described as $1.3^{\circ} \pm .2^{\circ}K/m/s$ which is less than that reported by Nordberg. The difference may be attributable to the foam, although had Nordberg fitted his data to include two data points near 10 knots, the slopes may not have differed significantly.

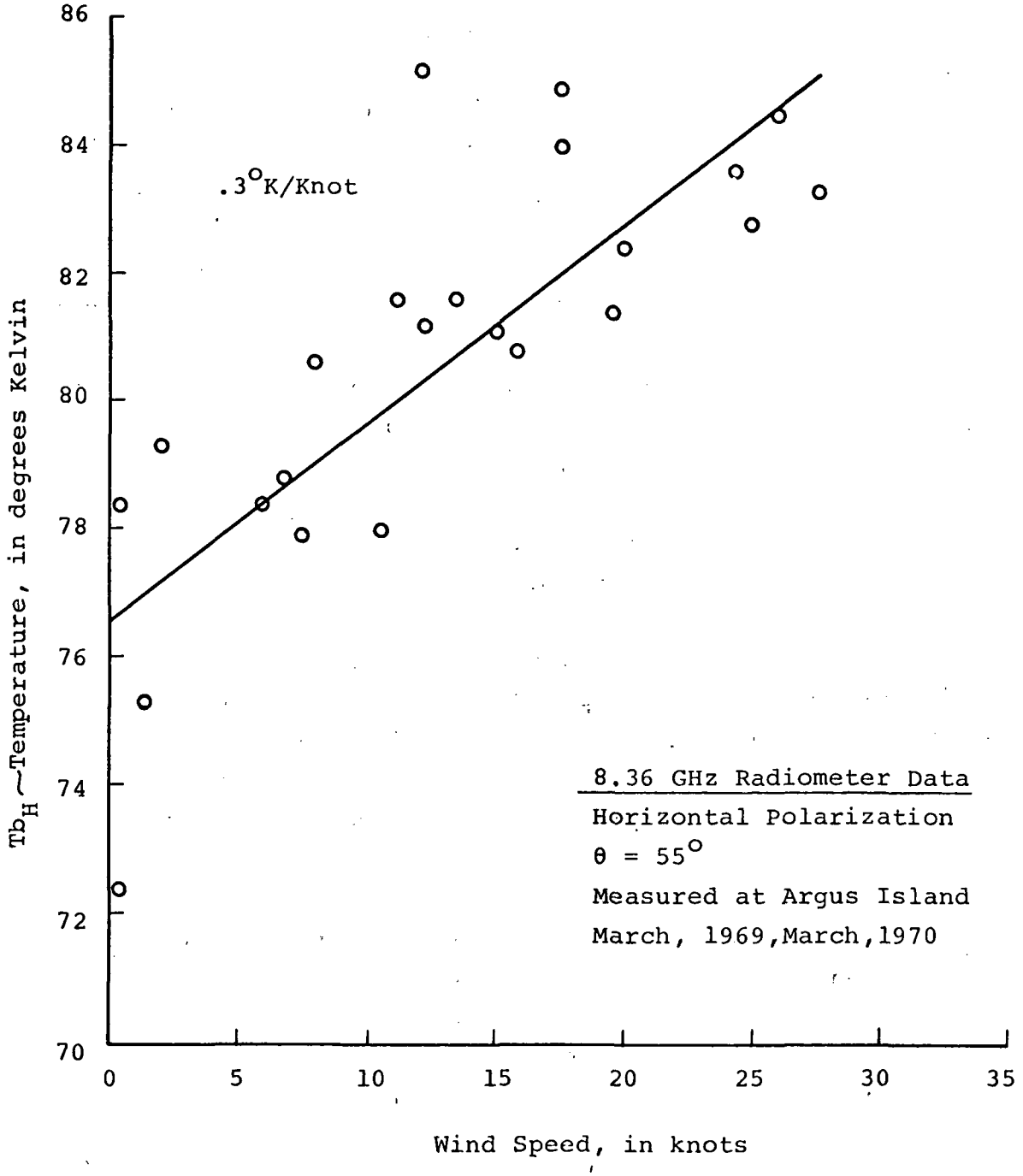

Figure 6. Radiometric wind response as reported by Hollinger.

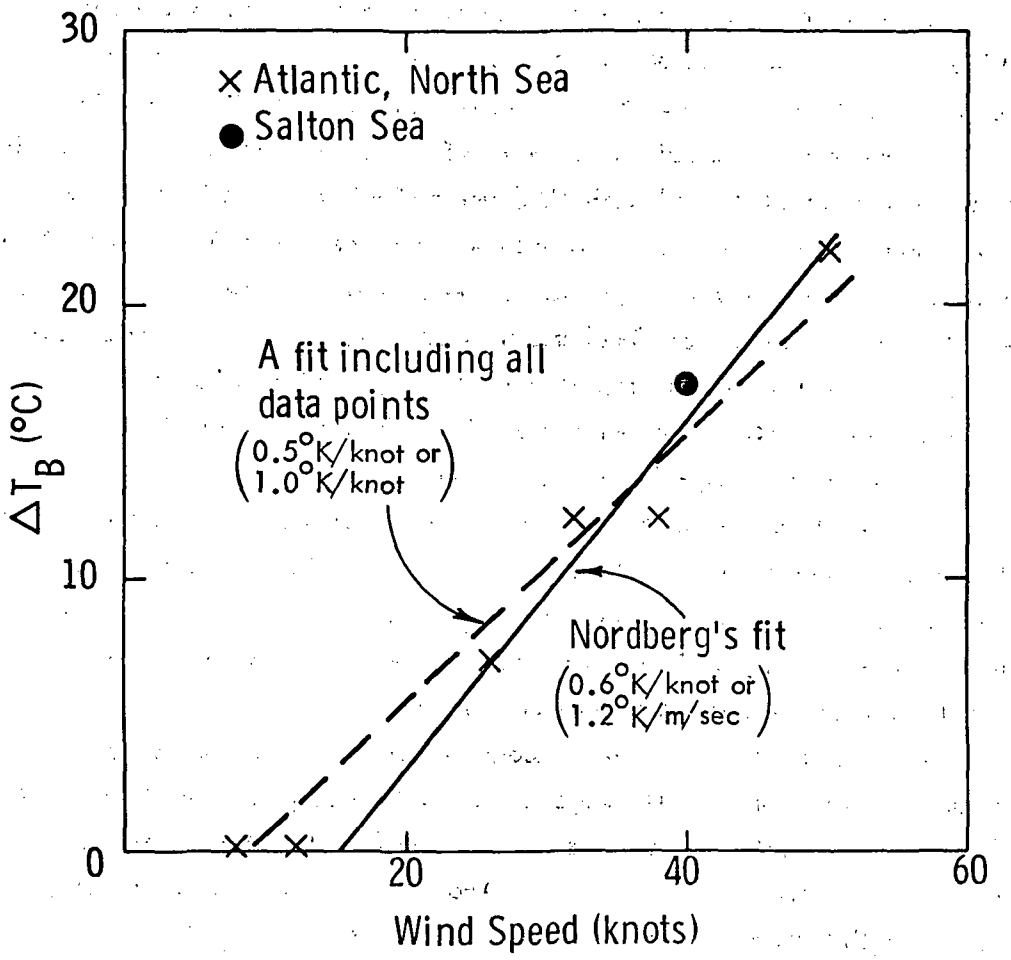

Figure 7. Wind dependence of Nordberg's observations at 19.34 GHz and the nadir angle.

C. Discussion of the Present Status

Scatter in the above results may well be primarily due to inadequate knowledge of the wind speed at the point of radar illumination. Bradley [3] was able to significantly reduce the scatter of data about the trend line by using only those runs made quite close to reliable wind sensors read continuously. Earlier data obtained both by NASA MSC and by NRL involved flights near weather reporting ships, but not as near as would be desirable; furthermore these ships sample the wind only once per hour. Hence scatter in the points is to be expected both because of non-simultaneity of wind measurements and because the wind measurements were made, at least in part, at some distance from the surface track of the radar. The wind speed in each observation cell is a difficult parameter to document, especially when the measurements are conducted miles from an anemometer. Future experiment efforts should emphasize even greater effort to obtain simultaneous wind and radar measurements at the same place. In addition it would be highly beneficial to document other parameters such as sea spectrum, foam and spray coverage, air and sea temperatures, swell, wind variability, wind gradients, surface pressure, surface humidity, etc.

Scatter in the trend with wind speed is also evident in the radiometric observations. The scatter in Hollinger's data, even though a strong trend with wind was shown, may be attributable to radiometric contributions from clouds for which compensation was inadequate. Another possibility may be associated with the fact that the effects of the wind profile inthe planetary boundary layer were not interpreted in terms of the wind gradient over a rough surface which is governed by wind speed and the air-sea temperature differential.[10]

D. Program Objectives

Experiments under well documented sea and wind conditions are clearly warranted. Under this contract suitable experiment configurations have been studied to permit good correlation between microwave observations and sea and

wind conditions. Selected aspects of the experiments are described in Section III of this report. Various meteorological and oceanographic situations which form the background for RADSCAT missions are also described. These situations represent an assortment of sea and wind conditions important to wave and weather forecasts. In addition, methods for implementing sea truth documentation are described. For a more comprehensive treatment of these experiments the reader is referred to "The Design of the RADSCAT Experiments," University of Kansas Center for Research, Inc., Technical Report 186-2, February, 1971.[11] The above mentioned report treats the design of several special experiments to observe the effects of clouds and rain on the scatterometric and radiometric observations. It also develops certain design requirements for the RADSCAT instrument to achieve certain experimental objectives.

A strong sea truth correlative basis is not the only objective of these experiments. The experiments and RADSCAT instrument have been designed to exploit the benefits of near simultaneity in measurements by the composite instrument. The joint measurements will provide a stronger interpretative basis for sea roughness and therefore wind. The measurements through clouds will afford an opportunity to assess the capability of inferring atmospheric attenuation from the composite sensor data and thereby correcting the scatterometer data. The experiments were also designed to determine the optimum frequency (within the RADSCAT band), polarization, and view angles for each sensor.

Other efforts under this contract have theoretically investigated the effects of clouds and rain on the observed microwave temperature. Various cloud and rain models have been employed to determine the rise in the microwave temperature when viewing downward through these model atmospheres. The effects of scattering on the radiative transfer process have been considered for heavy rain-fall rates. Emphasis has also been placed in correlating the temperature rise resulting from clouds and rain with atmospheric attenuation. These efforts are reported in Section IV.

A theory for microwave emission has been developed based upon a two scale roughness model for the sea surface. A non-coherent assumption[38] has been assumed to simplify the theory and consequently the numerical evaluation of the temperature values becomes quite feasible. These results are reported in Section V.

Backscatter theories were also considered to predict the backscatter characteristic of the sea. A new composite surface theory based on an equivalent surface field was developed. This theoretical model is simpler to interpret and reduces more readily to special cases than a previous theory.[61] Results from this theory are compared with measured backscatter from the sea. These results are described in Section VI.

These theoretical efforts form a strong interpretational basis for the existing scatterometric and radiometric observations as will be evident in the text. These findings are also converging to a better understanding of scatterometric and radiometric characteristics of the sea and their wind response.

This report describes the general approach and the specific results from these theoretical efforts. The detailed derivations may be found in the appropriate references listed below. Other reports and papers prepared under this contract are also included in the listing.

Technical Reports and Memorandum

Technical Report 186-1, "The Meteorological Effects on Microwave Apparent Temperatures Looking Downward Over a Smooth Sea," Steve Wu, October, 1970.

Technical Report 186-2, "Interim Report, Design of RADSCAT Experiments," J. P. Claassen, February, 1971.

Technical Report 186-3, "A Non-Coherent Model for Microwave Emission and Backscattering from the Sea," Steve Wu and A. K. Fung, July, 1971.

Technical Report 186-4, "Backscattering from a Two-Scale Rough Surface with Application to Radar Sea Returns," H. L. Chan and A. K. Fung, August, 1971.

Technical Report 186-5, "The Wind Response of Radar Sea Returns and its Implication on Wave Spectral Growth", J. P. Claassen and Mike Fung, September, 1971.

Technical Memorandum 186-1, "Accuracy Criterion for Estimating the Mean Squared Signal," John P. Claassen, December, 1970.

Open Literature

Fung, A. K. and H. L. Chan, "On the Integral for Backscattering from a Randomly Rough Surface," Proc. of IEEE, vol. 59, no. 8, pp. 1280-1281, August, 1971.

Symposiums

Fung, A. K. and H. L. Chan, "On Backscatter from Two-Scale Rough Surface," AGARD IXVII EPP Technical Meeting, June 21-25, 1971, Colorado Springs, Colorado.

Moore, R. K., J. P. Claassen, A. K. Fung, S. Wu and H. L. Chan, "Toward RADSCAT Measurements and Their Interpretation," AAFE Principal Investigator's Review, NASA Langley, October 4 & 5, 1971.

III. CERTAIN ASPECTS OF THE RADSCAT EXPERIMENTS

A. Introduction

In previous aircraft missions over the sea, microwave observations were often conducted over long traverses in the vicinity of a weather ship. In some cases the observations were conducted at distances actually remote from a weather ship. Most often the wind observations were documented by visually integrating an anemometer reading for short periods at widely spaced intervals. Wave conditions were also interpreted by a human observer, in some cases by untrained observers. To circumvent the problems associated with correlating the wind and wave observations by these methods with the microwave sensor data it is essential that well instrumented-well coordinated experiments be considered. JOSS I and JOSS II were attempts at such experiments.

In addition to the realization that coordinated remote and surface observations are essential, it is important to regard the ocean surface as a random process whose geometrical characteristics vary statistically over scales of distances both larger and smaller than the area observed by the RADSCAT sensor. The different scales of randomness are thought to be induced by inhomogeneities in the local wind field. This effect is especially prevalent at low wind speeds where the variations in the wind speed may be comparable to the average wind speed. To derive an average scattering coefficient and an average apparent temperature (and as a consequence an average wind effect) from this spatial random process will therefore require that the RADSCAT scan over distances which will sample the surface for lengths much longer than the largest local scale* of randomness. This implies that the number of independent samples of this random process could be dictated by the sea surface rather than the microwave bandwidth.

These random features of the surface have influenced the design of the RADSCAT instrument to include various mode sequences which provide different degrees of spatial averaging. But in addition, the above viewpoints dictate certain requirements in the execution of the RADSCAT experiments. These requirements are described below. Also, since the ocean surface is a random process which varies both spatially and temporally, various wind and wave conditions which

*As opposed to global scales.

dictate important measurement situations are also described in a subsequent section. These situations are also important to the oceanographer and meteorologist.

B. Suitable Experiment Configurations

To achieve well coordinated aircraft and sea truth observations, it is proposed that repeated flights be conducted in the vicinity of an instrumented site. There are several modes of the RADSCAT instrument which are well suited to measurements synchronized with surface instrumentation. The alternating scan angles mode with all of its options and fixed scan angle mode with its option can be employed for coordinated measurements. These mode sequences are shown in the diagrams of Figure 8. There are trade-offs among spatial average, coordination, and simultaneity of measurements for each mode and option. When the alternating scan angles mode is flown from 10,000 feet, nearly simultaneous measurements are realized for all submode conditions (Θ_1, VV, HH, f, S, R) from a common area of sea. For measurements coordinated with surface instruments, the mode may be initiated when directly over (near) an instrumented site. Subsequent measurements at other angles will occur on the same sea surface. At the time the mode is initiated the surface instruments could be cued either automatically from the aircraft or manually by sea based personnel.

Such coordinated measurements may be conducted at a weather ship, such as Weather Ship Hotel, or at a pre-designated site that is occupied by the Wallops Island ship, Range Recoverer. The measurement area should be staged a thousand yards or so from the lee or weather side of the ship. Repeated passage in the upwind, downwind, and diagonal-wind directions will document the directional character of the remote measurements. The experiment configuration is illustrated in Figure 9. When different mode options are employed different spatial coverage will be realized. Table I indicates the scatterometric linear surface coverage at each view angle for each option of the alternating scan angles mode when the aircraft flies at 140 knots.

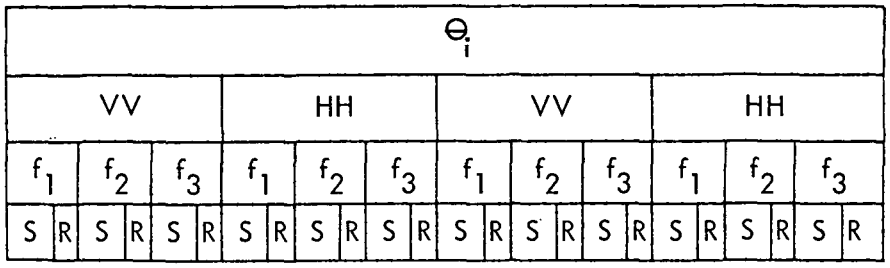

(a) The Basic Alternating Scan Angles Mode is Sequenced through Six Angles
(Options: $f_1 = f_2 = f_3$ or constant polarization)

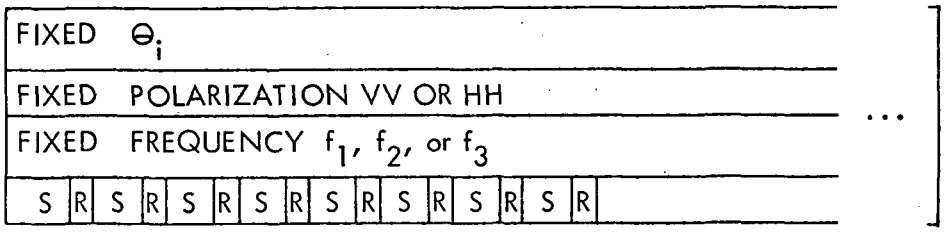

(b) The Basic Fixed Scan Angle Mode
(Option: Radiometer Only)

KEY:

Θ = Incident Angle
VV = Vertical Polarization Receive and Transmit
HH = Horizontal Polarization Receive and Transmit
f = Frequency
S = Scatterometer
R = Radiometer

Figure 8. Mode Sequences of the RADSCAT Instrument

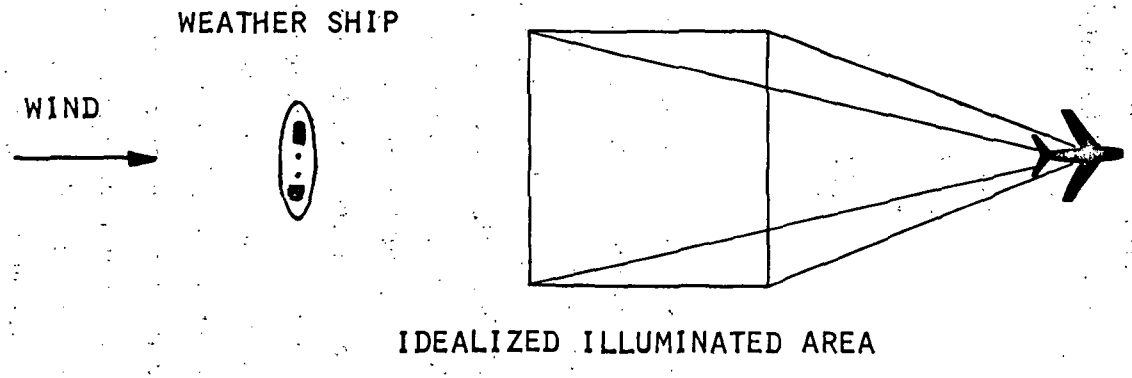

Figure 9. Experiment Configuration

TABLE I

SCATTEROMETRIC SURFACE COVERAGE

	UP-TRACK COVERAGE		
θ (Degrees)	MULTI-FREQUENCY MULTI-POLARIZATION (Feet)	FIXED FREQUENCY (Feet)	FIXED POLARIZATION (Feet)
0	1560	2090	2320
12.5	1730	2160	2380
24.5	1840	2340	2580
34.8	2120	2670	2930
43.7	2530	3160	3440
51.1	3100	3820	4020

More spatial coverage is, of course, realized in the fixed scan angle mode. An experiment configuration similar to that shown in Figure 9 may be employed; however, an illumination track about 7000 feet long will be sampled at roughly 1/2 second intervals. From records of this type variability in the RADSCAT observations may be compared with the variability in the wind field. In addition, the number of equivalent independent samples from the sea surface may be ascertained for various wind conditions. The remote measurements should be synchronized (cued) with the anemometer recording. The wind must be referred in time and space to the measurement track under the Taylor hypothesis which roughly asserts that the statistical moments of the wind speed in time are representative of those in space. Because of the difference in speed between aircraft and the wind a few minutes of RADSCAT measurements are equivalent to many minutes of anemometer record. The mean wind speed should be based on this long record which must be centered on the flight path by appropriately translating the anemometer record in time. A linear array of anemometers along the track would circumvent this interpretational problem, but almost certainly is not feasible.

C. Sea Truth Documentation

As indicated in Section II, extensive documentation is required to develop a fuller understanding of the influence of winds and seas on the RADSCAT measurements. In this regard it is extremely important that a recording anemometer be installed on board the ship.* Both wind speed and direction should be recorded during the experiment. It is also important to verify the calibration of the anemometer. It is highly beneficial to board a representative on the ship to observe, interpret, annotate, and operate the anemometer recorder during the course of the experiments. The initiation of a RADSCAT measurement sequence should be indicated on the anemometer record. A marker channel on the recorder would be helpful in this respect (the Brush Mark II recorder, for example).**

In addition to the wind speed and direction measurements, sea surface temperature, surface air temperature, surface pressure and humidity, should also be documented from the ship. The sea surface temperature is essential to the interpretation of the radiometric data. The air surface temperature and humidity are required to correct radiometric observations for atmospheric absorption. For more accurate correction (for atmospheric absorption), radiosondes may be launched during the experiment flights to profile temperature, humidity, and pressure. The air-sea temperature differential is necessary for deducing the wind profile over the sea. The air-sea temperature differential is extremely important to the proper interpretation of the wind dependence of the RADSCAT observations. The wind profile over the sea is sensitive to the air-sea temperature differential ΔT_{as} as illustrated in Figure 10. The graphs indicate that the wind stress on the sea is identical, even though the winds measured at anemometer heights are different (after Cardone [10]). The wind measurement and the air-sea temperature differential must be employed to compute an equivalent neutral wind at a given height.

---

*On Weather Ship Hotel an anemometer is already installed; provisions for recording its output in a calibrated fashion must be considered.

**A directional reference for the anemometer must also be established.

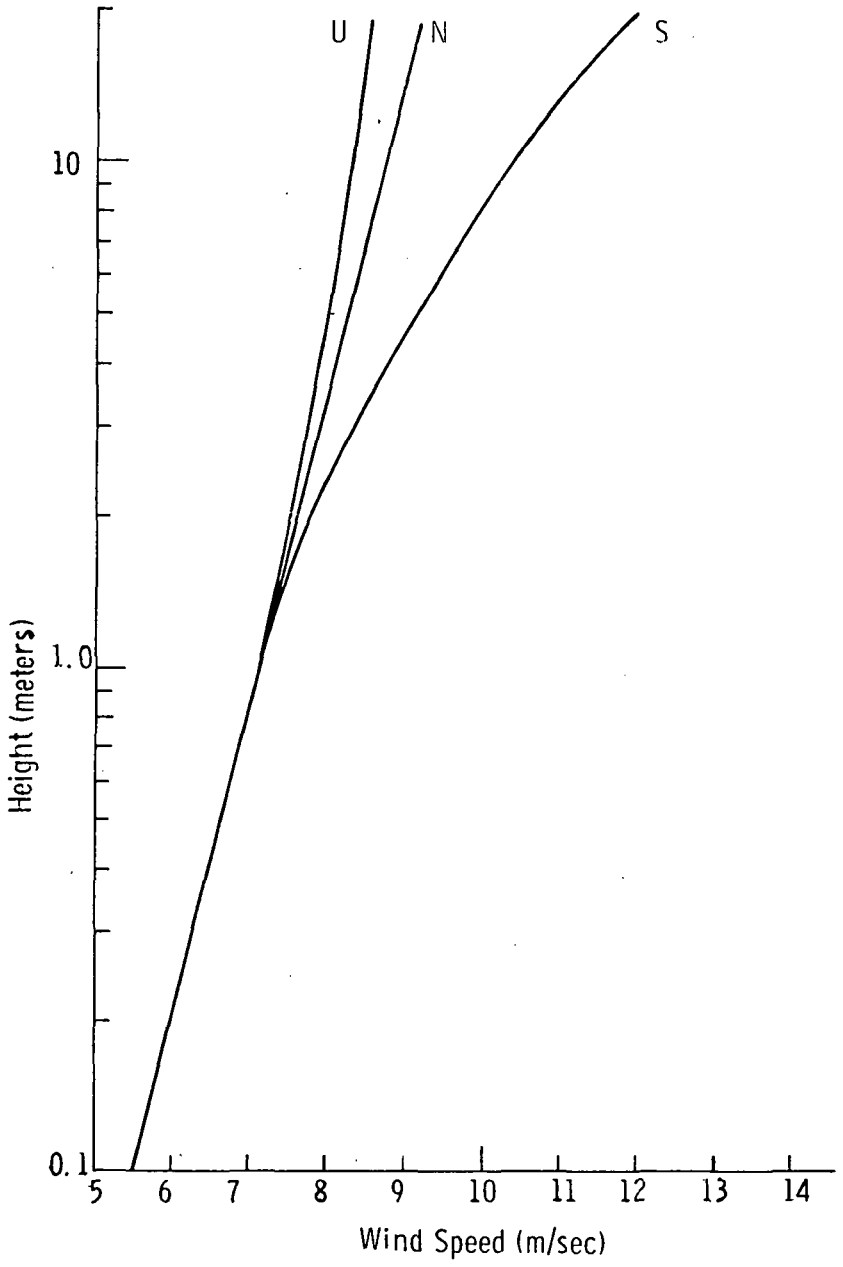

Figure 10. Theoretical wind profiles in the marine surface boundary layer for a surface stress of 1 dyne/cm^2 and neutral (N), unstable (U), and stable (S) stratification.

The spectrum of the ocean waves should be determined if at all possible. In deep oceanic waters there are two methods by which wave spectra may be measured, viz., with a laser profilometer or with special buoy systems which have velocimeters or accelerometers mounted on them. The laser profilometer is flown from an aircraft and its performance and effectiveness have been described by Ross, et al.[12] Of these two methods, the laser profilometer is the superior method since it can be easily transported to any experiment site. The records may not only be used to measure the wind induced spectrum but may be used to detect the presence of swell. The presence and magnitude of swell should also be documented by the wave hindcasting techniques developed by Pierson, et al.[13] In this method, ship reports in the form of wind speed and direction throughout the North Atlantic over a long period prior to the experiments are employed to estimate swell height and direction during the experiments.

If possible, capillary wave structure should be obtained by the Stillwell[65] technique. Foam and spray should be measured from vertical photographs. The IDECS at the University of Kansas can be used for automatic area measurements on the photos.

D. Choices of Weather and Wave Conditions

It is highly beneficial to conduct the experiments under carefully selected wind and wave conditions important to the oceanographer and meteorologist. The wind and wave conditions should also be chosen to differentiate a number of effects which can be potentially influence the RADSCAT measurements. The extratropical cyclone affords many of the important measurement opportunities.

(1) Low Wind Measurements

Several missions should be conducted under low and medium winds (summer winds) where significant variability in the wind amplitude and perhaps direction is anticipated. Close correlation of the wind measurements with the RADSCAT measurements should indicate the influence of variability in the local wind field on the measurements. The fixed angle mode is particularly adapted to observe the spatial

scale of wind variability. The results of the experiments should yield (1) the scatterometric and radiometric response to the small structure induced by the local wind field, (2) the importance of the large structure on the measurement, (3) the spatial coverage necessary to yield an indicator of the average wind field for given variability scales, and (4) the RADSCAT response to moderate wind conditions.

It is preferable to conduct these measurements under cloudless skies to assure that the radiometric measurements can be easily interpreted. This condition is preferred since direct and reflected cloud emissions will contribute to the radiometric observations. If the cloudless constraint cannot be realized, then the cloud contribution can be compensated for with some degree of accuracy if radiometric measurements are conducted above and below the clouds[9] or if opacity measurements are made.[11] These methods will undoubtedly be restricted to well stratified cloud conditions (horizontally homogeneous). However, when radiometric observations are conducted in this fashion, the cloud contribution may cause a scatter in the results which will make it difficult to interpret the radiometric response to the surface condition. As noted previously, this undoubtedly accounts to some extent for the scatter in or the selection of reported radiometric data. Most cloud conditions will not affect the scatterometric observations. As a consequence the influence of the surface conditions on the scatterometric response can be studied under less restrictive sky conditions.

(2) Wind and Wave Conditions Associated with Extratropical Cyclones

Similar measurements should be conducted under high wind conditions in either or both modes. A passage of an extratropical cyclone will afford measurement conditions to study high winds under a variety of wind speeds, wind direction, duration, fetch, etc. A cloud image of an extratropical cyclone located on the eastern seaboard is shown in Figure 11. The wind field associated with this system is shown in Figure 12. This isotach analysis was based on ship reports concurrent with the scene of Figure 11. These illustrations were prepared under Dr. W. J. Pierson, Jr., of New York University and appear in a Skylab Proposal jointly proposed by New York University, The University of Kansas, Colombia University, and NOAA. An examination of the wind field of Figure 12 indicates a number of weather and wave situations of particular interest to these experiments.

ESSA Spacecraft Cloud Mosaic for March 10, 1969
1800 GMT

Figure 11. A Cloud Image of an Extratropical Cyclone.

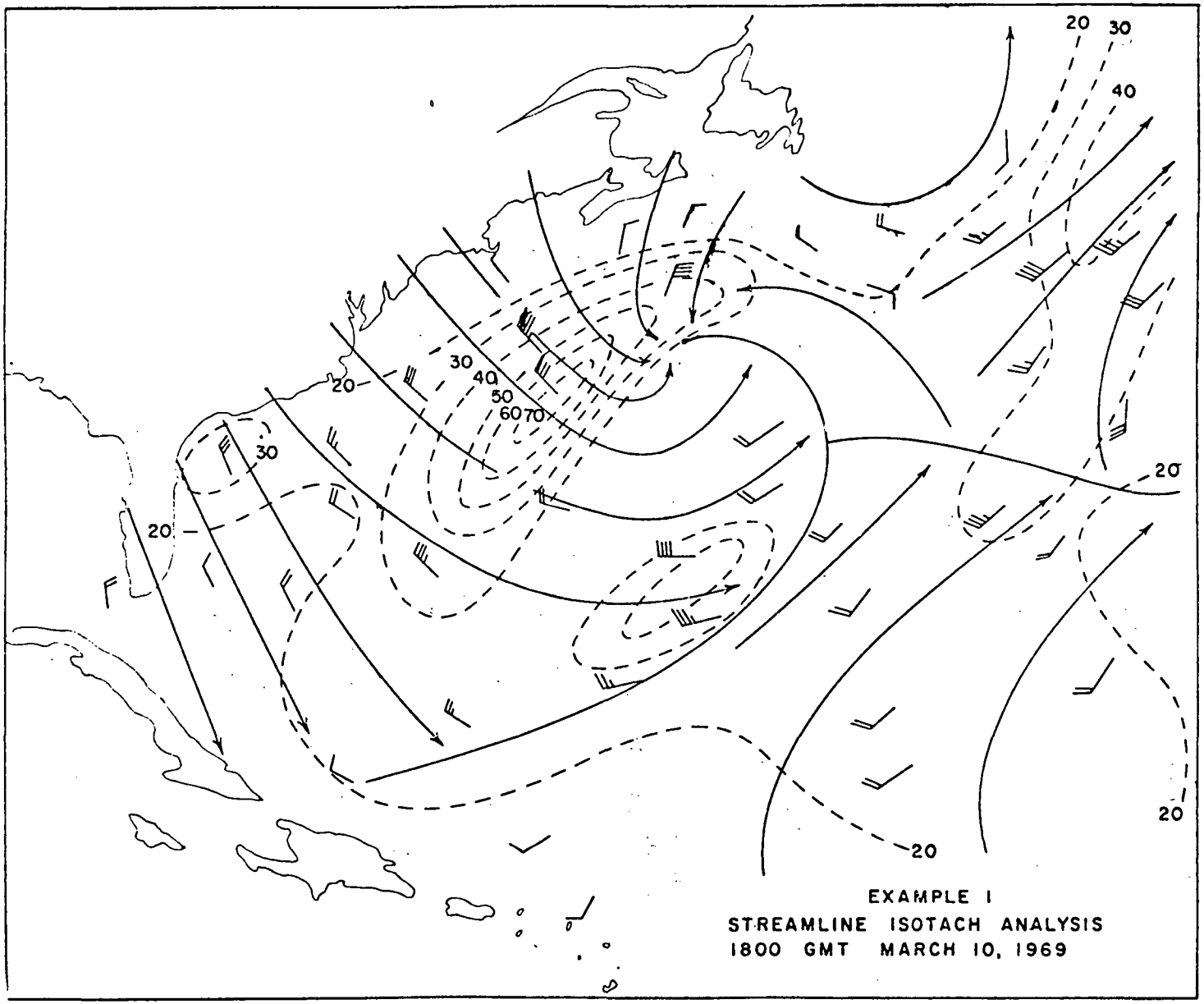

Figure 12. The Wind Field Associated with the Scene of Figure 11.

The warm sector preceding the cold front exhibits constant winds of about 20 knots over large regions. This condition is indicative of a fully developed sea whose spectral growth has attained its maximum under those wind conditions. It is further noted that, although some of this region is covered by a long bank of stratus, the region to the east of the cloud bank is essentially cloudless. These circumstances provide ideal conditions under which to execute RADSCAT observation under fully developed sea conditions. Both well coordinated measurements between the RADSCAT aircraft and sea based support and RADSCAT measurements away from an instrumented site are possible here.

The frontal band of clouds between the warm and cold sector provides a good opportunity to determine the effects of deep cloud covers on the scatterometric and radiometric observations. For more detail on these experiments the reader is referred to Section IV and reference [11].

The region immediately to the rear of the front affords conditions under which the development and decay of a confused sea condition may be documented. In this region the warm sector winds initially drove waves to the north; the cold front wind impinging on this region will develop waves propagating toward the southeast. Within a period of several hours after the passage of the front, significant waves will be superimposed on those propagating to the north. As a result, the large sea structure will be rather choppy. These conditions are likely to be found in the clear region behind the comma shaped stratus. As a consequence, radiometer observation will be unaffected by clouds. If, however, the stratus cloud deck cannot be avoided, corrections of the radiometric readings should be fairly accurate since the stratus of this type will be roughly horizontally homogeneous for significant distances.

In the high wind region marked by a cover of stratocumulus (Figure 11) there exists a good opportunity to document the development and decay of the sea under high winds and high wind gradients. The experiment may be staged at an instrumented site and the storm permitted to pass over the site. A wide latitude of high winds under limited fetch and duration can be observed within a six hour mission. Accurate scatterometric observations can be anticipated beneath or above this cloud deck; however, it may be difficult to correct and interpret the radiometric response.

Embedded within the stratocumulus cover will often occur isolated rain or snow showers. The upper boundary of these showers usually is beneath 10,000 feet. Occasionally several of these showers will coalesce. This situation is a fine opportunity in which to conduct the rain attenuation and surface impact experiments.[11]

A final examination of the cloud cover of Figure 11 and the associated wind field of Figure 12 indicates that experiments under fetch-limited conditions may be conducted off the eastern sea board. On a short time scale of several hours somewhat homogeneous, medium intensity winds will occur behind the most intense wind fields of Figure 12. The development of the sea will be almost totally governed by a homogeneous wind blowing from the shore out to sea. Measurement downwind or upwind would yield the effects of sea development on the RADSCAT measurements. It would be advantageous to fly between Range Recoverer and Weather Ship Hotel when they are separated 100 or more nautical miles as shown in Figure 13. The wind measurements at the two ships would attest to the homogeneity of the wind field. To sample the wind field between the two ships it would be highly beneficial to use an inertial navigational system which yields the wind speed and direction as a by-product of its navigational information or to provide a linear array of anemometers along the flight path. Intermittent flights are necessary at 150 feet altitude between RADSCAT measurements at 10,000 feet when the navigational system is used. The techniques developed by Cardone[10] may be employed to refer winds to the equivalent 19.5 meter height under neutral conditions. During these intervals the laser profilometer may be operated to obtain sea spectra and as a consequence wave development information.

E. Recommendations

Presently an unpressurized C-54 aircraft is specified as the vehicle from which RADSCAT observations are to be conducted. The altitude and speed limitations of this aircraft will often restrict the measurements which can be executed from this aircraft. The aircraft for example will not be capable of mounting the stratus/cumulus cloud cover found along cold fronts. This represents an important case in which deep cloud cover obscures (visually) much of the sea surface experiencing high gusting winds. Cloud attenuation may also be significant in this condition. An aircraft with higher altitude capability is recommended to achieve this objective. The instrument would also have to be modified for operation at higher altitudes.

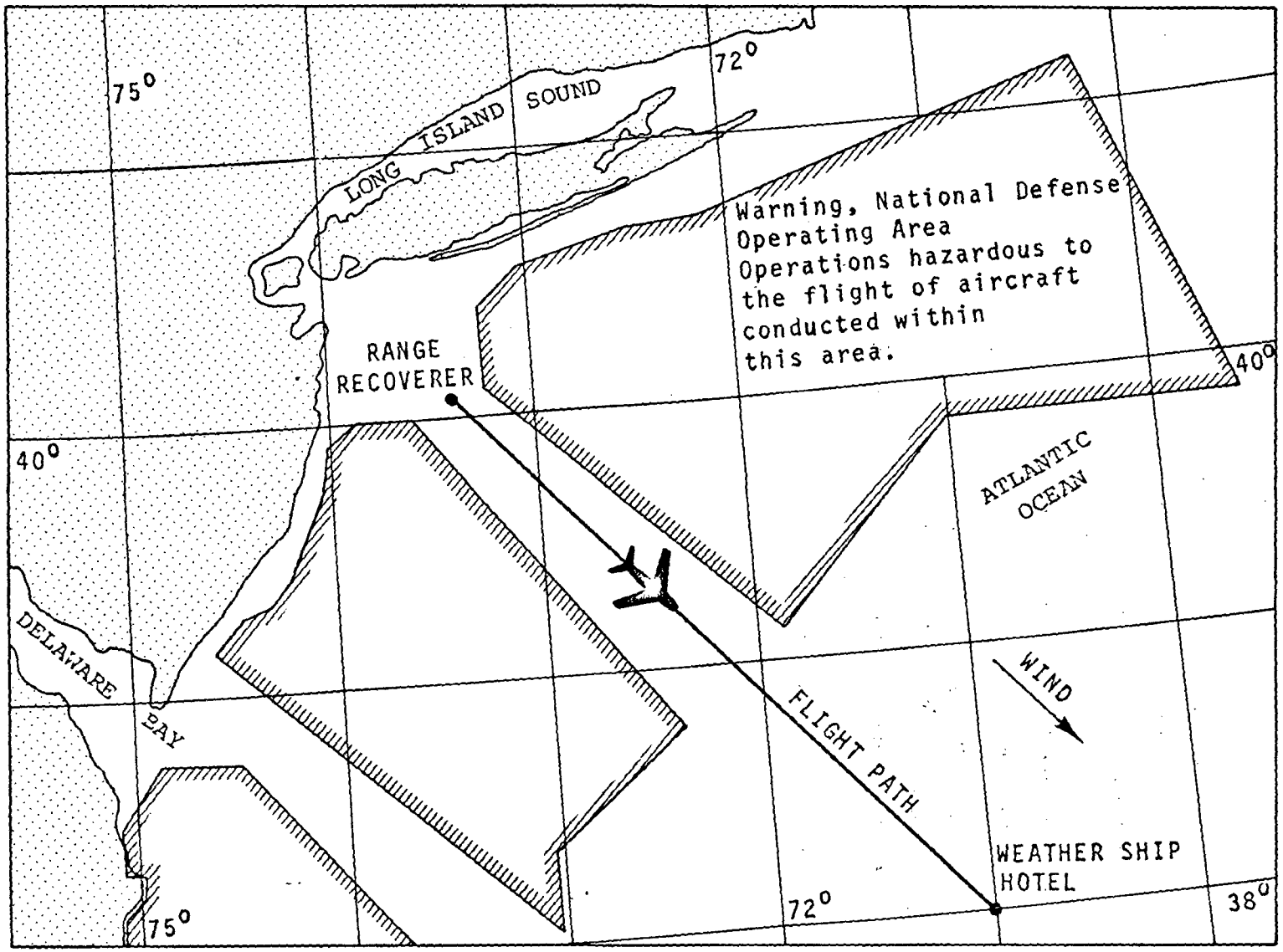

Figure 13. Fetch Limited Experiment Configuration.

In view of the importance of conducting measurements across cyclonic structures, it is recommended that segments of flight time be scheduled during the later winter and early spring months. These cyclonic structures move at about 30 knots and as a consequence during the course of such an event two or three flights separated roughly by 12 hours can be scheduled. The prediction and detection of these weather conditions, the flight scheduling and the designation of a probable experiment site, require the judgment of a qualified meteorologist/oceanographer. It is recommended that these services be arranged with Dr. Pierson's group of the Meteorology and Oceanography Department of New York University. His group has experience in providing these services and has access to cloud imagery, weather reports, weather radar displays, ship reports, etc. on which to base these decisions.

IV. THE EFFECTS OF CLOUDS AND RAIN ON THE APPARENT MICROWAVE TEMPERATURE

A. Introduction

(1) Background

High winds over the ocean are usually accompanied by clouds and rains (see Figure 11 of Section III and the accompanying text). These meteorological conditions influence scatterometric and radiometric observations, especially the latter, primarily because of atmospheric absorption (emission). The radiometric contributions to the surface brightness temperature by clouds and rains have been indicated by Singer and Williams[14] at 15.89 GHz. Additional observations at 19.45 GHz were reported by Conaway[15] and Kreiss.[16] On the other hand, theoretical investigations of cloud effects, except for the efforts of Kreiss, have largely been limited to cases in which the sky temperature is computed.[17,18]

Other radiometric measurements have documented the effect of clouds and rains on the sky temperature, i.e., looking upward. For example, Haroules and Brown[19] in a comprehensive set of measurements have measured sky temperature and inferred atmospheric attenuation. The attenuations and sky temperatures of various cloud and rain conditions shown in Table II are an excerpt of their data. Other extensive measurements of this type have been reported by Strickland,[20] Otsu, Yuichi,[21] Crane,[22] and Ippolito[23] in conjunction with the ATS-V communication satellite experiments. From these results the apparent temperature when looking downward may be qualitatively described.

Radiometric measurements conducted downward over clouds and rains will observe a slightly attenuated surface brightness temperature plus a cloud/rain contribution in excess of the sky temperature reported by the investigators above. In effect the radiometer loses contact with the surface when clouds or rain intervene.*

* The scatterometer, however, retains contact with the surface except under moderate to heavy precipitation, as a study of the entries of Table II will indicate.

TABLE II

ATTENUATION AND BRIGHTNESS TEMPERATURE OF CLOUDS AND RAIN

Cloud Type	One-Way Attenuation		T_{sky}	
	8 GHz dB	15 GHz dB	8 GHz °K	15 GHz °K
High Level	.02-.05	.03-.07	7	15
Medium Level	.03-.12	.08-.13	10	21
Low Level	.10-.25	.17-.40	14	30
Light Rain	.15-.25	.20-.60	16	38
Medium Rain	.80	3.2	20	43
Heavy Rain	1.5	5.4	70	140

(2) Objectives in Summary

The primary reason for proposing addition of a radiometer to a scatterometer for oceanic wind determination was the greater sensitivity of the radiometer to cloud and precipitation. Because of this, the combined instrument can use the radiometer to correct scatterometer measurements for small attenuation and to determine that scatterometer data should be discarded when heavy rain is indicated. Although the relation between attenuation and brightness temperature has been extensively studied for upward-looking radiometers, and measurements have shown that the expected temperature enhancements do indeed occur for downward-pointed radiometers, this is believed to be the first study aimed specifically at determining the relation between brightness temperature and attenuation for the downward-pointed radiometer. Computations have been made of the brightness temperature for a variety of meteorological conditions based on various models postulated by meteorologists. Comparison of the calculated temperature with attenuation has verified the general idea of the use of radiometer to calibrate scatterometer (see also Section V). These calculations have used a simplified ocean surface model, and further refinements are in order using a more representative description of ocean scatter.

B. Theoretical Approach

(1) Introduction

For a rough surface in thermal equilibrium the natural radiated power emitted by the surface is given by

$$P = K T_b B \tag{2}$$

where

K = Boltzmann's Constant
T_b = Brightness temperature
B = Equivalent bandwidth

The brightness temperature of the rough surface is dependent on the ability of surface to emit natural radiation and is given by

$$T_{bj}(\theta) = \epsilon_j(\theta)\, T_w \tag{3}$$

where

$\epsilon_j(\Theta)$ = emissivity in direction Θ for j polarization
T_w = surface temperature
j = vertical or horizontal polarization

The emissivity of a rough surface is dependent on the dielectric and geometrical properties of the surface and is given by

$$\epsilon_j(\theta) = 1 - \frac{1}{4\pi} \int\int \left[\gamma_{ji}(\theta,\theta') + \gamma_{jj}(\theta,\theta')\right] d\Omega' \tag{4}$$

where $\gamma_{ji}(\Theta,\Theta')$ is the bistatic differential scattering coefficient for j incident polarization and i reflected polarization for the Θ direction when illuminated from the Θ' direction. The integration is performed over a half space with respect to the primed variable.

The above expression for a quiet sea can be related to Fresnel reflection coefficient $R_j(\Theta)$ by

$$\epsilon_j(\theta) = 1 - |R_j(\theta)|^2 \qquad (5)$$

The evaluation of the Fresnel coefficient was based on the dielectric properties of sea water as given by Saxton and Lane.[24] Although this emissivity does not typify the sea well, it is adequate in indicating meteorological effects. The extension to realistic emissivity conditions for a rough sea can be based on the efforts reported in Section V .

(2) Theoretical Basis Excluding Scattering Effects

Measurement of the surface brightness temperature through a realistic atmosphere is affected by the emission, absorption and scattering characteristic of the atmosphere itself. The apparent surface temperature will contain direct and indirect contributions from the atmosphere. Under clear skies, cloudy skies, and light to moderate rains, the effects of scattering by the atmospheric constituents may be neglected for observations in the RADSCAT band. When scattering by atmospheric constituents is neglected, the observed (apparent) temperature at altitude z and nadir angle Θ will be given by

$$T_{aj}(\theta, z) = [T_{bj}(\theta) + T_{rj}(\theta)]\,\Gamma(\theta, z) + T_s(\theta, z) \qquad (6)$$

where

$$T_s(\theta, z) = \sec\theta \int_0^z \alpha(z'')\, T_{air}(z'') \exp\left[-\sec\theta \int_{z''}^{z} \alpha(z')\,dz'\right] dz'' \qquad (7)$$

$\alpha(z)$ = atmospheric absorption coefficient at height z

$T_{air}(z)$ = atmospheric temperature profile

$$T_{rj}(\theta) = T_s(\theta, \infty)\,|R_j(\theta)|^2 = T_s(\theta, \infty)\,[1 - \epsilon_j(\theta)] \qquad (8)$$

$$\Gamma(\theta, z) = \exp\left[-\sec\theta \int_0^z \alpha(z')\,dz'\right] \tag{9}$$

In the above expressions $T_s(\Theta, z)$ denotes the sky temperature as observed in the interval $(0, z)$, $T_{rj}(\Theta)$ the sea reflected sky temperature, and $\Gamma(\Theta, z)$ the atmospheric transmittance in the interval $(0, z)$.

To describe atmospheric effects the atmosphere was considered to be horizontally stratified and the total absorption coefficient was described as

$$\alpha(z) = \alpha_{cs}(z) + \alpha_{cloud}(z) + \alpha_{rain}(z) \tag{10}$$

$\alpha_{cs}(z)$ is the absorption profile associated with clear skies and is composed of a sum of absorption components resulting from various oxygen and water vapor absorption bands. The absorption coefficient α_{cs} is temperature and pressure dependent. As a consequence, the temperature profile was assumed to be given by

$$T(z) = \begin{cases} T_w - 6.46z \ ^\circ K & \text{for } 0 \le z \le 11 \text{ km} \\ 217 \ ^\circ K & \text{for } z > 11 \text{ km} \end{cases} \tag{11}$$

and the pressure profile by

$$P(z) = 1.33\ P_w\ e^{-0.143z} \quad mb \tag{12}$$

where P_w is the sea surface pressure.

The absorption coefficient for clouds was based on a model suggested by Benoit[25]

$$\alpha_{cloud}(z) = M\,\nu^{b(z)}\,e^{a(z)} \quad dB/km \tag{13}$$

where

M = liquid water content

ν = propagating frequency

b(z) = frequency index

a(z) = temperature coefficient

The empirical expression proposed by Gunn and East[26] was employed to specify rain attenuation

$$\alpha_{rain}(z) = d[p(z)]^c \tag{14}$$

where p(z) is the precipitation rate and c and d are frequency dependent parameters.

A thorough treatment of this theoretical basis is described in reference [27]. The apparent temperature was numerically computed for various cloud and rain models. These models and their apparent temperature characteristics are described in Section IV.C below.

(3) Theoretical Basis Including Scattering Effects[17,28,29,30]

Under heavy precipitation a larger percentage of precipitation particles exhibit diameters comparable to wavelengths characteristic to the RADSCAT band. As a consequence scattering cannot be neglected in considering the transfer of radiation through heavy precipitation. The physical effects are clear. The radiation from the surface not only encounters absorption but also scatters in all directions on its upward course. The addition of "collisions" on its upward course, as a consequence, attenuates the surface radiation and reflections more effectively. Similar physical processes describe the propagation of the inherent radiation of the atmosphere. A decrement in the apparent temperature can therefore be anticipated. The solution technique for radiation transfer through a scattering atmosphere is presented below.

In a precipitating atmosphere, the source of emission in the medium consists of two terms: the unpolarized thermal radiation and the emission induced by scattering. The basic equation of radiative transfer becomes an integral differential equation; it is given by

$$\cos\theta \frac{dI_\nu(\theta,\varphi)}{dz} + \beta_{ex} I_\nu(\theta,\phi) = \beta_{sc}\int_0^{2\pi}\int_0^{\pi} I_\nu(\theta_s,\varphi_s)\gamma(\cos\Theta)\sin\theta_s\, d\theta_s\, d\varphi_s$$

$$+ \frac{1}{2}\beta_{ab} B_\nu(T) \qquad (15)$$

where

$I_\nu(\Theta,\phi)$ = radiation intensity of the system in direction (Θ,ϕ) at frequency ν. For a fixed frequency, the subscript is usually ignored to simplify the notation.

Θ_s,ϕ_s = direction of the scattered radiation.

$\beta_{ex},\beta_{sc},\beta_{ab}$ = the extinction, the scattering, and the absorption coefficients, respectively. These can be calculated using Mie's theory for a specific rain model. The values used in this investigation are shown in Table III.

$\gamma(\cos\Theta)$ = scattering phase function subject to

$$\int_0^{2\pi}\int_0^{\pi}\gamma(\cos\Theta\sin\theta_s\, d\theta_s\, d\varphi_s = 1$$

$\cos\Theta = \cos\Theta\cos\Theta_s + \sin\Theta\sin\Theta_s\cos(\phi_s - \phi)$

$B_\nu(T)$ = Planck's function at microwave frequencies

$$= \frac{2K\nu^2}{c^2} T_{air}$$

K = Planck's constant

c = velocity of light

T_{air} = air temperature in the precipitating atmosphere.

Equation (15) can be expressed in terms of microwave temperature by the formula

$$I_\nu = \frac{K\nu^2 T}{c^2} \qquad (16)$$

Prior to this conversion, it is necessary to consider the polarized characteristics of microwave radiation. The unpolarized thermal radiation in the medium may be decomposed into equal components for horizontal and vertical polarization, but

TABLE III

THE EXTINCTION COEFFICIENT, THE SCATTERING COEFFICIENT, AND THE ALBEDO OF PRECIPITATION

Freq. GHz	Temp. °K	273			283			293		
	Coefficient / $P_{mm/hr}$	$k_m^{-1}\beta_{ex}$	$k_m^{-1}\beta_{sc}$	ω	$k_m^{-1}\beta_{ex}$	$k_m^{-1}\beta_{sc}$	ω	$k_m^{-1}\beta_{ex}$	$k_m^{-1}\beta_{sc}$	ω
8.9	10	.0318	.00147	.046	.0307	.00151	.049	.0288	.00157	.054
	20	.0729	.00426	.058	.0735	.00440	.060	.0723	.00460	.064
	30	.1185	.00792	.067	.1222	.00821	.067	.1230	.00859	.070
	40	.1669	.01229	.074	.1743	.01278	.073	.1774	.01333	.075
11.1	10	.0558	.00372	.067	.0574	.00383	.067	.0582	.00397	.068
	20	.1251	.01070	.086	.1322	.01101	.083	.1380	.01142	.083
	30	.1998	.01977	.099	.2133	.02031	.095	.2251	.02101	.093
	40	.2777	.03042	.110	.2985	.03148	.105	.3158	.03219	.102
13.9	10	.0942	.00949	.101	.0994	.00971	.098	.1051	.00998	.095
	20	.2065	.02684	.130	.2201	.02740	.124	.2350	.02800	.119
	30	.3253	.04881	.150	.3470	.04959	.143	.3708	.05051	.136
	40	.4465	.07339	.164	.4800	.07609	.159	.5080	.07557	.149

the emission induced by scattering is a polarized radiation which contributes to the two polarizations in a random fashion. As a result it is conceivable to assume that the emission induced by scattering has equal probability for horizontal and vertical polarization. With this assumption in mind, the coupled polarization equation can be decoupled and the equation of radiative transfer becomes:

$$\cos\frac{dT_j(\theta,\varphi)}{dz} + \beta_{ex}T_j(\theta,\varphi) = \frac{\beta_{sc}}{2}\int_0^{2\pi}\int_0^{\pi} T_j(\theta_s,\varphi_s)\,\gamma(\cos\Theta)\sin\theta_s\,d\theta_s\,d\varphi_s$$

$$+ \beta_{ab}T_{air}(z) \qquad (17)$$

$$j = h \text{ or } v$$

Introducing the optical depth $\tau = \int_z^{\infty}\beta_{ex}dz$, and defining $\omega = \beta_{sc}/\beta_{ex}$ (albedo of scattering), $\mu = \cos\Theta$, $\mu_s = \cos\Theta_s$, Equation (17) can be rewritten as follows:

$$\mu\frac{dT_j(\mu,\varphi)}{d\tau} + T_j(\mu,\varphi) = \frac{\omega}{2}\int_0^{2\pi}\int_{-1}^{1} T_j(\mu_s,\varphi_s)\,\gamma(\cos\Theta)\,d\mu_s\,d\varphi_s$$

$$+ (1-\omega)\,T_{air}(\tau) \qquad (18)$$

where

$$\cos\Theta = \mu_s\mu + \sqrt{1-\mu^2}\sqrt{1-\mu_s^2}\cos(\varphi_s-\varphi)$$

The scattering phase function, $\gamma(\cos\Theta)$, can be represented in a finite series of Legendre polynomials:

$$\gamma(\cos\Theta) = \sum_{\ell=0}^{N} r_\ell P_\ell\left[\mu\mu_s + \sqrt{1-\mu^2}\sqrt{1-\mu_s^2}\cos(\varphi_s-\varphi)\right] \qquad (19)$$

where P_l is the Legendre polynomial of order l. Additional simplification will result when the following identity is employed.

$$P_l(\cos\Theta) = P_l\left[\mu\mu_s + \sqrt{1-\mu^2}\sqrt{1-\mu_s^2}\cos(\varphi_s - \varphi)\right]$$

$$= P_l(\mu)P_l(\mu_s) + 2\sum_{m=1}^{l}\frac{(l-m)!}{(l+m)!}P_l^m(\mu)P_l^m(\mu_s)\cos m(\varphi_s - \varphi) \tag{20}$$

where

P_l^m = Associated Legendre polynomial of order l degree m.

We have

$$\gamma(\cos\Theta) = \gamma(\mu, \varphi, \mu_s, \varphi_s)$$

$$= \sum_{l=0}^{N} r_l\left[P_l(\mu)P_l(\mu') + 2\sum_{m=1}^{l}\frac{(l-m)!}{(l+m)!}P_l^m(\mu)P_l^m(\mu_s)\cos m(\varphi_s - \varphi)\right]$$

$$= \sum_{m=0}^{N} A^m \cos m(\varphi_s - \varphi) \tag{21}$$

where

$$A^m = (2 - \delta_{o,m})\left[\sum_{l=m}^{N} r_l^m P_l^m(\mu)P_l^m(\mu_s)\right] \tag{22}$$

$$(l = m, \ldots, N \quad , \quad 0 \le m \le N)$$

$\delta_{o,m}$ = 1 if m = 0
= 0 otherwise

$$\gamma_l^m = \gamma_l\frac{(l-m)!}{(l+m)!}$$

Equation (21) suggests that we expand $T_j(\tau,\mu,\phi)$ in the form

$$T_j(\tau,\mu,\varphi) = \sum_{m=0}^{N} T_j^m(\tau,\mu)\cos m\varphi \tag{23}$$

When Equations (21) and (23) are substituted into Equation (18), the following independent equations result:

$$\mu \frac{dT_j^m(\tau,\mu)}{d\tau} + T_j^m(\tau,\mu) = \frac{\varpi\omega}{2}\int_{-1}^{1} A^m(\mu,\mu_s)\, T_j^m(\tau,\mu_s)\, d\mu_s + (1-\omega)\, T_{air}(\tau)$$

$$(m = 0, 1, \cdots, N) \tag{24}$$

The boundary conditions for a plane surface bounded below and the atmosphere extended to infinity are

$$T_j(\tau_o,\mu) = \epsilon_j(\mu)\, T_g + [1-\epsilon_j(-\mu)]\, T_j(\tau_o,-\mu) \qquad \mu \geq 0$$

$$T_j(0,\mu) = 0 \qquad \mu \leq 0 \tag{25}$$

where τ_o is the total optical depth of the precipitating atmosphere. $\epsilon_j(\mu)$ is the plane surface emissivity and T_g is the surface temperature.

Since the plane surface is isotropic, and since there are no sources above the atmosphere, and since the thermal radiation in the medium is also isotropic in nature, the solution of Equation (24) consists of one term (m = 0) only and it becomes a function τ, μ, and independent of ϕ.

In order to obtain the function $T_j(\tau,\mu)$ numerically, the approximate problem is formulated by confining ourselves to (N =) 5 terms in the expressions shown in Equations (21) and (23) and requiring that Equation (24) and boundary condition (25) be fulfilled at the points $\mu_1, \mu_2, \ldots, \mu_N$ of the interval (0, 1) and

$(\mu_{-1}, \mu_{-2}, \ldots, \mu_{-N})$ in the interval $(0,-1)$. The integrals are here replaced by quadrature summations.

A system of ordinary differential equations of the first order with N boundary conditions at $\tau = 0$ and N at $\tau = \tau_o$ is obtained for the 2N unknown functions $T_j^i(\tau) = T_j(\mu_i, \tau)$, $(i = 1,2,\ldots,N,-1,-2,\ldots,-N)$ of this approximate problem.

We introduce a difference net in τ in such a way that the boundaries of the different substances in the points of discontinuity of the coefficients of Equation (24) are points of the net. A finite difference system is obtained by integration over each step of the net (τ_l, τ_{l+1}) of the system of differential equations for the functions $T_j^i(\tau)$ on the assumption that these functions can be interpolated linearly over the step. For N = 5, the system of equations with the subscript j removed, is represented as follows:

$$\frac{\mu_1}{\tau_l}\left(T_{l+1}^1 - T_l^1\right) + \frac{1}{2}\left(T_{l+1}^1 + T_l^1\right) = \frac{\pi\omega}{2}\sum_{i=1}^{5} a_i\left[A(\mu_1,\mu_i)\left(T_{l+1}^i + T_l^i\right) + A(\mu_1,-\mu_i)\left(T_{l+1}^{-i} + T_l^{-i}\right)\right]$$

$$+ (1-\omega)\, T_{air}(\tau_l)$$

$$\vdots \qquad (26)$$

$$\frac{\mu_5}{\tau_l}\left(T_{l+1}^5 - T_l^5\right) + \frac{1}{2}\left(T_{l+1}^5 + T_l^5\right) = \frac{\pi\omega}{2}\sum_{i=1}^{5} a_i\left[A(\mu_5,\mu_i)\left(T_{l+1}^i + T_l^i\right) + A(\mu_5,-\mu_i)\left(T_{l+1}^{-i} + T_l^{-i}\right)\right]$$

$$+ (1-\omega)\, T_{air}(\tau_l)$$

$$\frac{\mu_1}{\tau_l}\left(T_l^{-1} - T_{l+1}^{-1}\right) + \frac{1}{2}\left(T_l^{-1} + T_{l+1}^{-1}\right) = \frac{\pi\omega}{2}\sum_{i=1}^{5} a_i\left[A(\mu_1,\mu_i)\left(T_l^{-i} + T_{l+1}^{-i}\right) + A(\mu_1,-\mu_i)\left(T_l^i + T_{l+1}^i\right)\right]$$

$$+ (1-\omega)\, T_{air}(\tau_l)$$

$$\vdots \qquad (27)$$

$$\frac{\mu_5}{\tau_l}\left(T_l^{-5} - T_{l+1}^{-5}\right) + \frac{1}{2}\left(T_l^{-5} + T_{l+1}^{-5}\right) = \frac{\pi\omega}{2}\sum_{i=1}^{5} a_i\left[A(\mu_5,\mu_i)\left(T_l^{-i} + T_{l+1}^{-i}\right) + A(\mu_5,-\mu_i)\left(T_l^i + T_{l+1}^i\right)\right]$$

$$+ (1-\omega)\, T_{air}(\tau_l)$$

Note that

$$\int_{-1}^{1} f(\mu)\, d\mu = \int_{0}^{1} [f(\mu) + f(-\mu)]\, d\mu$$

$$\cong \sum_{j=1}^{N} a_j [f(\mu_j) + f(-\mu_j)] \qquad (28)$$

$a_1 = 0.11846,\ a_2 = 0.23931,\ a_3 = 0.28444,\ a_4 = 0.23931,\ a_5 = 0.11846$

$\mu_1 = 0.04691,\ \mu_2 = 0.23077,\ \mu_3 = 0.50000,\ \mu_4 = 0.76923,\ \mu_5 = 0.93509$

where a_j's are the weighting factors and μ_j's are elements of the domain of T when a five point Gaussian quadrature integration technique is employed.

Equivalently this can be written in matrix form as:

$$A_\ell T_{\ell+1}^{+} + B_\ell T_\ell^{+} + C_\ell (T_{\ell+1}^{-} + T_\ell^{-}) = F_\ell^{+}$$

$$C_\ell (T_{\ell+1}^{+} + T_\ell^{+}) + B_\ell T_{\ell+1}^{-} + A_\ell T_\ell^{-} = F_\ell^{-} \qquad (29)$$

with

$$T_\ell^{+} = \begin{bmatrix} T_\ell^{1} \\ \vdots \\ T_\ell^{5} \end{bmatrix}, \quad T_\ell^{-} = \begin{bmatrix} T_\ell^{-1} \\ \vdots \\ T_\ell^{-5} \end{bmatrix}, \quad F_\ell^{+} = F_\ell^{-} = (1-\omega)\, T_{air}(\tau) \begin{bmatrix} 1 \\ \vdots \\ 1 \end{bmatrix}$$

$$A_\ell = [a_{ij}] \qquad a_{ij} = \left(\frac{\mu_i}{\tau_\ell} + \frac{1}{2}\right)\delta_{ij} - \frac{\pi\omega}{2} A(\mu_i, \mu_j)\, a_j$$

$$B_\ell = [\, b_{ij} \,] \qquad b_{ij} = \left(-\frac{\mu_i}{\tau_\ell} + \frac{1}{2}\right)\delta_{ij} - \frac{\pi w}{2} A(\mu_i, \mu_j)\, a_j \tag{30}$$

$$C_\ell = [\, c_{ij} \,] \qquad c_{ij} = -\frac{\pi w}{2} A(\mu_i, -\mu_j)\, a_j$$

$$\delta_{ij} = 1 \quad , \quad i = j$$

$$= 0 \quad \text{otherwise}$$

The boundary conditions of Equation (25) imply: (a) on the plane surface

$$T^+(\tau_0) = T_g\, \epsilon_j^+ + \left\{ [I] - \epsilon_j^+ \right\} \cdot T^-(\tau_0)$$

where

$$\epsilon_j^+ = \begin{bmatrix} \epsilon_j(\mu_1) \\ \vdots \\ \epsilon_j(\mu_s) \end{bmatrix}$$

(b) with no incident radiation above the layer L

$$T^-(0) = [0]$$

(c) an invariance principle is based on the general reflection and emission properties of the layer (τ_ℓ, τ_0),

$$T_\ell^+ = \hat{\sigma}_\ell\, T_\ell^- + \pi_\ell \tag{31}$$

with

$$\hat{\sigma}_0 = [I] - \epsilon_j^+ \quad , \quad \pi_0 = T_g\, \epsilon_j^+$$

where [I] is the unit vector, ϵ_j^+ is the emission vector of the plane surface, and $\hat{\sigma}_\ell, \pi_\ell$ are the reflection and emission vector of the layer (τ_ℓ, τ_0). When Equation (31) is substituted in (28) and solved for $\hat{\sigma}_\ell$, and π_ℓ, we get

$$\hat{\sigma}_{\ell+1} = -\epsilon_{\ell}^{-1}\left[C_{\ell} - (B_{\ell}\hat{\sigma}_{\ell} + C_{\ell})(C_{\ell}\hat{\sigma}_{\ell} + A_{\ell})^{-1}B_{\ell}\right]$$

$$\pi_{\ell+1} = \epsilon_{\ell}^{-1}\left[F_{\ell+1}^{+} - B_{\ell}\pi_{\ell} - (B_{\ell}\hat{\sigma}_{\ell} + C_{\ell})(C_{\ell}\hat{\sigma}_{\ell} + A_{\ell})^{-1}(F_{\ell+1}^{-} - C_{\ell}\pi_{\ell})\right]$$

$$\epsilon_{\ell} = A_{\ell} - (B_{\ell}\hat{\sigma}_{\ell} + C_{\ell})(C_{\ell}\hat{\sigma}_{\ell} + A_{\ell})^{-1}C_{\ell} \qquad (32)$$

It is also known from the transmission properties of the layer that

$$T_{\ell-1}^{-} = \hat{\gamma}_{\ell}\, T_{\ell}^{-} + \delta_{\ell} \qquad (33)$$

where

$\hat{\gamma}_{\ell}$ = attenuation coefficient of the layer

δ_{ℓ} = emission coefficient of the layer

From Equations (33) and (28), the following expressions result

$$\hat{\gamma}_{\ell} = -(C_{\ell}\hat{\sigma}_{\ell} + A_{\ell})^{-1}(C_{\ell}\hat{\sigma}_{\ell+1} + B_{\ell})$$

$$\delta_{\ell} = (C_{\ell}\hat{\sigma}_{\ell} + A_{\ell})^{-1}\left[F_{\ell+1}^{-} - C_{\ell}(\pi_{\ell+1} + \pi_{\ell})\right] \qquad (34)$$

The matrix functional equations shown in Equations (28) to (34) which represent the original finite difference equation are applied to solve the integral differential equation with two boundary conditions given in Equation (25).

Computationally, the coefficients $\hat{\sigma}_{\ell}, \hat{\gamma}_{\ell}, \pi_{\ell}, \delta_{\ell}$ are first found for $\ell = 0, 1, \ldots, L$, using $\hat{\sigma}_{o} = [I] - \epsilon_{1}^{+}$, $\pi_{o} = T_{g}\epsilon_{1}^{+}$, and the recursive relations given in Equations (32) and (34). These coefficients do not depend on τ. With these coefficients calculated at every net point, Equations (31) and (33) therefore enable us to find the solutions T_{ℓ}^{+} and T_{ℓ}^{-} for all values of ℓ. To increase the accuracy of the numerical computation, the number of nets for μ_{i} and τ_{ℓ} can be increased. Under the assumption that the emission induced by scattering contains equal probability for both polarizations, the system of difference equations presented

in Equations (28) through (34) is applicable for either horizontal or vertical polarization; the only difference is the surface reflection and emission characteristics, namely $\hat{\sigma}_o = [1] - \epsilon_j^+$, $\pi_o = T_g \epsilon_j^+$, where j = "h" or "v".

C. Computed Cloud and Rain Effects

(1) Introduction

The presence of clouds and rain as shown above can be expressed as a change in the absorption coefficient. Even though the absorption coefficient may be specified for a given water content or precipitation rate, computation of the total absorption or emission requires that meteorologically realistic models for clouds and rain be selected. According to meteorological classifications there are three basic cloud forms, namely, cirrus, cumulus, and stratus. All cloud formations consist of these standard forms, a combination of these forms, or a modification of these forms.

Since cirrus clouds are typically thin layers of ice, their absorption and emission are relatively insignificant compared to the other cloud types. In the results reported below only stratus and cumulus cloud formations and various rain conditions are therefore considered. The sea surface is considered calm and at a temperature of 290°K. Rain impact effect on the surface is not included.

(2) Clouds

Extratropical cyclones have an assortment of overcast conditions. A prominent band of clouds is found along the cold front. It may be considered an overcast condition composed of stratus and cumulus clouds. The cloud structure is usually deep and may be classified as a heavy overcast. Frequently an overcast condition can be associated with the warm sector preceding the cold front. When this overcast is not precipitating it may be classified as a medium or heavy overcast condition.

To study these overcast conditions Porter's overcast models[31] were employed. See Table IV for a description of three overcast situations.

TABLE IV
PORTER'S OVERCAST MODELS

CLASSIFICATION	ALTITUDE EXTENT (m)	WATER CONTENT (gm/m^3)
Light (sun visible)	300-650	0.33
Medium (light sky)	400-900	0.67
Heavy	500-3200	1.00

This model can be considered a combination of stratus and cumulus. The apparent temperature characteristic for these overcast conditions are shown relative to a clear sky characteristic* in Figures 14 and 15 for horizontal and vertical polarization, respectively, for observations at 13.9 GHz. A comparison of these graphs indicates that horizontal polarization exhibits an increasing sensitivity to the overcast condition with view (incident) angle. A 70°K separation between the heavy overcast and the clear condition can be observed at view angles in the vicinity of 70 degrees. The response for vertical polarization on the other hand shows maximum sensitivity to clouds at nadir only.

Cumulus clouds are prevalent over the ocean at any season. To typify their effect Levine's descriptions[32] for cumulus were employed (see Table V below).

TABLE V
LEVINE'S CUMULUS MODELS

CASES	ALTITUDE EXTENT (m)	WATER CONTENT (gm/m^3)
Case 1	457-1068	0.5
Case 2	457-2590	1.0
Case 3	457-3810	1.25

*The clear sky apparent temperature includes the effects of absorption and emission by oxygen and water vapor in the atmosphere.

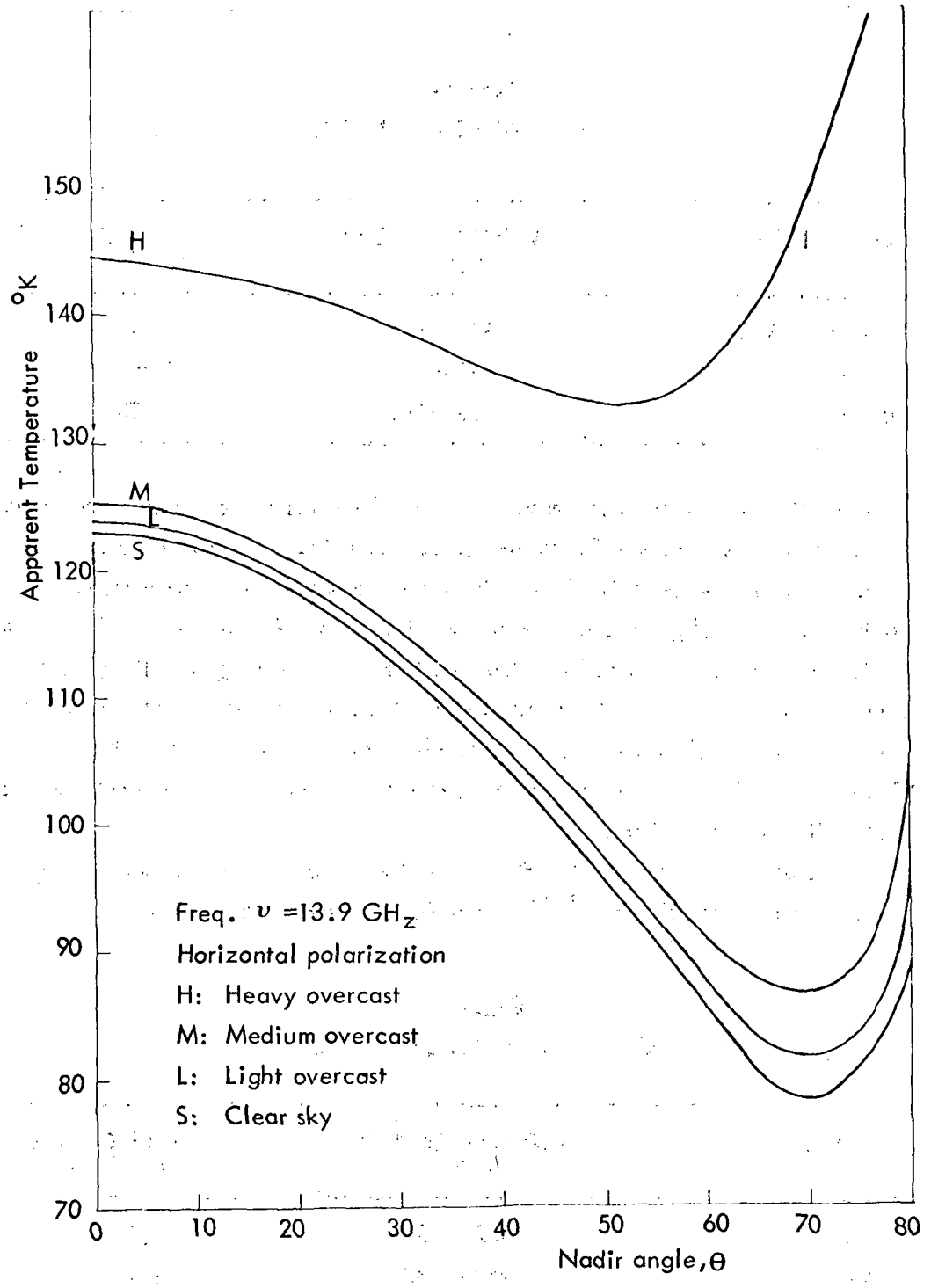

Figure 14. The computed apparent temperature characteristic for three overcast conditions - horizontal polarization.

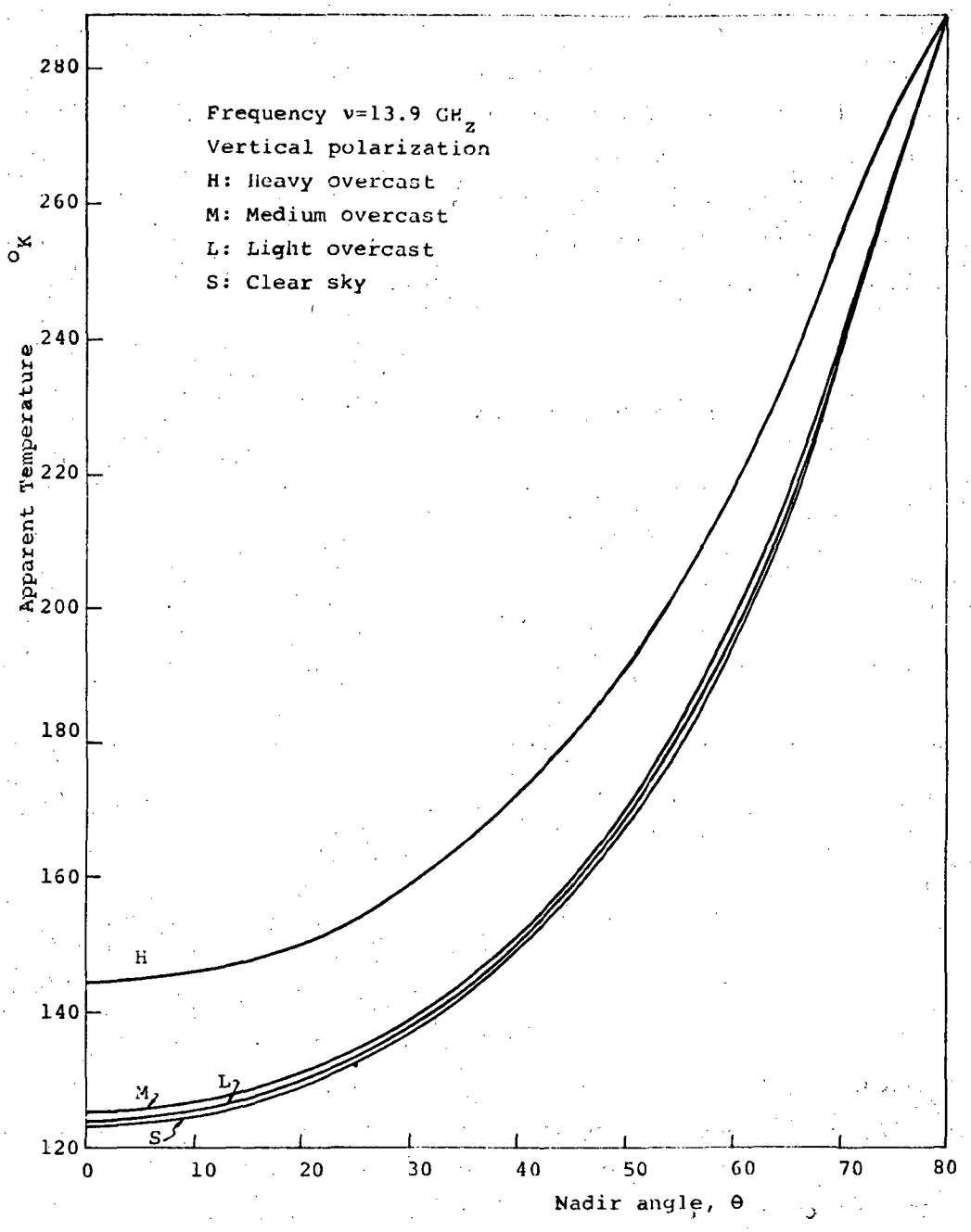

Figure 15. The computed apparent temperature characteristic for three overcast models - vertical polarization.

The apparent temperature responses with view angle for these three cases are shown in the graphs of Figure 16 for horizontal polarization. Frequency responses in the RADSCAT band for these cases are shown in the graphs of Figure 17 for two view angles. The warmth of this cloud condition can be associated with the high moisture content and depth of these clouds.

Stratus are typified by a thin band of low moisture content clouds. The apparent temperature response of these cloud conditions are based on Neiburger's investigation[33] (see Table VI). The results for horizontal polarization are shown

TABLE VI
NEIBURGER'S STRATUS MODELS

CASES	ALTITUDE EXTENT (m)	MOISTURE CONTENT (gm/m^3)
Case 1	30-580	.35
Case 2	152-520	.25
Case 3	213-490	.20

in the graphs of Figure 18. It is evident here that stratus do not contribute much to the rise in the apparent temperature.

(3) Light to Moderate Rains

The extent of precipitation over the world at any time is small in comparison to the extent of the non-precipitating regions. The frequency of rain over oceans is known to be even lower than that over land. As a consequence the operation of the combined radiometer-scatterometer will not be impeded often by rain. It is important, however, to estimate the effects of rain on the radiometric observation to attempt to discriminate between precipitating and non-precipitating regions since the interpretation of the scatterometric output will undoubtedly differ in the two regions.*

*Also helpful in mapping precipitation over the oceans.

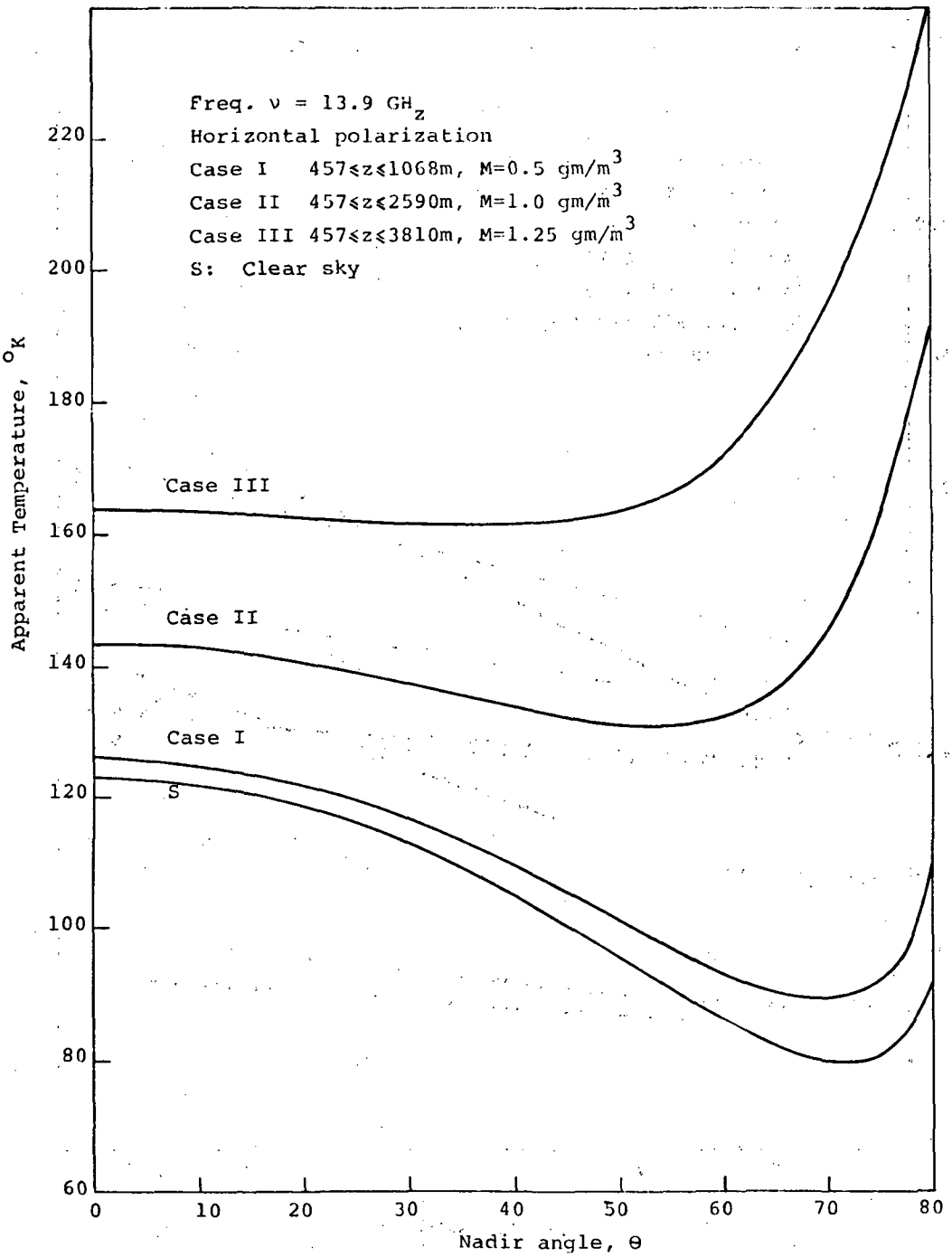

Figure 16. The computed apparent temperature characteristic for observations through cumulus clouds.

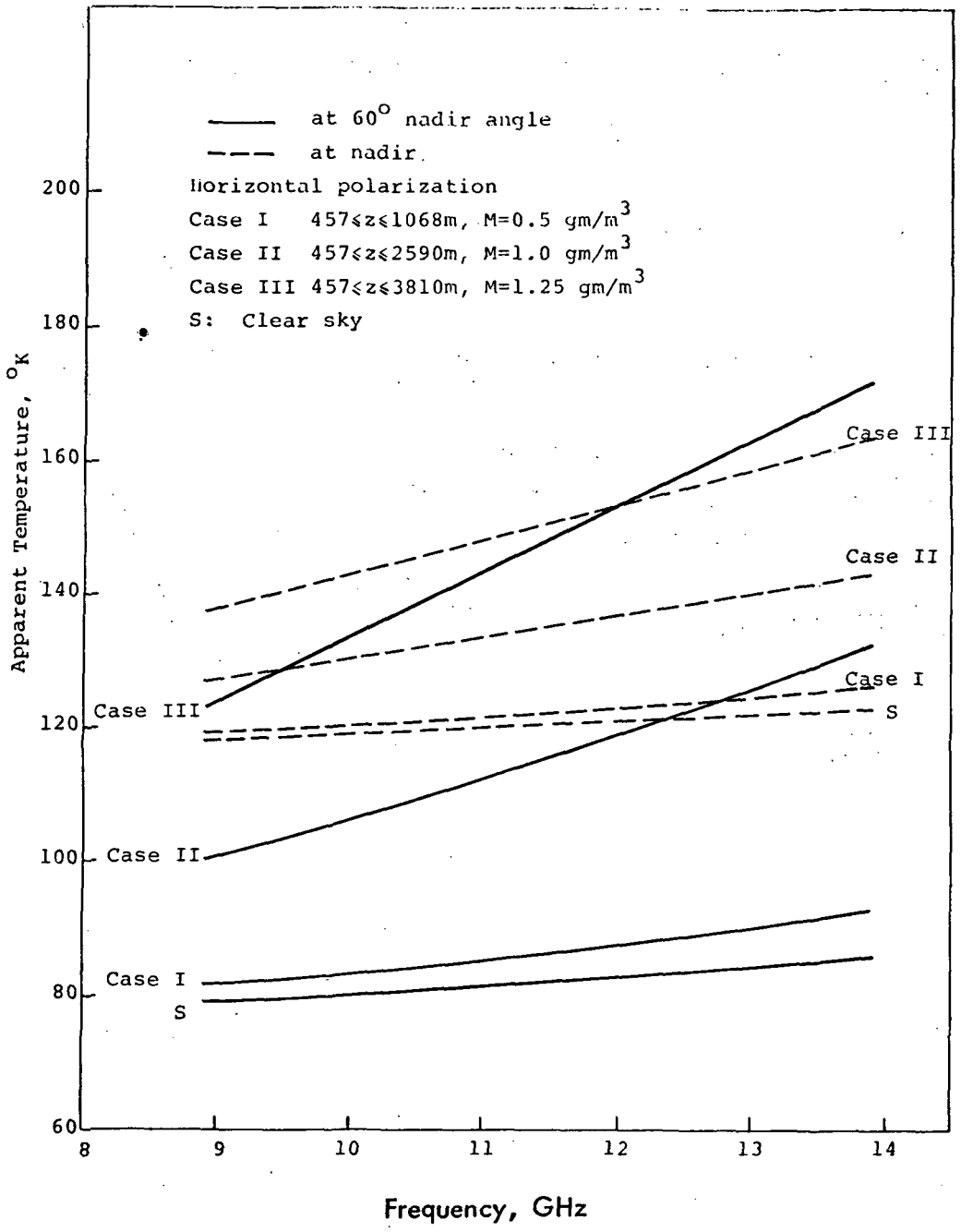

Figure 17. The computed frequency response of the apparent temperature above cumulus.

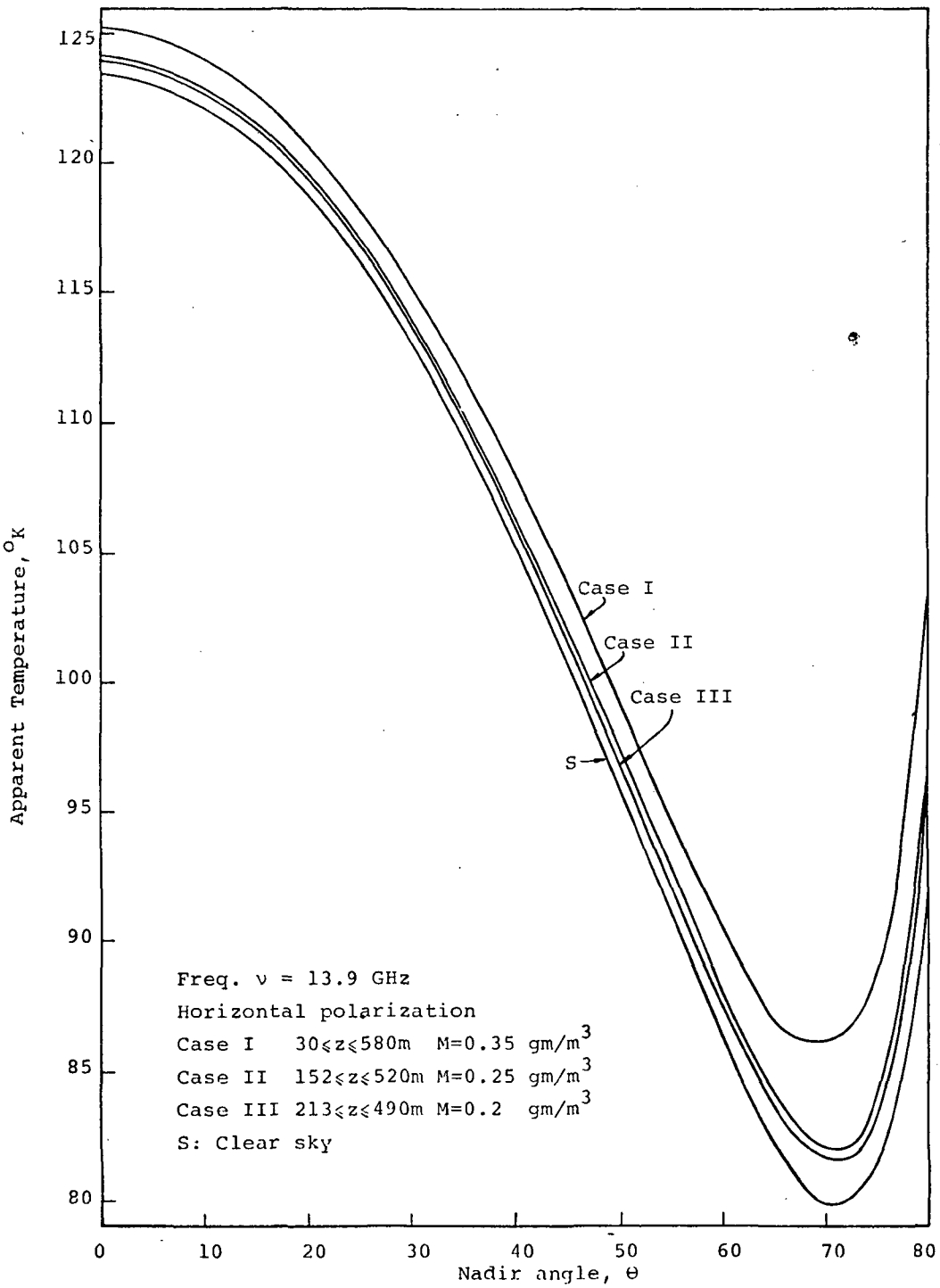

Figure 18. The computed apparent temperature characteristic for observations through stratus clouds.

The characteristics of rainfall have largely been described over land. No information regarding vertical rainfall distributions was found for rain over oceans. In this effort it is presumed that the rain characteristics over land and sea are similar. In this respect Valley's rain models[34] were used in describing the radiometric response to rain. He describes several cases; however, only one case is treated here. This case is representative of summer rain in temperate latitudes and, with a slight increase in temperature, of wide-spread tropical rains as well. This model typifies widespread uniform precipitation and not showery conditions. The precipitation and cloud characteristics are shown in Figure 19 and in Table VII, respectively. As a result of different updrafts, four different precipitation rates can be described for each case.

TABLE VII
VALLEY'S RAIN MODEL

UPDRAFT CONDITION (m/sec)	RAIN PARAMETERS		CLOUD PARAMETERS	
	Altitude Extent (m)	Precipitation at z = 0 (mm/hr)	Altitude Extent (m)	Water Content (gm/m^3)
0.4	0-3100	10.3	3100-7000	0.30
0.3	0-3200	7.9	3200-7000	0.25
0.2	0-3300	5.2	3300-7000	0.15
0.1	0-3500	2.8	3500-7000	0.10

The computed apparent temperature characteristics are shown in Figures 20 and 21. From Figure 20 it is evident that the sensitivity to rain is greater at higher angles for small rainfall rates than for larger rainfall rates. Figure 21 demonstrates that sensitivity to rainfall rate is larger at higher RADSCAT frequencies (a result to be expected). The radiometric contributions by rain are notably larger than those of clouds.

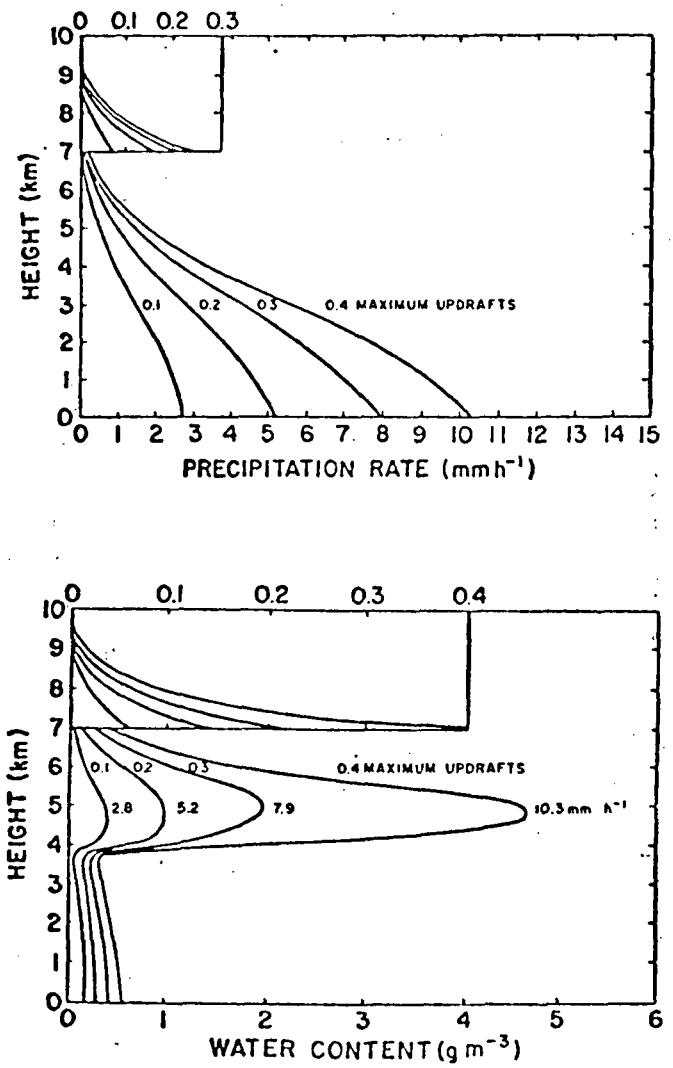

Figure 19. Precipitation and water content distribution for extensive showers.

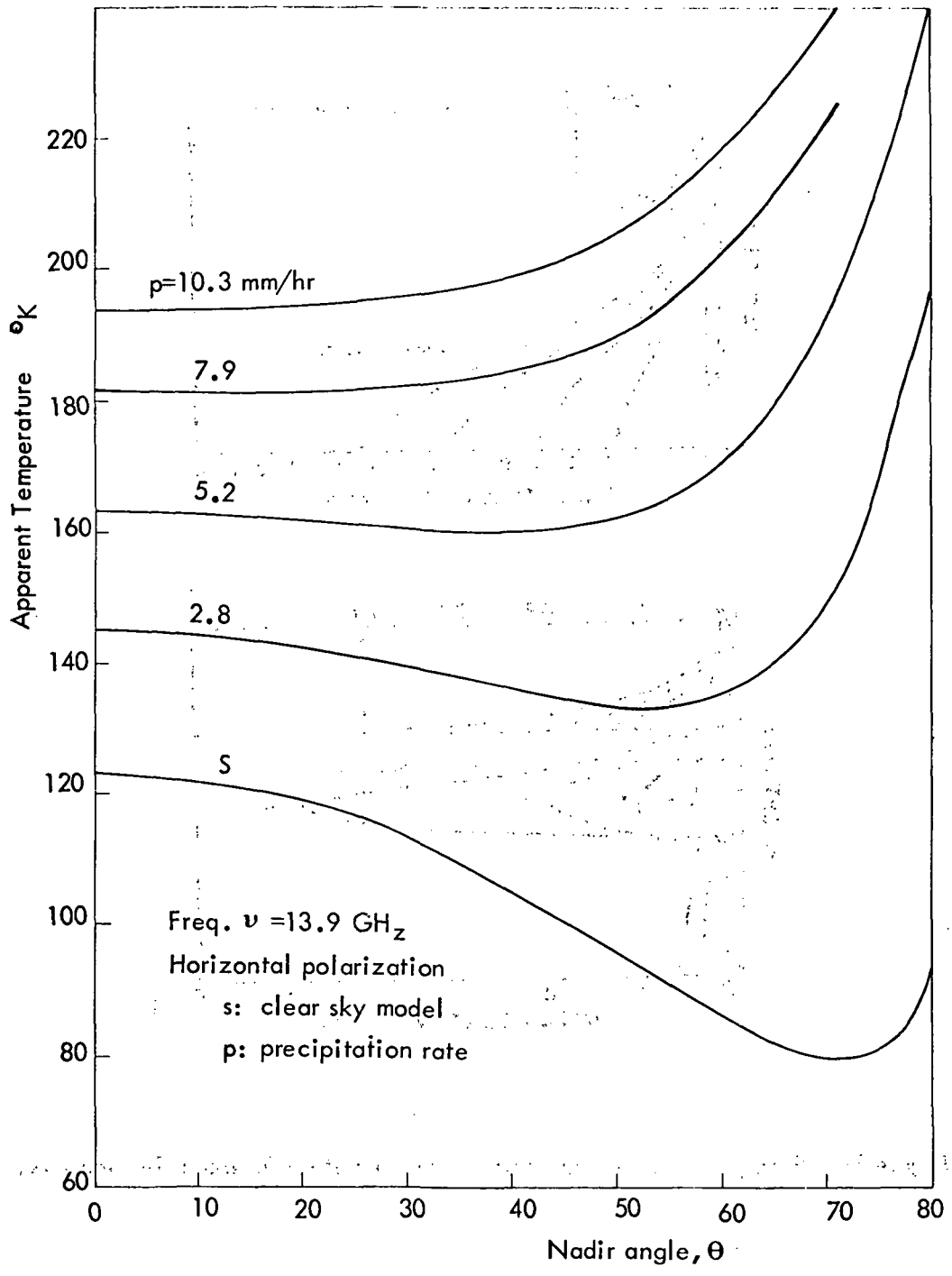

Figure 20. The computed apparent temperature characteristic for observations through rain.

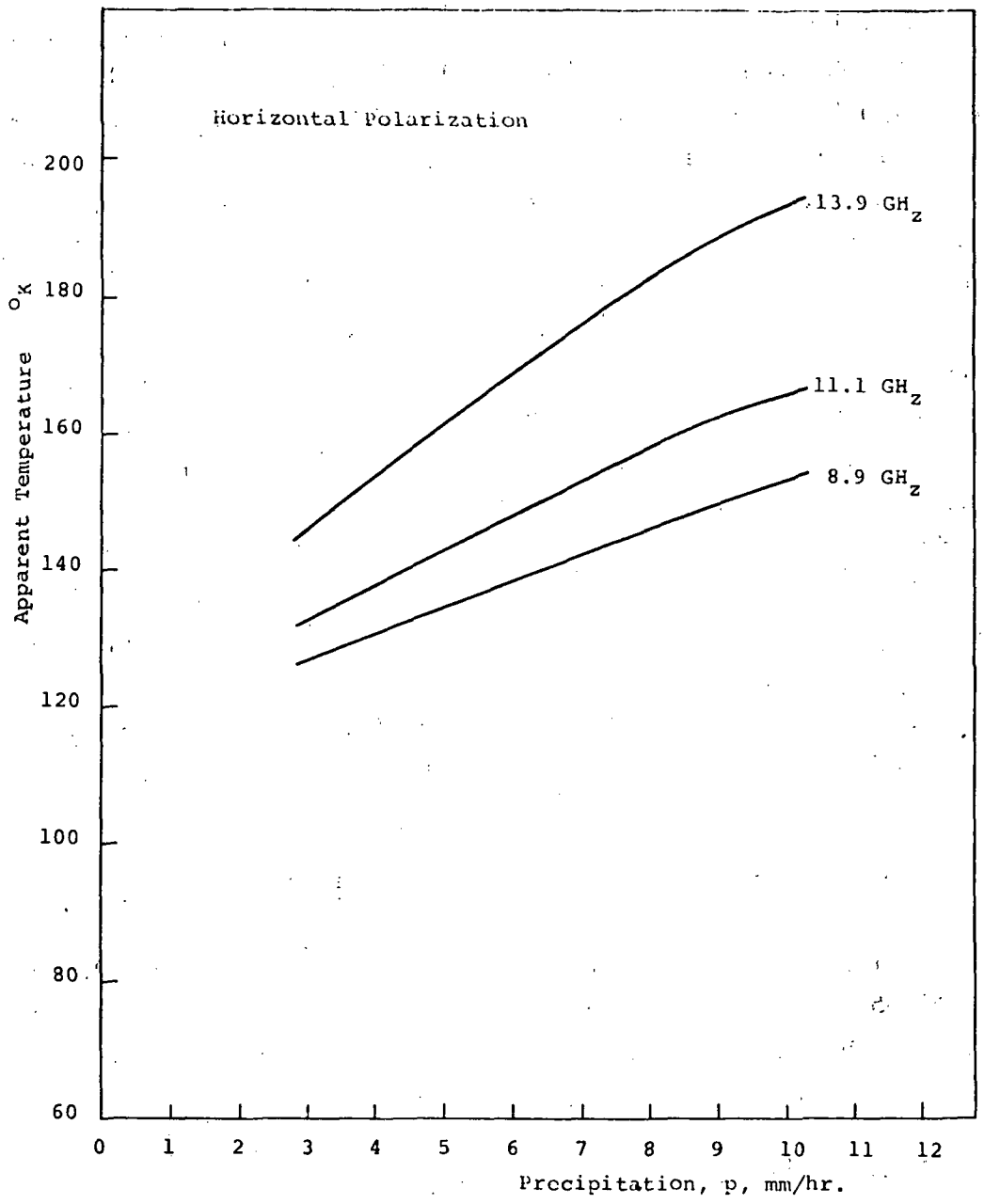

Figure 21. The computed apparent temperature response at nadir as a function of precipitation rate.

(4) Heavy Rains

Based on the theory described in Section III.B above, computer techniques were developed to predict the emission characteristic as would be observed above heavy rains. The effects of scattering by rain drops in the radiative transfer process are included and the computed results are compared with the apparent temperature when scattering is neglected. The results for two precipitation cases, 10 mm/hr and 30 mm/hr, are shown in Figures 22 through 25 for both polarizations. A decrement in the observed temperature is clearly evident when the scattering effect is included. At higher observation angles it is apparent that the scattering mechanism dominates and causes a decrease in the temperature except in the case of Figure 22. The effect of scattering is very significant at larger rainfall rates.

An examination of Figures 26 through 29 where the computed sky temperature is graphed for the same cases indicates that the decrease in temperature at higher angles must be associated with the loss of surface emission and surface reflections since the sky temperature exhibits no decrease at higher angles. An interesting characteristic is evident at higher precipitation rates. The sky temperature differs for horizontal and vertical polarization. The effect was also reported by Stogryn[17] and is attributable to multiple scattering between the surface and the sky. The surface scattering characteristic introduces the separation. This observation implies that the ratio of the polarized emissions looking downward will be altered by multi-scattering between the rain and the surface. This is somewhat evident in Figures 22 through 25.

D. Correlation of the Rise in the Apparent Temperature with Attenuation

The usefulness of the radiometer as an attenuation sensor has been verified in the ATS-5 communication experiments.[21] In this technique absorption by the atmosphere is inferred from radiometric observations of the natural radiation of the atmosphere or the radiation of an exo-atmospheric source such as the sun. The response of the radiometer to the natural radiation of the atmosphere has led several investigators[35,36] to suggest that it may be possible to infer atmospheric attenuation over the sea with the combined radiometer-scatterometer sensor. The advantage of deriving atmospheric attenuation lies in the ability to correct the scatterometric observation through dense cloud covers where the radiometer senses large contributions by the atmosphere (as shown above). Efforts under this contract have further verified the potential to infer atmospheric attenuation with the RADSCAT instrument.

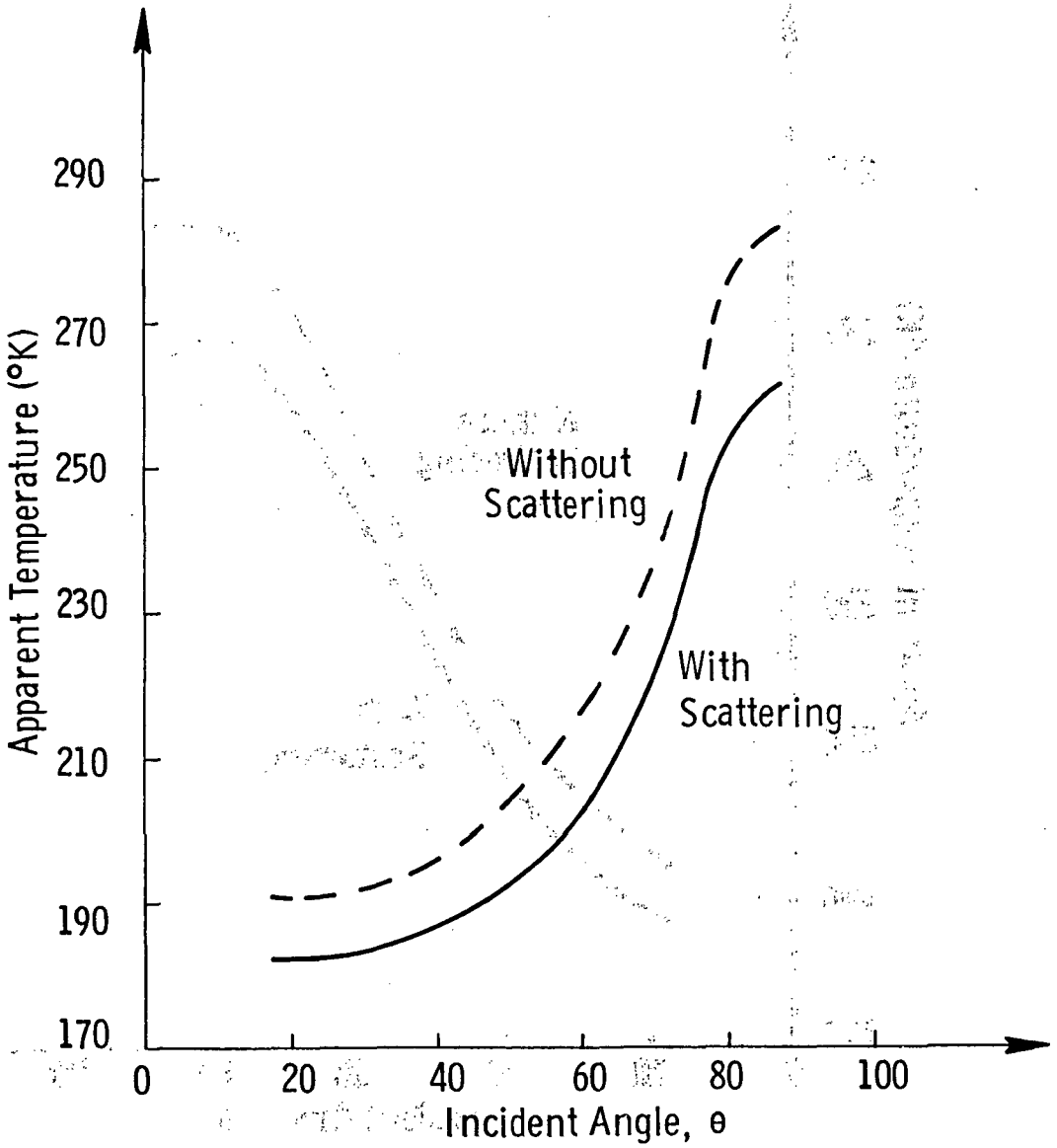

Figure 22. The Computed Apparent Temperature for Horizontal Polarization and a Precipitation Rate of 10 mm/hr.

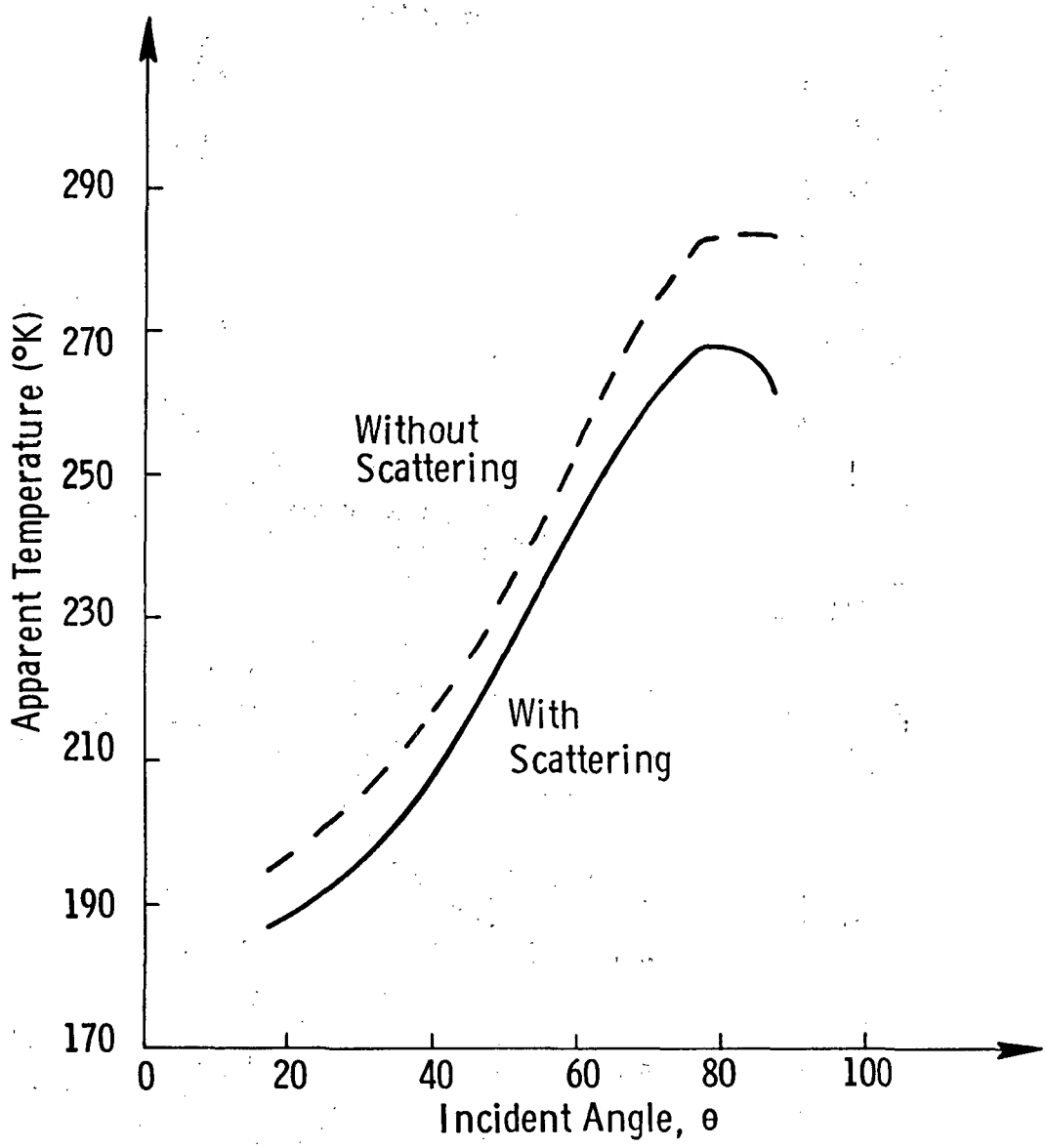

Figure 23. The Computed Apparent Temperature for Vertical Polarization and a Precipitation Rate of 10 mm/hr.

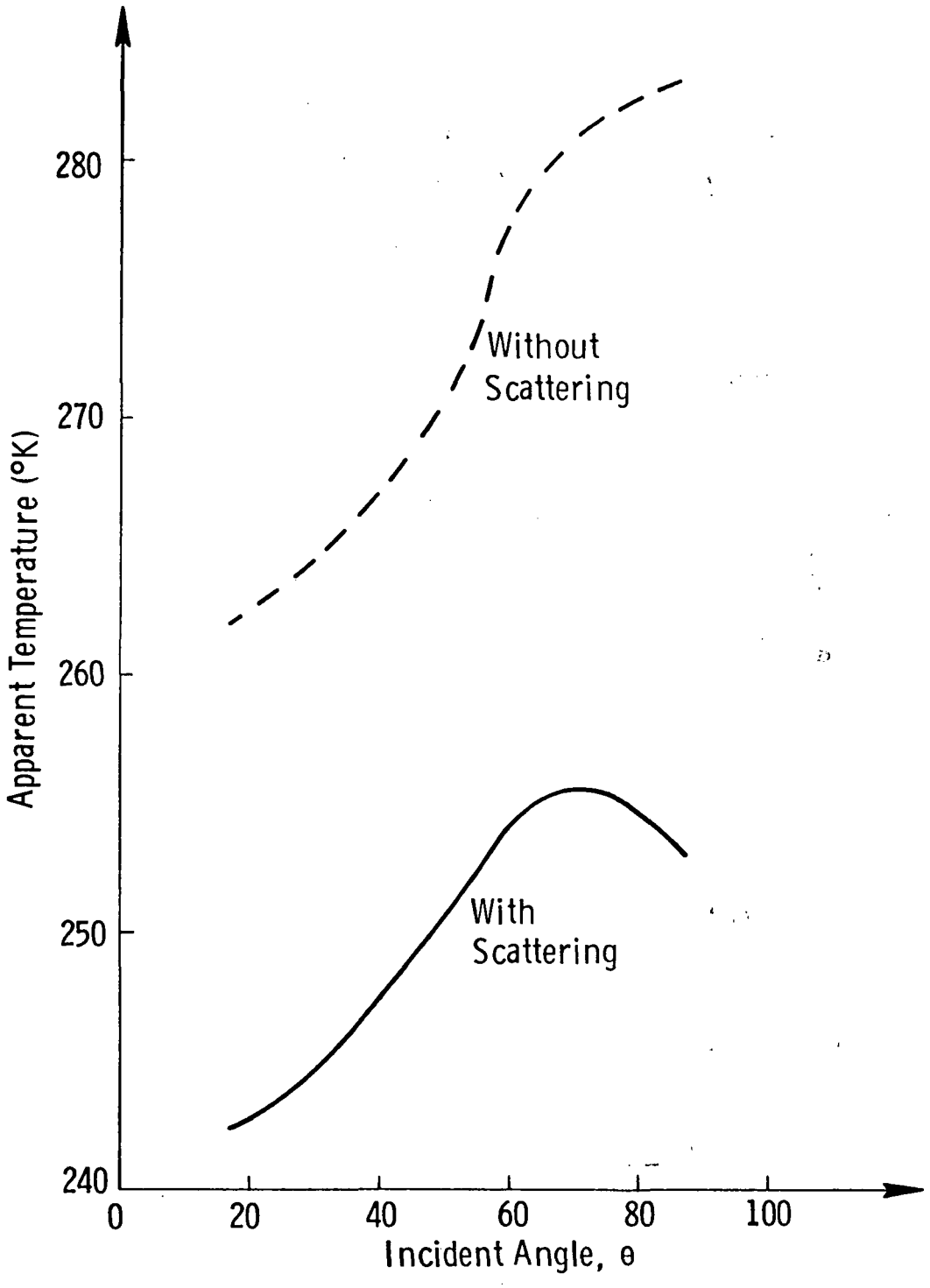

Figure 24. The Computed Apparent Temperature for Horizontal Polarization and a Precipitation Rate of 30 mm/hr.

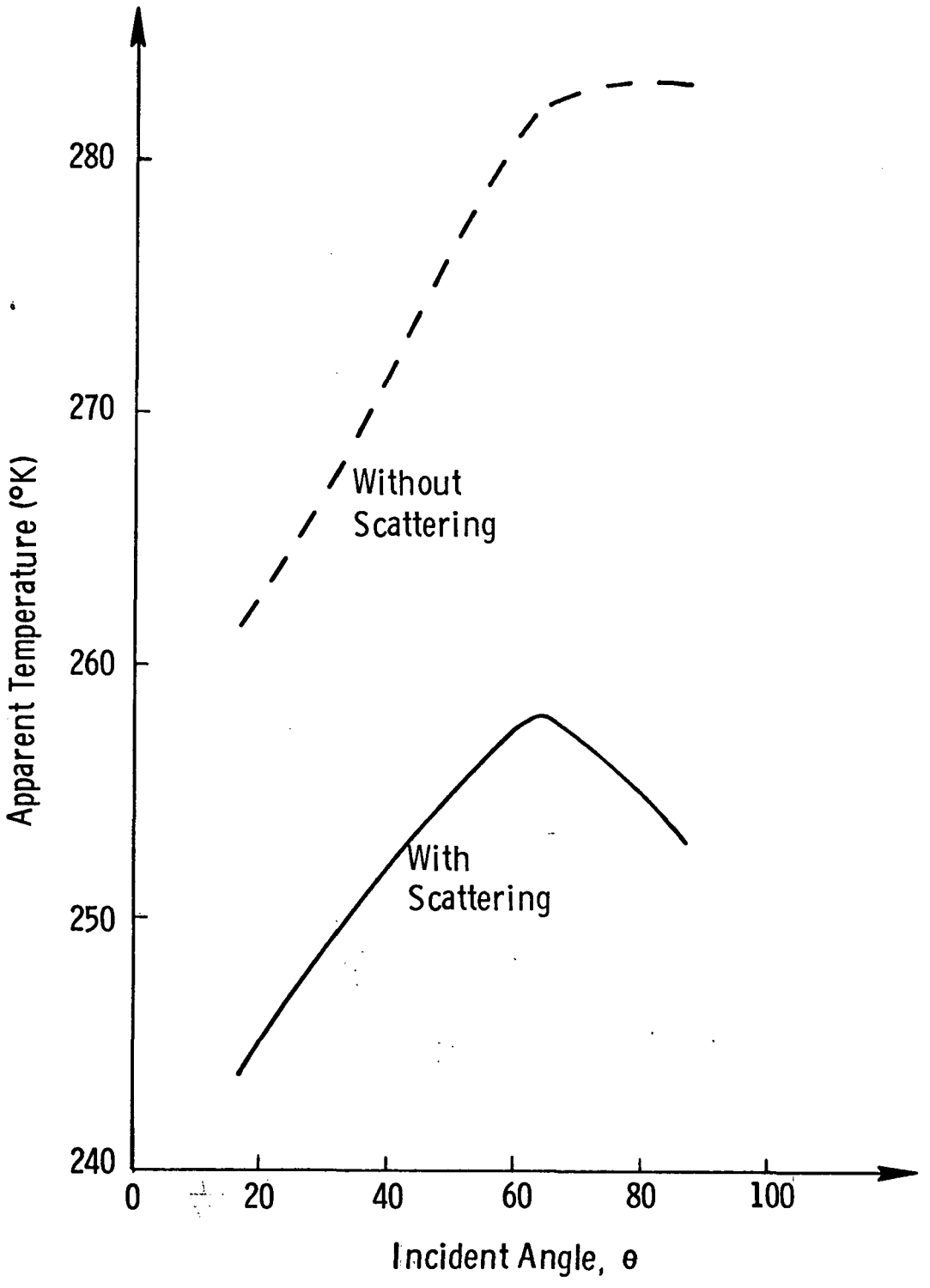

Figure 25. The Computed Apparent Temperature for Vertical Polarization and a Precipitation Rate of 30 mm/hr.

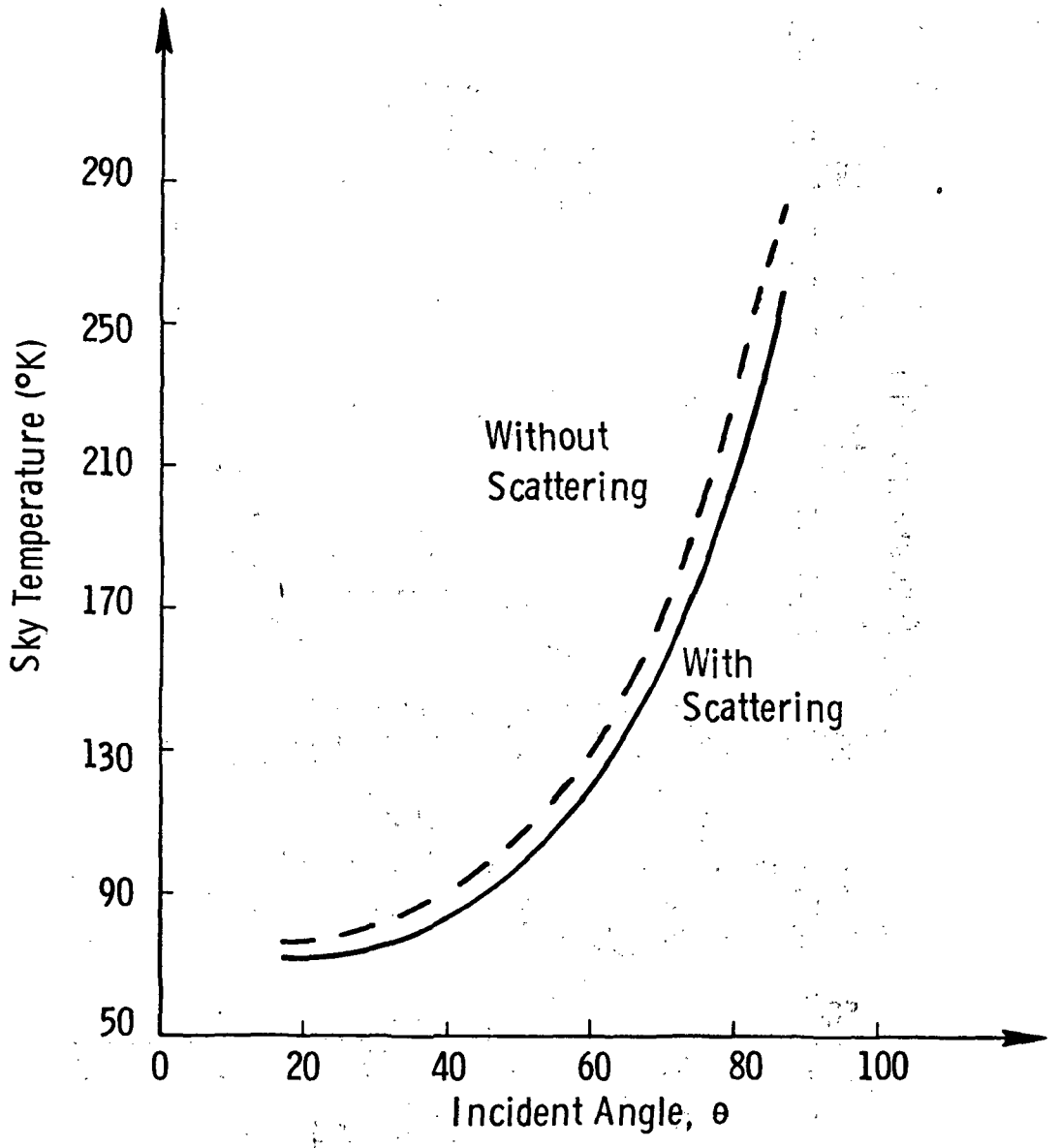

Figure 26. The Computed Sky Temperature for Horizontal Polarization and a Precipitation Rate of 10 mm/hr.

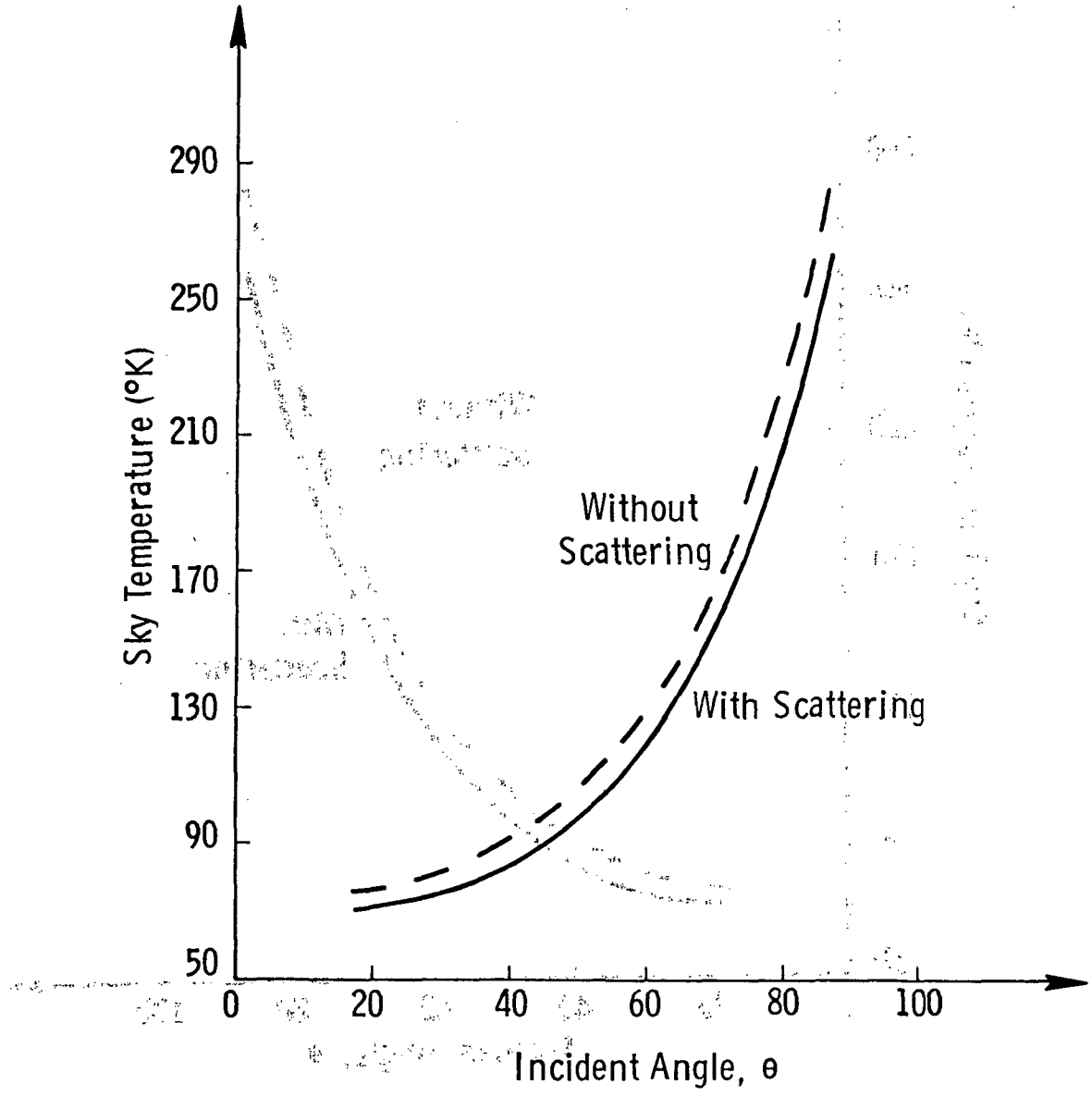

Figure 27. The Computed Sky Temperature for Vertical Polarization and a Precipitation Rate of 10 mm/hr.

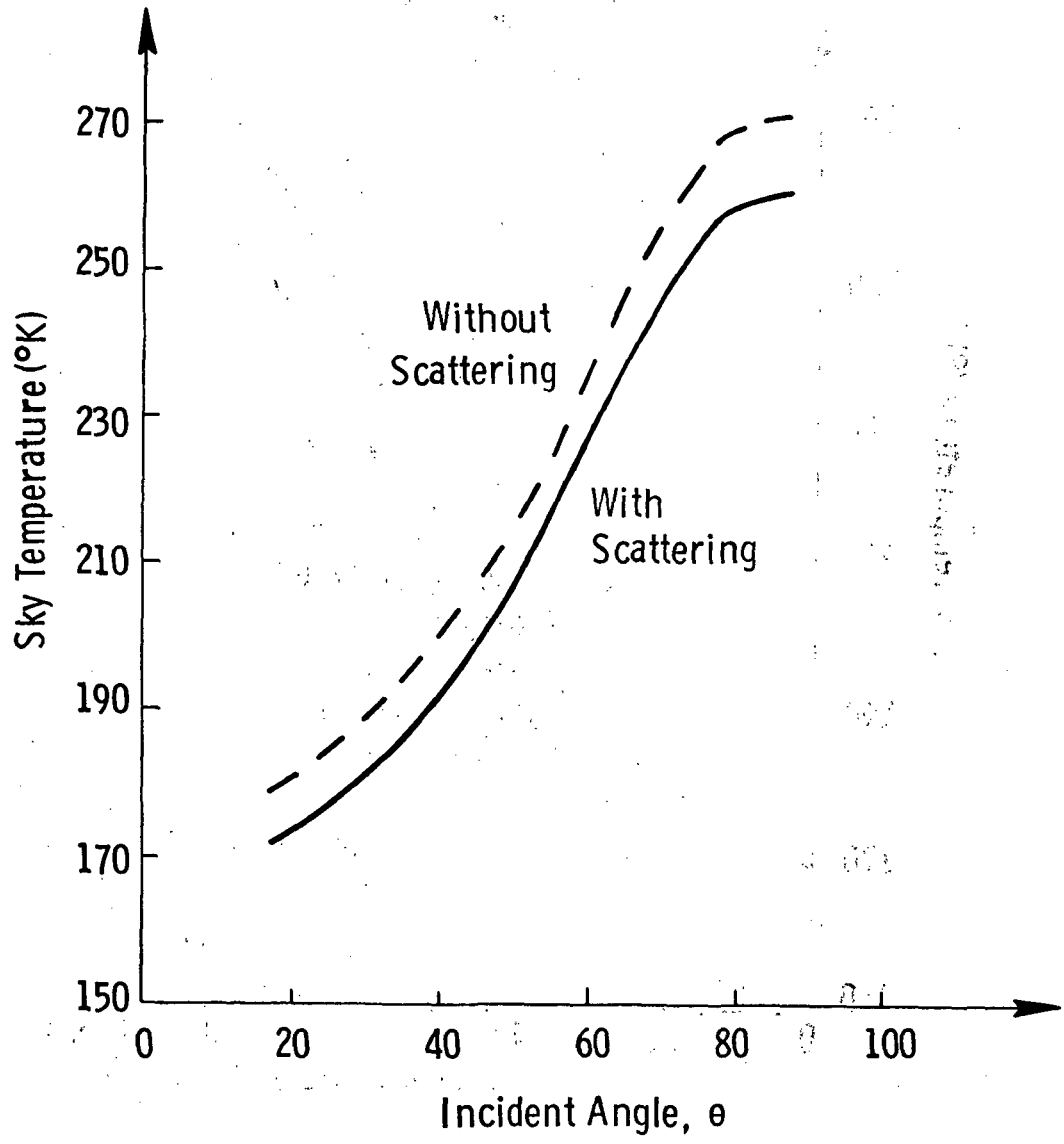

Figure 28. The Computed Sky Temperatures for Vertical Polarization and a Precipitation Rate of 30 mm/hr.

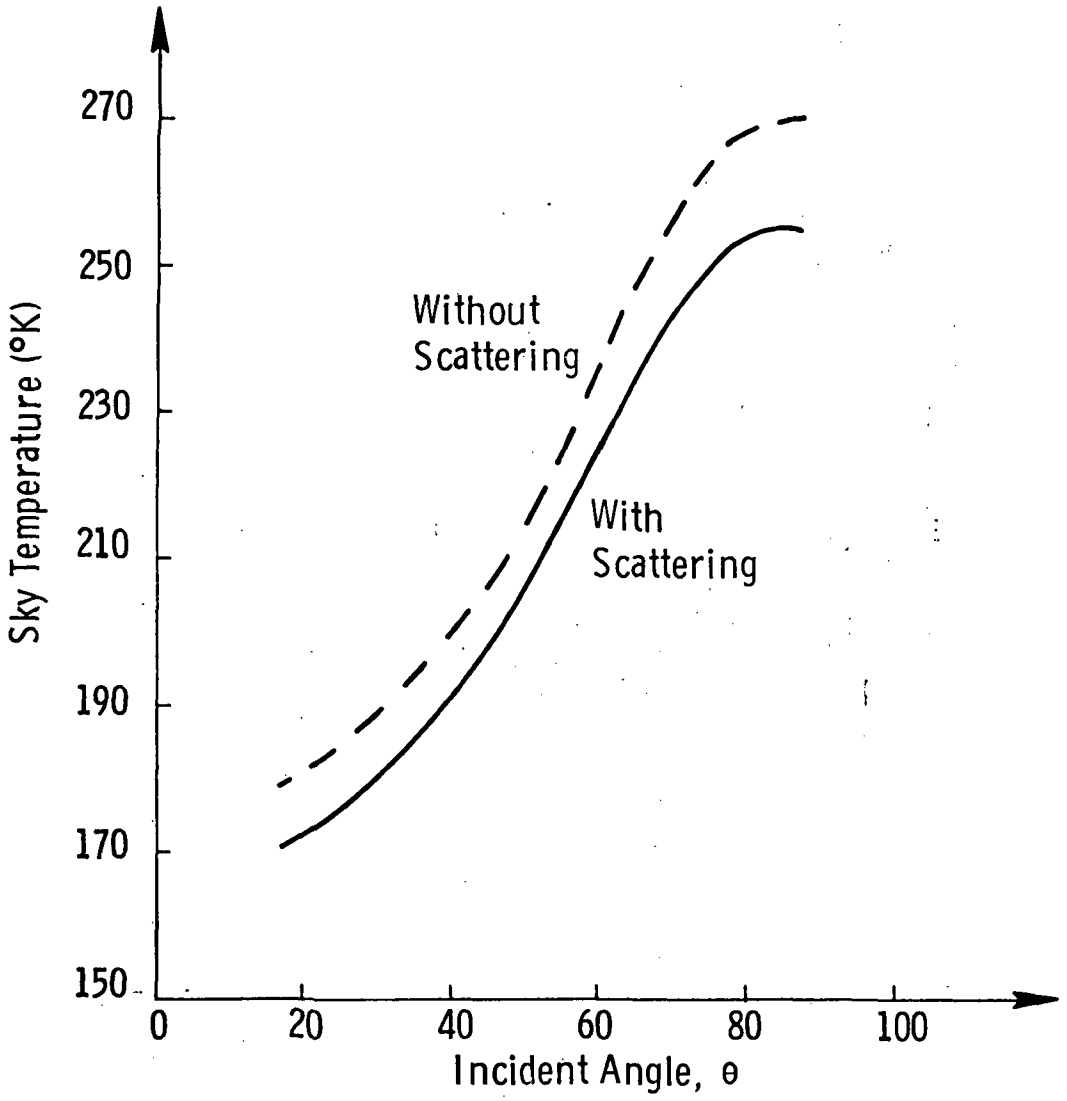

Figure 29. The Computed Sky Temperature for Horizontal Polarization and a Precipitation Rate of 30 mm/hr.

As a by-product of the theoretical investigation described earlier in this section, it was possible to correlate the excess temperature

$$\Delta T_j(\theta) = T_{aj}(\theta, \infty) - T_{bj}(\theta) \tag{35}$$

as caused by the atmosphere with atmospheric attenuation for various cloud and rain models. The results for three observation angles are shown in the graphs of Figures 30 through 32; the correlation is largely independent of view angle. Depending on view angle, excess temperature associated with rains lies to the right of that associated with clouds. This result may serve as a basis for identifying observations through rain. The correlation of attenuation with excess temperature depends somewhat on atmospheric structure, as shown (the points come from several atmospheric models). The variation from the mean curve is small enough, however, to verify clearly the postulated ability to determine attenuation from radiometric temperature.

A close examination of these results and those of Section V indicates a good potential that the excess temperature may be inferred from simultaneous scatterometric and radiometric observations. A combination of verified theoretical models and empirical models could be used to correct the scattering cross-section for attenuation in an iterative procedure. The technique is based on the ability to infer an estimate of the surface brightness temperature from the scatterometric data σ^o. This σ^o in turn implies a certain wind (although incorrect since an unknown attenuation has altered the measurement); associated with this wind speed is an estimated brightness temperature. The estimated brightness temperature and the measured apparent temperature are employed to estimate the excess temperature from which the attenuation is computed. The attenuation is then used to correct the measured σ^o. The process is then repeated until no improvement in the attenuation is observed. The technique is illustrated in the logic diagram of Figure 33. The convergence of the solution is assured since the error in σ^o attributable to attenuation is always one sided. This technique, however, must account for the small variation in σ^o associated with scatterometric measurements at different aspect angles with respect to the wind direction (squint). Correction of this nature may be possible in an operational system where the wind field is estimated on the basis of RADSCAT observations combined with scattered ship and shore reports also.

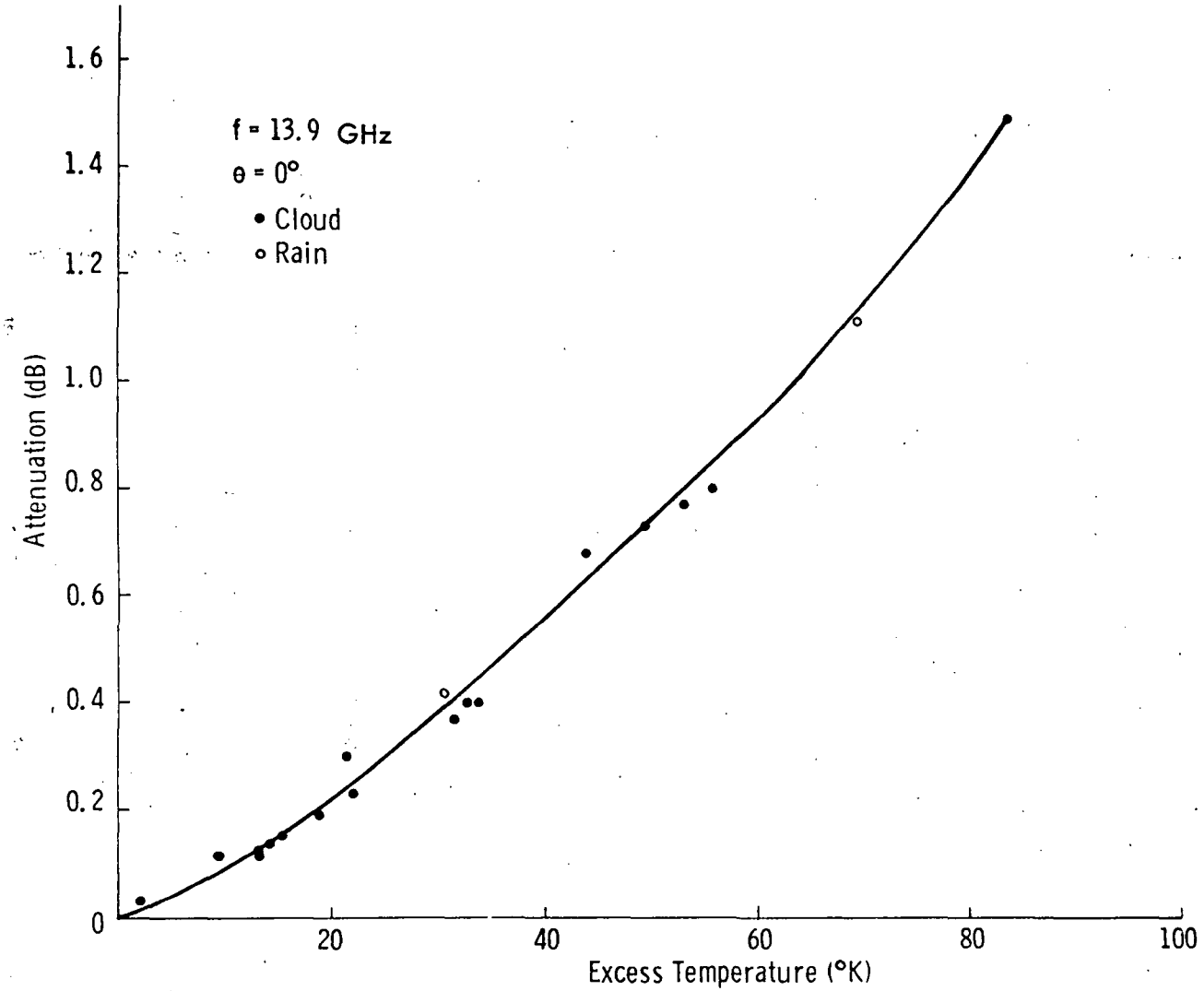

Figure 30. Attenuation as a Function of Excess Temperature for the Conditions Noted

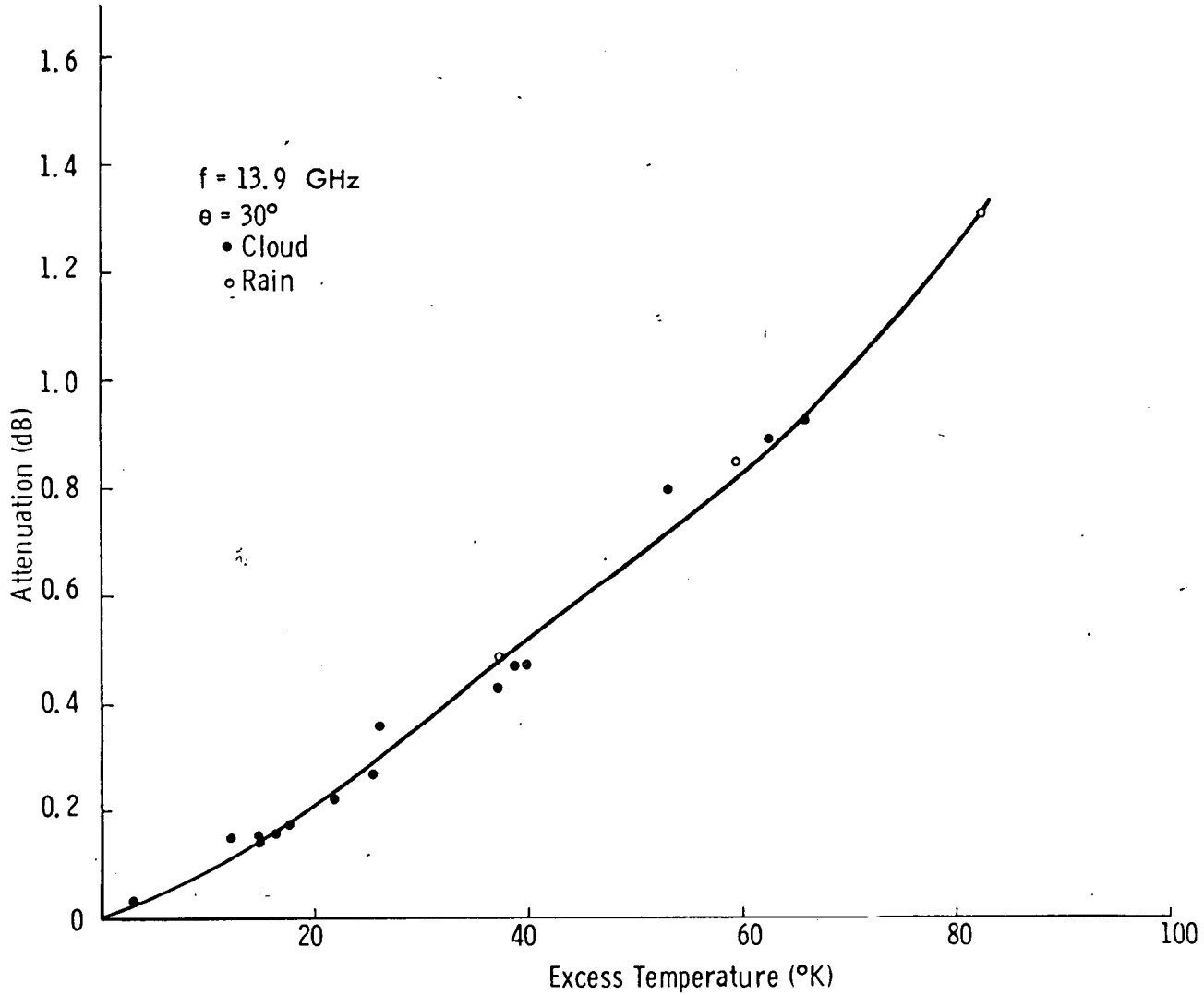

Figure 31. Attenuation as a Function of Excess Temperature for the Conditions Noted

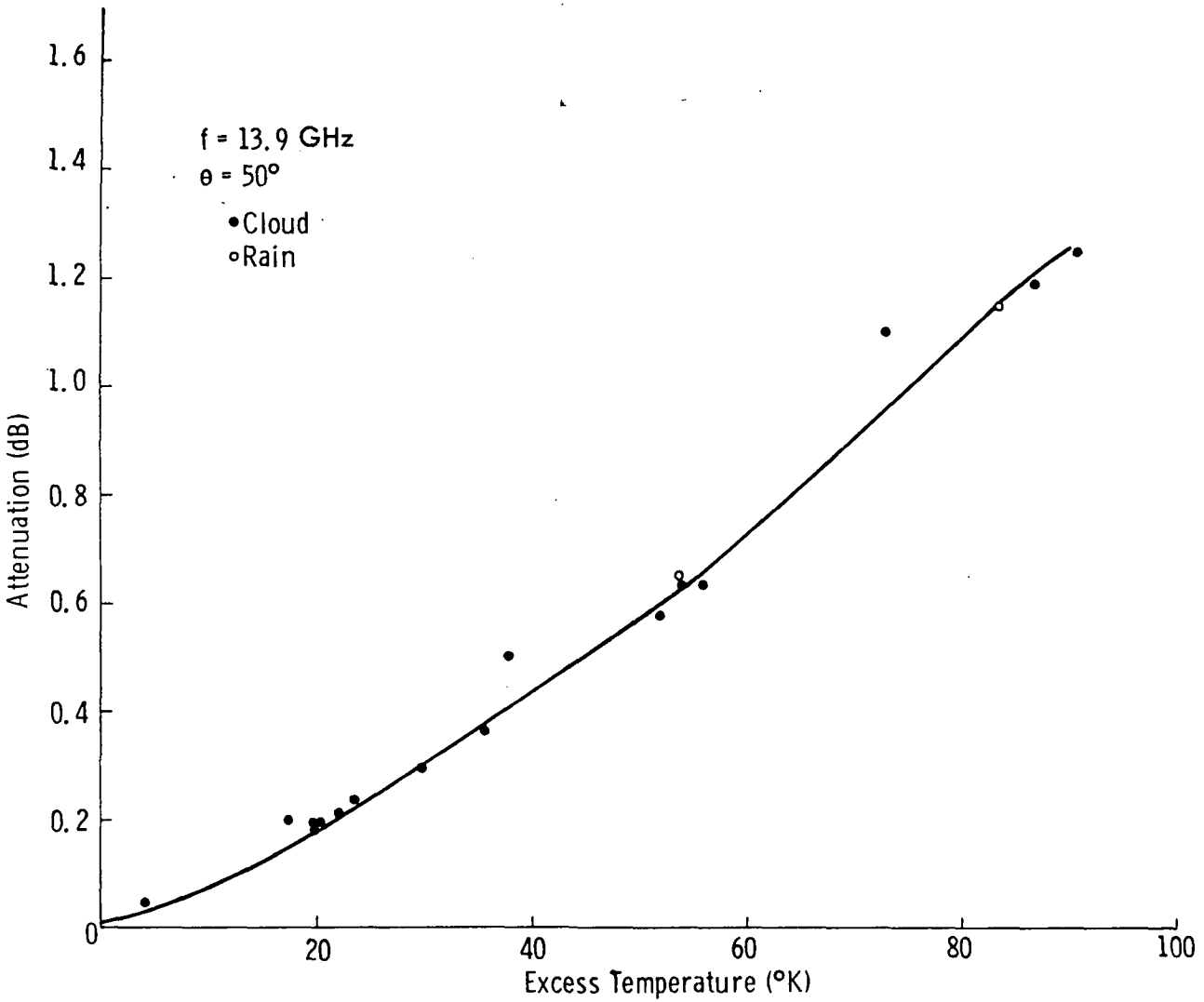

Figure 32. Attenuation as a Function of Excess Temperature for the Conditions Noted

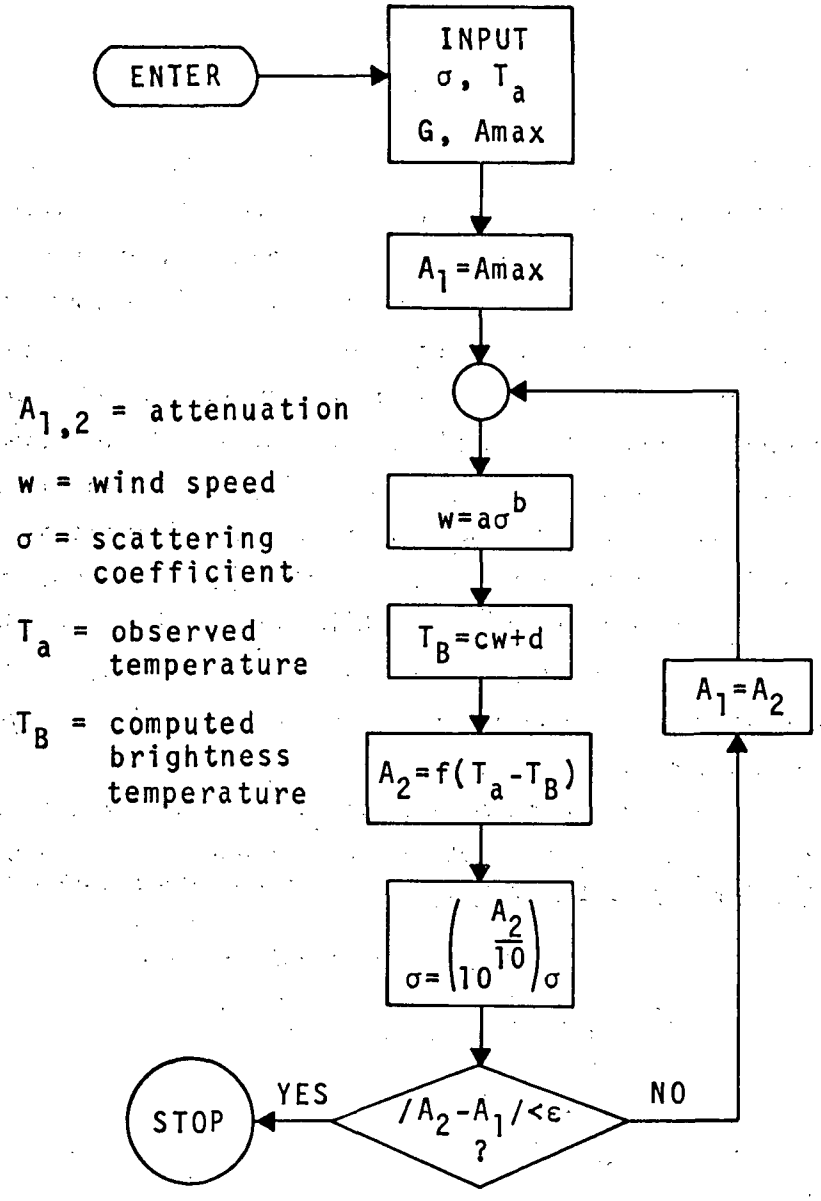

Figure 33. A Logic Diagram for Estimating Attenuation.

E. Recommendations

In view of the radiometric observations of the sea reported recently[6] and the theoretical fitting of these results as reported in Section VI, extension of the above efforts to include a realistic sea surface is warranted. These improved computations should include sensitivity studies to determine the response to clouds and rains having various temperature and pressure profiles. Meteorological profiles over Ship Hotel could be used and temperature and pressure profiles of recent cloud modeling investigations could also be considered. The above refined results could then be used for developing methods of extracting atmospheric attenuation from scatterometer-radiometer data. The accuracy of the various methods should be examined. Other techniques should also be sought. The insensitivity of vertical polarization emissivity to wind speed also should be considered when seeking other methods. In view of the good correlation between excess temperature and attenuation as a result of numerical studies, a better phenomenological model for the theoretical basis for this correlation should also be sought.

These refined results should also be examined for features definitive of rain and rainfall rate. This investigation would serve as an indication of the precipitation sensing capability of the composite sensor.

V. A THEORY FOR MICROWAVE EMISSIONS FROM THE SEA

A. Introduction

(1) Background

As described in Section II the microwave emission characteristic of the sea has been measured by several investigators. These investigators have compared their observations with predictions from geometric optics theory which uses a single surface model and found some but not satisfactory agreement between predictions and measurements. The wind dependence of the geometric optics approach was based on measured rms sea slope data reported by Cox and Munk.[37] However, the theory failed to predict the observed wind dependence at nadir and only loosely fitted the observed emission characteristic for nadir angles between 30 and 70 degrees. The failure of the simple geometric optics model to account for wind dependence at nadir was first reported by Nordberg, et al.,[8] and verified by Hollinger.[6]

(2) Objectives in Summary

In view of the above deficiencies an investigation was undertaken to seek a more adequate model for microwave emissions from the sea. The emphasis in this investigation was oriented toward using a composite surface scattering theory which better describes the roughness characteristic of the sea. The brightness temperature was, of course, computed from the bistatic scattering coefficient in the standard way (see Section IV). Since several lengthy numerical integrations are required to yield the emissivity, a more adequate model was sought among the simpler composite scattering theories. With this perspective a non-coherent scattering theory of the type described by Semyonov[38] was extended to yield the bistatic characteristic. An isotropic surface characteristic, although not realistic for the ocean surface was assumed. A justification for this assumption is based on the observed directional insensitivity of emissions from the sea.[39]

The composite theory yields a scattering coefficient consisting of a sum of two terms. One term reflects mainly the large structure contribution with an appropriate modification in the Fresnel reflection coefficient resulting from small

surface irregularities and is described by the geometric optics method. The second term reflects small structure contributions which are compensated for large structure tilting effects.

The wind dependence of the surface parameters in the composite model was introduced in accordance with rms slope data measured by Cox and Munk for the large undulations and Sutherland's results[40] for the small irregularities. The notable features of Sutherland's results are that the high frequency portion of the sea spectrum grows over a significant region of wind speeds and varies like K^{-4}, where K is the wave number of the sea waves. Details for the theory and the choice of surface parameters will be discussed in the Section V.B below.

Comparisons of the computed brightness temperature and backscatter characteristics at two different wind speeds were made with measured data and with predictions from a single surface model. The results are presented in Section V.C.

B. A Theory for Microwave Emissions from the Sea

The basic theory of surface brightness temperature was developed by Peake.[41] The relationship between the surface emissivity, the surface temperature and the brightness temperature is as follows:

$$T_{Bi}(\theta) = \epsilon_i(\theta)\, T_g \qquad i = h \text{ or } v \qquad (36)$$

where $T_{B_i}(\Theta)$ is the brightness temperature; $\epsilon_i(\Theta)$ the emissivity; T_g the surface temperature; h denotes horizontal polarization and v vertical polarization. Note that the azimuthal angle ϕ needed together with Θ to specify a direction has been chosen to be zero without loss of generality.

The connection between the emissivity and the bistatic scattering coefficient of the surface, $\gamma_i(\Theta, \Theta_s, \phi_s)$ is

$$\epsilon_i(\theta) = 1 - \frac{1}{4\pi} \int_0^{2\pi} \int_0^{\frac{\pi}{2}} \gamma_i(\theta, \theta_s, \varphi_s) \sin\theta_s \, d\theta_s \, d\varphi_s \qquad (37)$$

where Θ_s, ϕ_s are angles defining the direction of scatter corresponding to a wave incident at an angle Θ.

The basic formulation of the problem indicated above shows that the bistatic scattering coefficient is the quantity that defines the angular characteristics of the brightness temperature of a given surface. Consequently, different brightness temperature theories are also distinguished by the different models assumed for the bistatic scattering coefficient.

The bistatic scattering coefficient derived from a two-scale rough surface model with Gaussian surface height distribution and Gaussian surface correlation for both scales can be shown to be of the form[42]

$$\gamma_i(\theta, \theta_s, \varphi_s) = \gamma_i^o(\theta, \theta_s, \varphi_s) + \langle \gamma_i^1(\theta, \theta_s, \varphi_s) \rangle \tag{38}$$

$\gamma_i o(\Theta, \Theta_s, \phi_s)$ denotes the main contribution by the large undulations. For horizontal polarization

$$\gamma_h^o(\theta, \theta_s, \varphi_s) = \frac{2a_1^2 [\,|\langle R_h \rangle|^2 a_2^2 + |\langle R_v \rangle|^2 q_y^2\,]}{\cos\theta\, q_z^4\, m^2 (a_2^2 + q_y^2)} \cdot \exp\left[-(q_x^2 + q_y^2)/2m^2 q_z^2\right] \tag{39}$$

and for vertical polarization

$$\gamma_v^o(\theta, \theta_s, \varphi_s) = \frac{2a_1^2 [\,|\langle R_v \rangle|^2 a_2^2 + |\langle R_h \rangle|^2 q_y^2\,]}{\cos\theta\, q_z^4\, m^2 (a_2^2 + q_y^2)} \cdot \exp\left[-(q_x^2 + q_y^2)/2m^2 q_z^2\right] \tag{40}$$

where

$$|\langle R_i \rangle|^2 = |R_i|^2 \left\{1 - 4k^2\sigma_i^2 \exp\left[-\frac{\sin^2\Theta}{2}\right]\cos\Theta\right\} \tag{41}$$

R_i = Fresnel reflection coefficient of a plane surface

$\cos\Theta = (a_1/2)^{1/2}$

$a_1 = 1 + \cos\Theta\cos\Theta_s - \sin\Theta\sin\Theta_s\cos\phi_s$

$a_2 = \sin\Theta\cos\Theta_s + \cos\Theta\sin\Theta_s\cos\phi_s$

$q_x = \sin\Theta_s\cos\phi_s - \sin\Theta$

$q_y = \sin\Theta_s\sin\phi_s$

$q_z = \cos\Theta + \cos\Theta_s$

k = wave number

m = rms surface slope of the large undulations

σ_1^2, ℓ = variance and correlation length of the small irregularities, respectively.

$\langle \gamma_i^1(\Theta, \Theta_s, \phi_s) \rangle$ denotes the bistatic scattering coefficient of the small irregularities where the averaging occurs over the distribution of the surface normals of the large undulations. Specifically

$$\langle \gamma_i^1(\theta, \theta_s, \varphi_s) \rangle = \int_{-\frac{\pi}{2}}^{\frac{\pi}{2}} \int_{-\frac{\pi}{2}}^{\frac{\pi}{2}} \gamma_i^1(\theta', \varphi', \theta_s', \varphi_s') \, P(\theta_n, \varphi_n) \, d\theta_n \, d\varphi_n \qquad (42)$$

where

$P(\Theta_n, \phi_n)$ = surface slope distribution of the large undulations.

$$= \frac{1}{2\pi m^2} \exp\left[- \tan^2 \theta_n / 2m^2 \right] \qquad (43)$$

Θ_n, ϕ_n = tilting and rotating angles of the large undulations.

Also

$$\gamma_i^1(\theta', \varphi', \theta_s', \varphi_s') = 4 k^4 \sigma_i^2 \ell^2 \exp\left[-\left(\frac{\ell t}{2}\right)^2 \right] \left[|M_{ih}|^2 + |M_{iv}|^2 \right] \cdot \cos\theta' \cos^2\theta_s' \qquad (44)$$

$$t = k \left(\sin^2\theta' - 2 \sin\theta' \sin\theta_s' \cos(\varphi_s' - \varphi') + \sin^2\theta_s' \right)^{\frac{1}{2}}$$

$$M_{hh} = \frac{(\epsilon_r - 1) \cos(\varphi_s' - \varphi')}{(\cos\theta' + \sqrt{\epsilon_r - \sin^2\theta'})(\cos\theta_s' + \sqrt{\epsilon_r - \sin^2\theta'})}$$

$$M_{hv} = \frac{(\epsilon_r - 1) \sin(\varphi_s' - \varphi') \sqrt{\epsilon_r - \sin^2\theta_s'}}{(\cos\theta' + \sqrt{\epsilon_r - \sin^2\theta'})(\epsilon_r \cos\theta_s' + \sqrt{\epsilon_r - \sin^2\theta'})}$$

$$M_{vh} = \frac{(\epsilon_r - 1) \sin(\varphi_s' - \varphi') \sqrt{\epsilon_r - \sin^2\theta'}}{(\epsilon_r \cos\theta' + \sqrt{\epsilon_r - \sin^2\theta'})(\cos\theta_s' + \sqrt{\epsilon_r - \sin^2\theta_s'})}$$

$$M_{vv} = \frac{(\epsilon_r - 1) \left[\cos(\varphi_s' - \varphi') \sqrt{\epsilon_r \sin\theta'} \sqrt{\epsilon_r - \sin^2\theta_s'} - \epsilon_r \sin\theta' \sin\theta_s' \right]}{(\epsilon_r \cos\theta' + \sqrt{\epsilon_r - \sin^2\theta'})(\epsilon_r \cos_s' + \sqrt{\epsilon_r - \sin^2\theta_s'})}$$

ϵ_r = relative complex dielectric constant

$\Theta', \phi', \Theta_s', \phi_s'$ = local incident and scattered angles based on the large undulations, respectively

$$\cos\Theta' = \cos\Theta_n\cos\Theta + \sin\Theta_n\sin\Theta\cos\phi_n$$

$$\sin\phi' = -\sin\Theta\sin\phi_n(1 - \cos^2\Theta')^{-1/2}$$

$$\cos\Theta_s' = \cos\Theta_n\cos\Theta_s - \sin\Theta_n\sin\Theta_s\cos(\phi_s - \phi_n)$$

$$\sin\phi_s' = \sin\Theta_s\sin(\phi_s - \phi_n)(1 - \cos^2\Theta_s')^{-1/2}$$

The surface parameters appear in the above theory as the rms slope of the large structures m, the standard deviation of the small structures σ_1, and the correlation length of the small structures l. This scattering model can be adapted to predict sea returns by noting that the rms slope can be based on measurements by Cox and Munk[37] and by noting that the assumed Gaussian spectrum for the small irregularities can approximate the high frequency portion of the sea spectrum BK^{-4} where the Bragg scatter condition applies, i.e., $K = 2k\sin\Theta$. In view of the requirements of the composite surface theory it is reasonable to choose the oil slick sea measurements by Cox and Munk, since the small irregularities have been suppressed. The value of m is thus assigned. The value of kl was assigned so that the correct angular behavior of the Gaussian spectrum approximated BK^{-4} well over the angular range, $30^\circ \leq \Theta \leq 70^\circ$, i.e., BK^{-4} was approximated by $(\sigma_1 l)^2/\pi \exp[-(Kl/2)^2]$ where $K = 2k\sin\Theta$, the Bragg scatter condition. This was achieved by noting that when $kl = 2$ similar behavior was realized. This is demonstrated in the graph of Figure 34. The factor 35.3 appears in the Gaussian approximation to bring the levels into agreement at 60 degrees. The value of B must yet be assigned.

Oceanographic investigations indicate values of B in the range from 4.6×10^{-3} to 3.26×10^{-2}. [37,43,44] This implies that $k\sigma_1$ should lie in the range from 0.084 to 0.24 when BK^{-4} is equated to $(\sigma_1 l)^2/\pi \exp[-(Kl/2)^2]$ at 60 degrees. These values of $k\sigma_1$ are consistent with the assumptions of the small perturbation theory, an encouraging result.

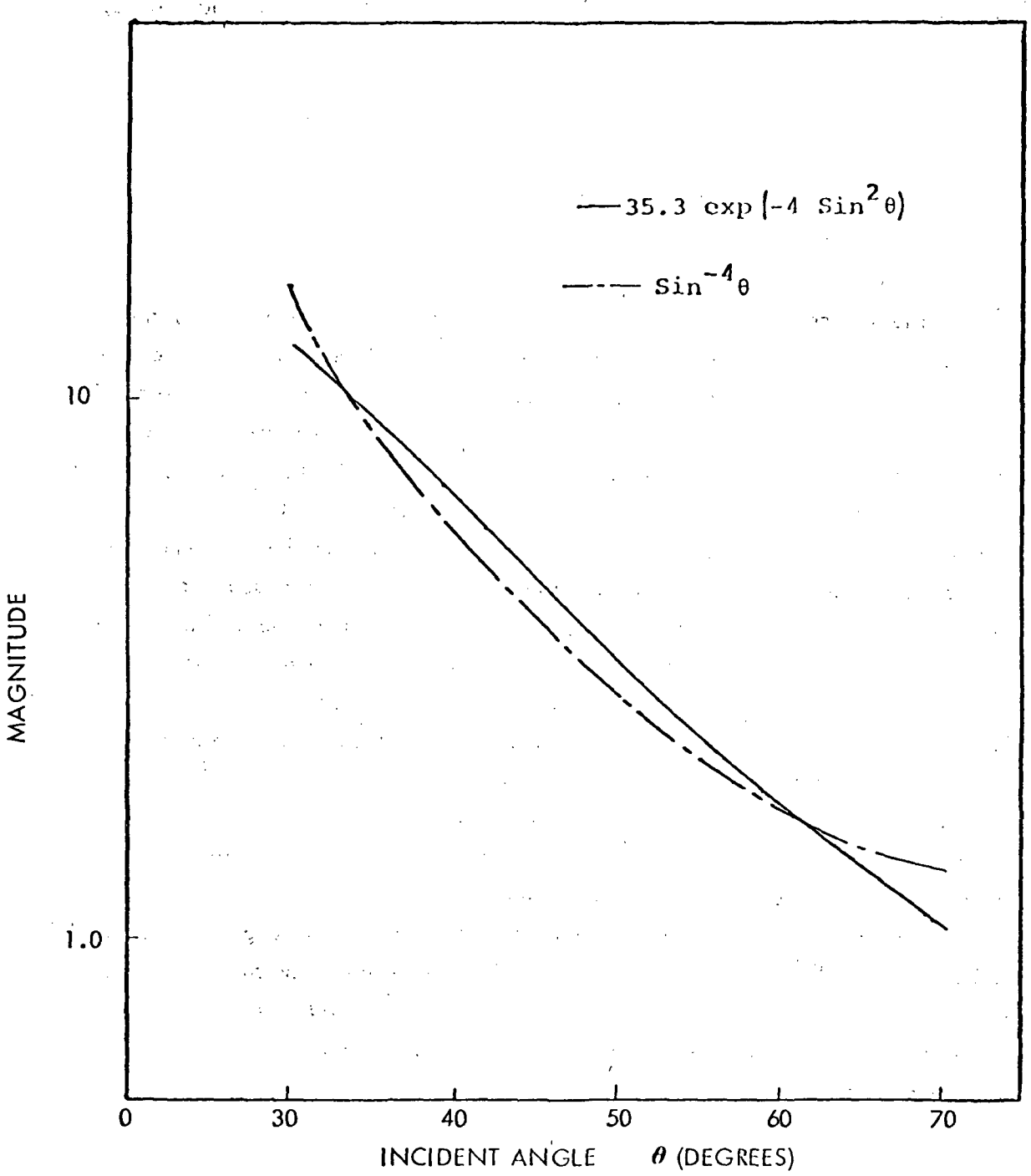

Figure 34. Comparison of the Angular Variations of $Sin^{-4}\theta$ and $35.3\exp(-4Sin^2\theta)$

C. Presentation and Discussion of the Results

As indicated in the previous section (V.B), the surface parameter m can be based on results reported by Cox and Munk and l can be estimated by bringing BK^{-4} into approximate agreement with the Gaussian spectrum over the domain of K where the Bragg scatter condition applies. The wind dependence in this model, however, not only enters through the factor m but also through the factor $k\sigma_1$. B which is known to be wind dependent[40, 45] can be related to $k\sigma_1$. However, at this writing the wind dependence of B is not yet available. To circumvent this lack of information it was noted that the horizontally polarized emission characteristic for nadir angles about 30° is very sensitive to $k\sigma_1$. So in the interim, the parameter $k\sigma_1$ can be estimated by fitting the predicted emission characteristics to the measured characteristics for large nadir angles.* With $k\sigma_1$ established in this manner, the backscatter characteristic may also be computed and compared with reported measurements.

The parameter $k\sigma_1$ was estimated from horizontally polarized emission characteristics at 8.36 GHz associated with two distinct wind speeds. The emission characteristics were based on an average of several of Hollinger's experiment runs** under similar wind stress conditions.*** The vertically polarized emission characteristic was then computed from the estimated $k\sigma_1$. These results are shown in the graphs of Figures 35 and 36. The dielectric constant was based on data reported by Saxton and Lane.[24]

Comparison of the predictions of this emission model indicates a significantly improved agreement over that predicted by a single surface model. Better level and trend agreement is evident for both horizontally and vertically polarized emissions. Sensitivity to wind speed is evident at nadir which was not noted with the single surface model. The sensitivity at nadir is carried by the modified Fresnel coefficient (see Equation 41).

---

*It appears that the wind sensitivity of B may be assigned by this technique. However, this is left as future effort.

**The authors are indebted to Dr. J. P. Hollinger of NRL for making his radiometric measurements available to us.

***The authors are also grateful to Dr. V. J. Cardone of NYU for interpreting Hollinger's wind speed measurements under comparable wind stress conditions.[10]

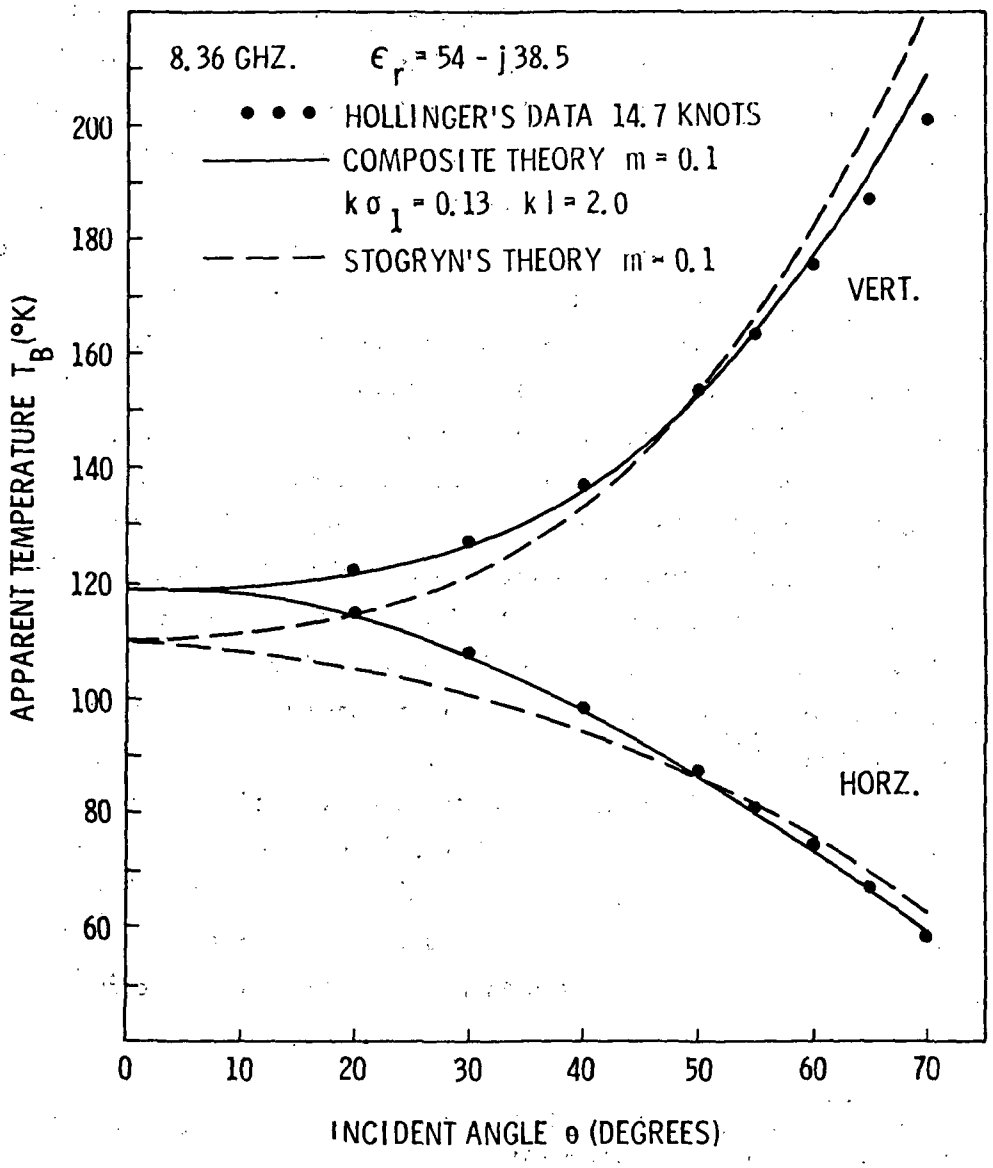

Figure 35. Comparison of Computed and Measured Emission Characteristics for Horizontal Polarization.

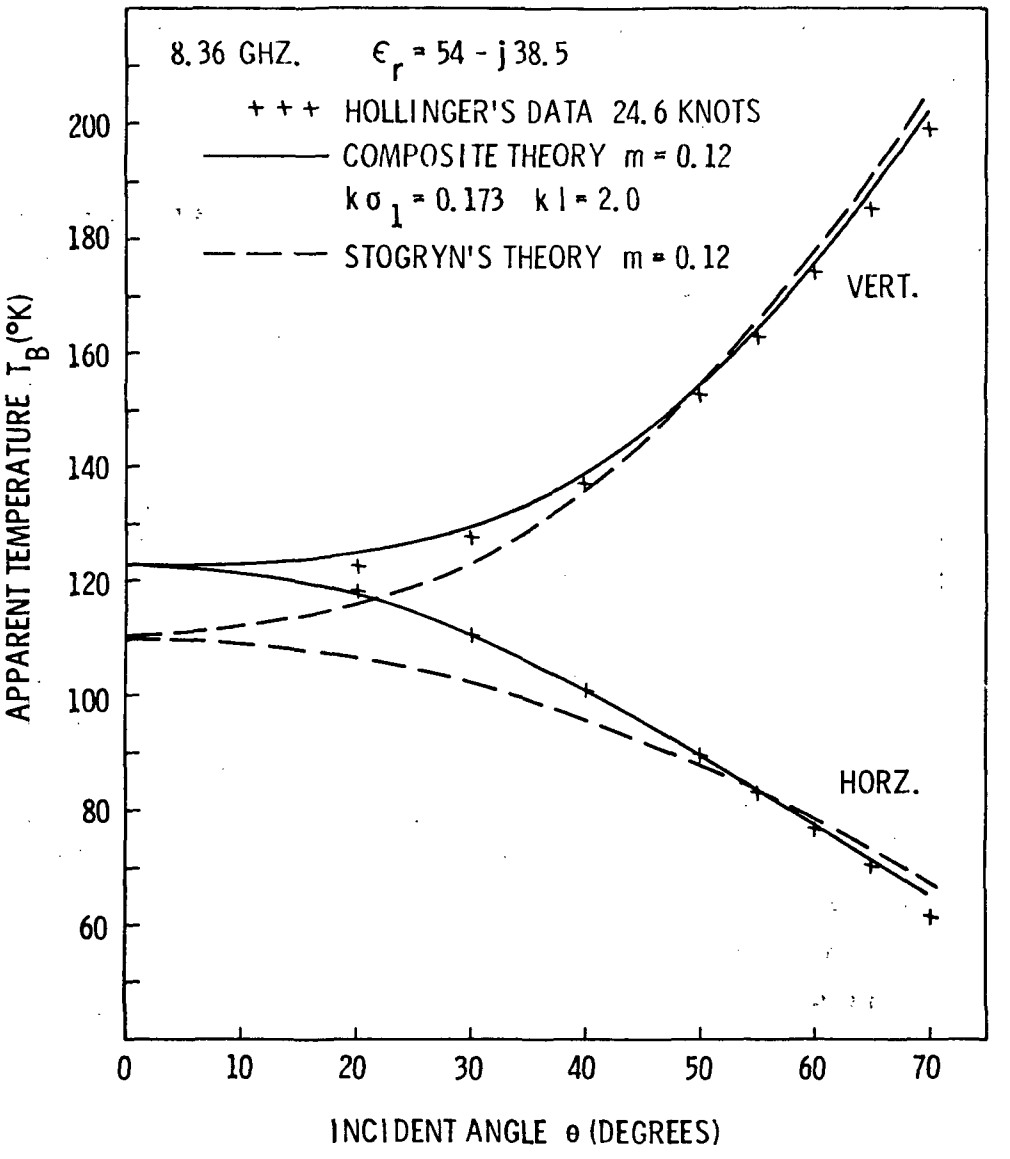

Figure 36. Comparison of Computed and Measured Emission Characteristics for Vertical Polarization.

The adequacy of the composite surface theory is further demonstrated when the predicted backscatter characteristics are compared with measured characteristics. Data at 8.91 GHz reported by Daley, et al.*,[46] at similar wind stress conditions were chosen as a basis for comparison. The dielectric constant was changed to reflect the influence of the slightly different frequency. The comparison of predicted and measured characteristics are shown in Figures 37 through 40. These results indicate reasonable agreement with measurements and improved agreement over the predictions of the simple geometric optics approach (single surface model). It is noted that the best agreement with measurements occurs primarily at larger angles and for vertical polarization. There is some uncertainty in the accuracy of the measurements near nadir[46] so lack of agreement may be anticipated there. The discrepancy at large angles for horizontally polarized cross sections may be attributable to receiver noise at these small cross sections. This statement is, however, speculative.

In the above composite theory, the same set of parameters (m, σ_1, l) has been employed at a given wind speed to predict both the scattering and the emission characteristics for both polarizations (see Figures 35 through 40). Much improved agreement with measured results (especially the scatterometric measurements) over a single surface theory indicates that the sea surface is better modeled by a composite rather than a single surface. It also indicates that the adequacy of a scattering model is best exemplified when it is used to predict both the scattering and the emission characteristics.

The level of NRL data which are based on the statistical median had to be raised by 6 dB to realize the agreement. Valenzuela[47] indicated that the average cross section was about 4.6 dB above the median based on exponential statistics assumed for the returns. As a consequence, 1.4 dB remains unaccounted for. Perhaps the remaining 1.4 dB may be partially associated with the biases disclosed by Claassen and Fung.[4]

*The authors are indebted to Mr. N. W. Guinard of NRL for making these backscatter data available to us.

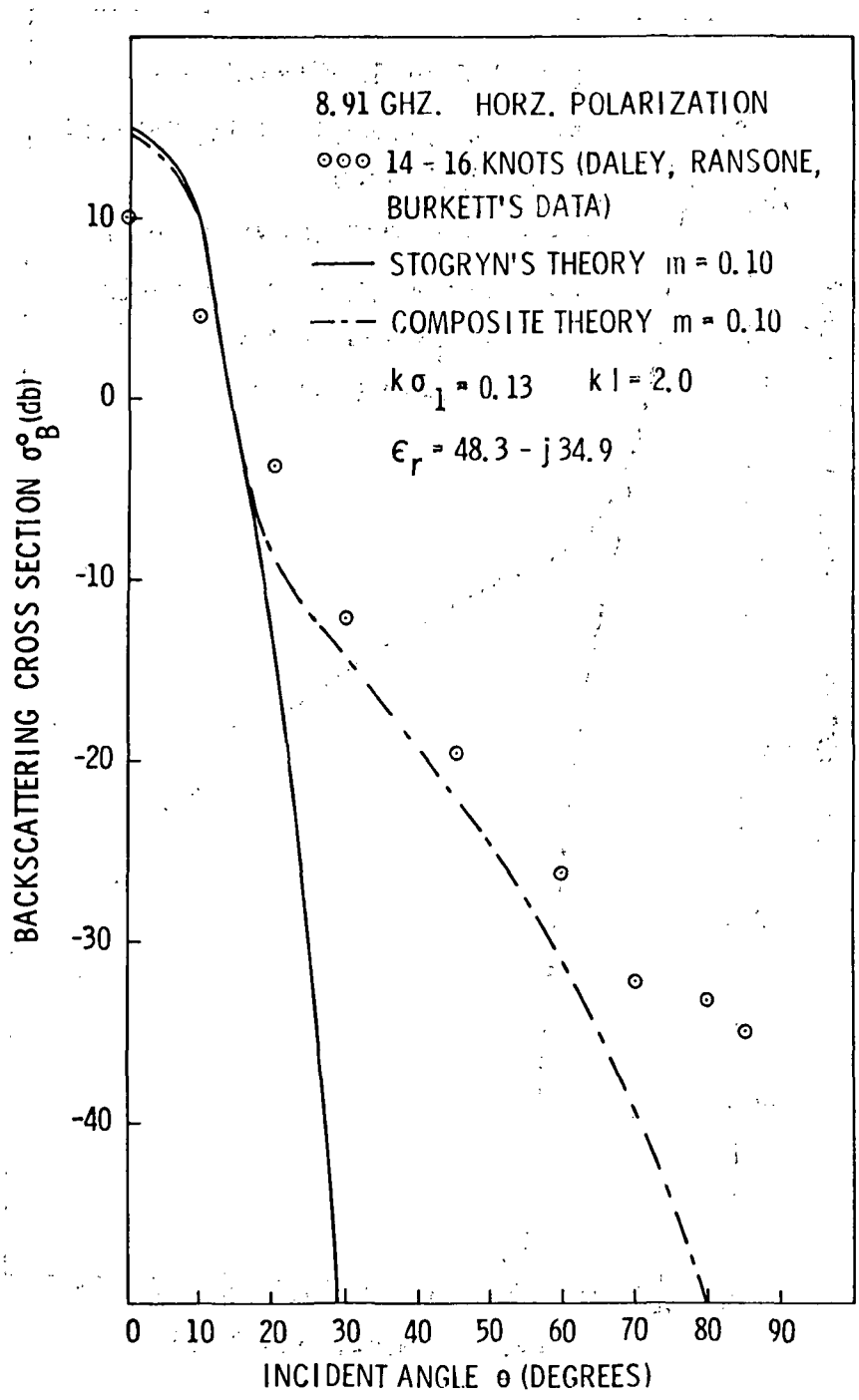

Figure 37. Comparison of Computed and Measured Backscatter Characteristics.

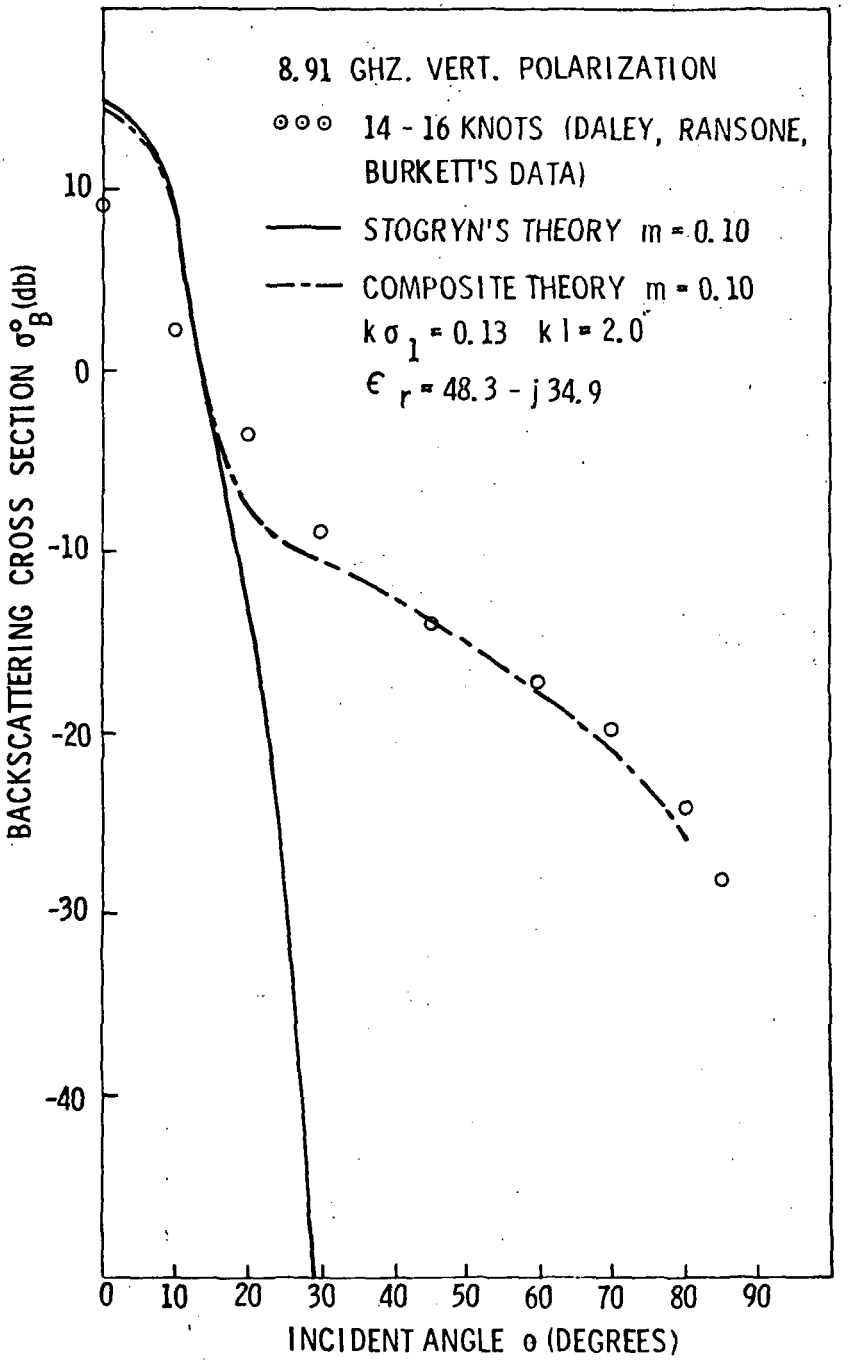

Figure 38. Comparison of Computed and Measured Backscatter Characteristics.

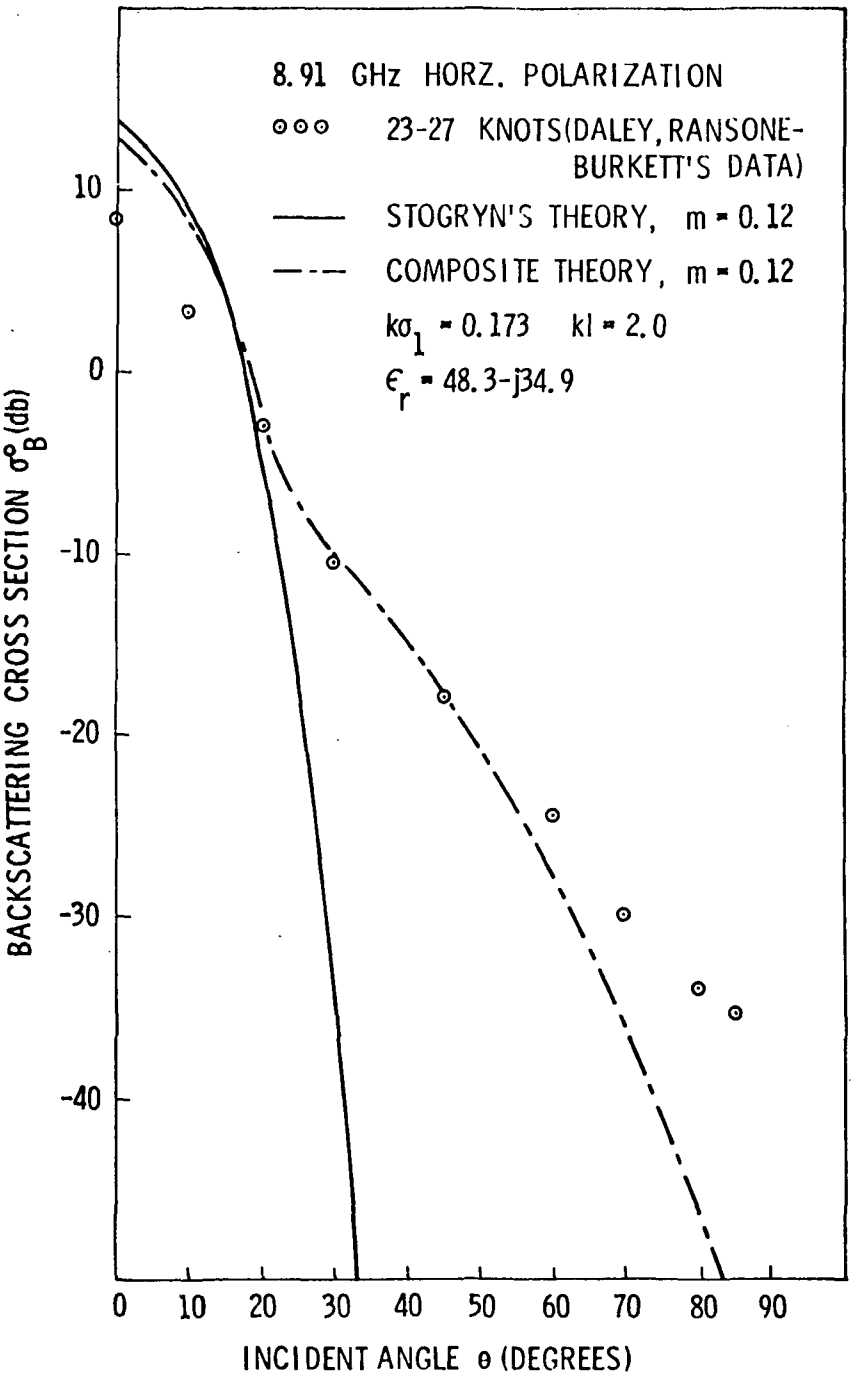

Figure 39. Comparison of Computed and Measured Backscatter Characteristics.

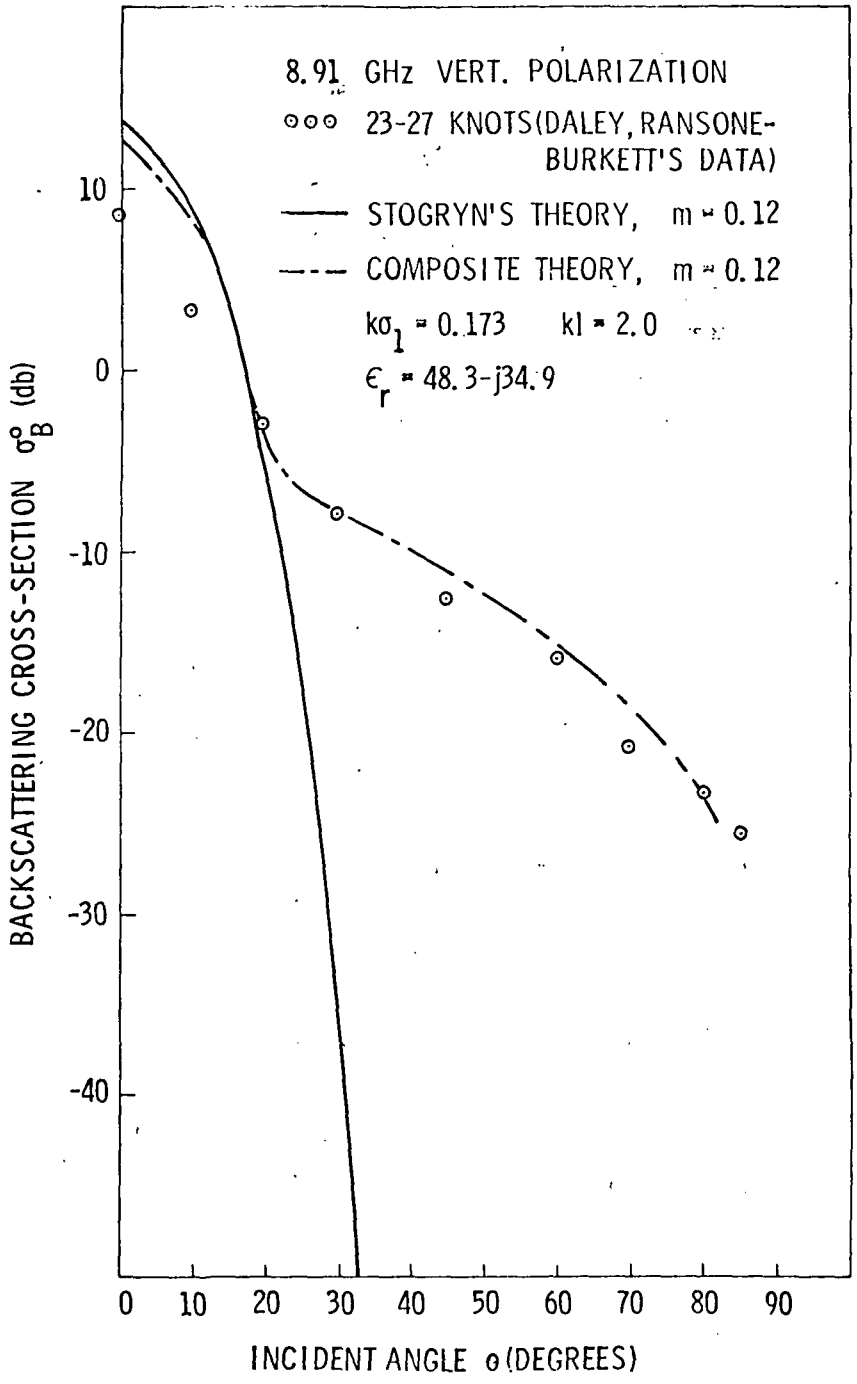

Figure 40. Comparison of Computed and Measured Backscatter Characteristics.

D. Recommendations

The simplified composite model was shown to predict scatterometric and radiometric responses of the sea with reasonable accuracy. The use of an isotropic surface model, however, has completely ignored the anisotropic characteristics of the sea surface. The cross wind response, for instance, cannot be distinguished from that of the upwind. Also, the evaluation of the scattering integral by the stationary phase approximation results in a wind speed dependence of the large undulations only through the rms slope of the large structures and not the specific shape of the surface spectrum. It remains to be seen as to whether or not such a simplification is acceptable. Future efforts should, therefore, be directed towards developing a two dimensional sea scatter theory which employs the two dimensional sea spectrum proposed by oceanographers. Complete anisotropic characteristics of the sea surface as well as the wind dependence of sea surface should be embodied in such an approach. This approach may, however, be too involved for microwave emission theory due to the many lengthy numerical integrations required for a number of multiple integrals, but is certainly feasible for radar sea scatter with the present computer capabilities (see reference [62] for a composite theory based on an anisotropic surface).

VI. BACKSCATTER THEORY FOR A COMPOSITE SURFACE WITH APPLICATION TO SEA RETURNS

A. Background

Many theories have been developed for predicting radar returns from the sea surface during the last two decades. The theoretical models treated varied rather widely but in general four different types of models may be identified, namely, (1) a slightly rough surface,[48,49,50] (2) a surface made up of a collection of randomly oriented facets,[51,52] (3) a smoothly undulating surface,[48,53] and (4) a two-scale composite surface consisting of small irregularities superimposed upon large, gentle undulations.[54,55,56,57,58] In the past most theories were concerned with predicting returns either close to the vertical[52,53,59] or away from the vertical,[50,51] but not both. They all fall under categories (1) to (3). More recently two-scale models have been proposed to account for the radar returns over the entire angular range. It is generally believed that such models may serve as a good approximation to the true sea surface (in so far as predicting the return signal is concerned) so that some practically useful results can be derived.

As a justification for the two-scale model, it has been observed experimentally[60] that the polarization dependence is small for small incident angles (less than about 30°). This suggests a quasi-specular type return which is typical for structures at least several wavelengths in size. It has also been observed that at larger incident angles vertically polarized returns are in general significantly higher than the horizontally polarized returns. This indicates that structures of the order of the incident wavelength or less are effective.[51,56] Consequently, the two-scale model appears to be a very reasonable model for sea scatter. Another significant point about the two scale theory is that it predicts greater wind speed dependence for large incident angles, especially for horizontal polarization. This follows from the fact that the larger the incident angle the greater is the enhancement of the return signal from the small structures by the large undulations. Such an indication is again confirmed by available experimental data (see Figures 2 through 5). On the other hand if a single surface theory is used, say, the perturbation theory, then the wind speed dependence would be uniform for all incident

angles where the theory is applicable.[40] This again indicates that a two-scale model is needed to account for sea scatter.

The general two-scale model applied to sea scatter is typified by a large undulating surface on which small irregularities are superimposed. More specifically two types of composite surface models may be identified: (1) the large undulations are larger in dimension than the illuminated area and thus within the beam of illumination the surface appears as a tilted perturbed plane and (2) the illuminated area contains at least several large undulations. For model (1) the problem remains essentially the same as a small perturbation problem since the effect of any tilt can be accounted for by a change in the angle of incidence and by resolving the incident plane wave into horizontally and vertically polarized components. Such a simple treatment is not possible for model (2) for which two different approaches are in existence: (1) the "non-coherent" assumption method[38] and (2) the "coherent" approach (where the non-coherent assumption is not made).[61,62]

In the past, most studies were restricted to either a one-dimensional sea model or an isotropic sea model. It is well known that the wind induces a non-isotropic characteristic in the surface. As a consequence a realistic treatment of sea returns should consider the two-dimensional character of the sea. Thus, studies to date are capable of providing at most an estimate of sea return for some specific cases. To obtain a more satisfactory theory for sea scatter it is necessary that the theory (1) handle at least two scales of roughness, (2) be general enough for a two-dimensional non-isotropic surface, and (3) incorporate an adequate two-dimensional sea model. A theory which achieves the first two objectives has been developed and is described in detail elsewhere.[62] A simplified version of this theory is presented in Section VI.B below. Section VI.C describes the results of this simplified theory when applied to sea returns.

B. A Scattering Theory for A Composite Rough Surface

A backscatter theory for a two-scale rough surface has been developed for a two-dimensional, non-isotropic surface without using the non-coherent assumption. The approach reduces the composite surface problem to a single surface problem by applying the concept of the equivalent surface field. This can be achieved by

modifying the surface fields on the large undulations Z(x,y) to include the effects of the small irregularities s(x,y). Once this equivalent surface field is obtained, the Stratton-Chu integral may be employed to calculate the far zone scattered field. It can be shown that the backscattering cross section, σ_{pp}, obtained by this technique may be expressed as a sum of two terms, i.e.,

$$\sigma_{pp} = \sigma_{1pp} + \sigma_{2pp} \tag{45}$$

where σ_{1pp} is identical with that obtained by the classical Kirchhoff's method.* σ_{2pp} is a term that represents the interaction between the larger undulations and the small irregularities. It vanishes, if the small irregularities are absent. On the other hand, if the larger undulations should be absent, σ_{2pp} will reduce to the small perturbation results.

Completely general results for σ_{pp} have been derived for a two-dimensional anisotropic composite surface. Expressions for both the horizontally and the vertically polarized scattering cross-sections were developed. The derivation of these very complicated expressions may be found in reference.[62] To assess the capabilities of this new composite theory the general results were reduced under the assumptions that the rough surface was isotropic and had a Gaussian height distribution for both scales of roughness. In addition the autocorrelations of the two types of roughness were assumed to be Gaussian. Under these assumptions the general expressions for either polarization (pp = hh or vv) reduce to

$$\sigma_{1pp} = \frac{1}{2}\left(4m^2\cos^2\theta\right)^{-1} \left|A_{pp} + B_{pp}\tan\theta\right|^2 \exp\left[-\tan^2\theta/2m^2\right] \tag{46}$$

and

$$\sigma_{2pp} = \pi k^2 \sigma_1^2 \iint \left\{ \left|C'_{pp} + G D'_{pp}\right|^2 W + \right.$$
$$\left. \mathrm{Re}\left[\left(C'_{pp} + G D'_{pp}\right) C_{pp}^{*} G\right] V_z \frac{dW}{dq} \right\} V_z^{-2} m^{-2} \cdot$$
$$\exp\left\{-\left[(u + k\sin\theta)^2 + v^2\right]/2 V_z^2 m^2\right\} du\, dv \tag{47}$$

*An equivalent reflection coefficient as discussed by Rice should really be used in place of the Fresnel reflection coefficients. Such a correction, however, is minor for the entire cross section.

where Re means "the real part of" and

$$m^2 = \sigma^2 \, | \rho''(0) |$$

$$q = u - k \sin\theta$$

$$v_z = 2k \cos\theta$$

$$G = (u + k \sin\theta) / V_z$$

$$W = W(\sqrt{q^2 + v^2})$$

$$T_p = 1 + R_p$$

$$R_p = \begin{cases} R_\perp \text{ for horizontal polarization} \\ R_\parallel \text{ for vertical polarization} \end{cases}$$

R'_p = derivative of T_p with respect to Z_x

Θ = angle of incidence

In particular, for horizontal polarization it is required that

$$A_{hh} = 2 R_\perp \cos\theta$$

$$B_{hh} = 2 (R_\perp \sin\theta + R'_\perp \cos\theta)$$

$$C'_{hh} = T_\perp C_{hh}$$

$$D'_{hh} = T_\perp D_{hh} + R'_\perp C_{hh} \qquad (48)$$

$$C_{hh} = Q[u^2(b-c)/k + kc + (u^2+bc)\cos\theta]$$

$$D_{hh} = Q(u^2+bc)\sin\theta$$

$$\theta = (k'^2 - k^2)[2\pi(k^2 c + k'^2 b)]^{-1}$$

Whereas for vertical polarization it is required that

$$A_{vv} = -2 R_\parallel \cos\theta$$

$$B_{vv} = -2(R_\parallel \sin\theta + R_\parallel \cos\theta)$$

$$C'_{vv} = T_{\parallel} C_{vv}$$

$$D'_{vv} = T_{\parallel} D_{vv} + R'_{\parallel} C_{vv} \qquad (49)$$

$$C_{vv} = Q\{[u(b + k\cos\theta)]\sin\theta + [\cos(v^2c - v^2b - ck^2) - k(v^2 + bc)]\cos\varphi/k'\}$$

$$D_{vv} = Q\{\sin\theta[ku\sin\theta + (v^2c - v^2b - ck^2)\cos\varphi/k'] + k^2\sin\theta\cos\theta[\cos\theta(v^2c - v^2b - ck^2) - k(v^2 + bc)]/k'^3\cos\varphi - u\cos\theta(b + k\cos\theta)\}$$

In the above expressions σ_1^2 and σ^2 are the variances of the small irregularities $s(x,y)$ and the large undulations $Z(x,y)$, respectively; ρ is the correlation coefficient of $Z(x,y)$; $W(K) = \ell^2/2 \exp[-(K\ell/2)^2]$ is the roughness spectrum of $s(x,y)$ related to its correlation coefficient by the Bessel transform; is the correlation length of the surface, $s(x,y)$; $\rho''(0)$ is the second derivative of ρ evaluated at zero.

This simplified scattering model was adapted to predict sea returns in the same manner as described in Sections V.B and V.C where m was determined from slick sea rms slope data and σ_1 from measured horizontally polarized emissions.

C. Presentation and Discussion of the Results

(1) Comparison with Experimental Results

The surface parameters were chosen by the method discussed in Sections V.B and V.C and the backscatter characteristics at 8.91 GHz and 1.228 GHz were computed on this basis for two different wind speeds. These results were then compared with the backscatter data reported by Daley, et al.,[46] from JOSS I mission. (see Figures 41 through 48). The scattering characteristics at L band were based on the same parameters as used for X-band predictions. JOSS I data were raised 6 dB to be consistent with level adjustments used in Section V. Reasonable agreement is observed in trend over all angles. See Section II.B and V.C for a discussion on the discrepancies in the level. It is noted that the value $k\sigma_1$ increases with increasing wind speeds. This observation is in agreement with recent observations of the sea spectrum.[40,63]

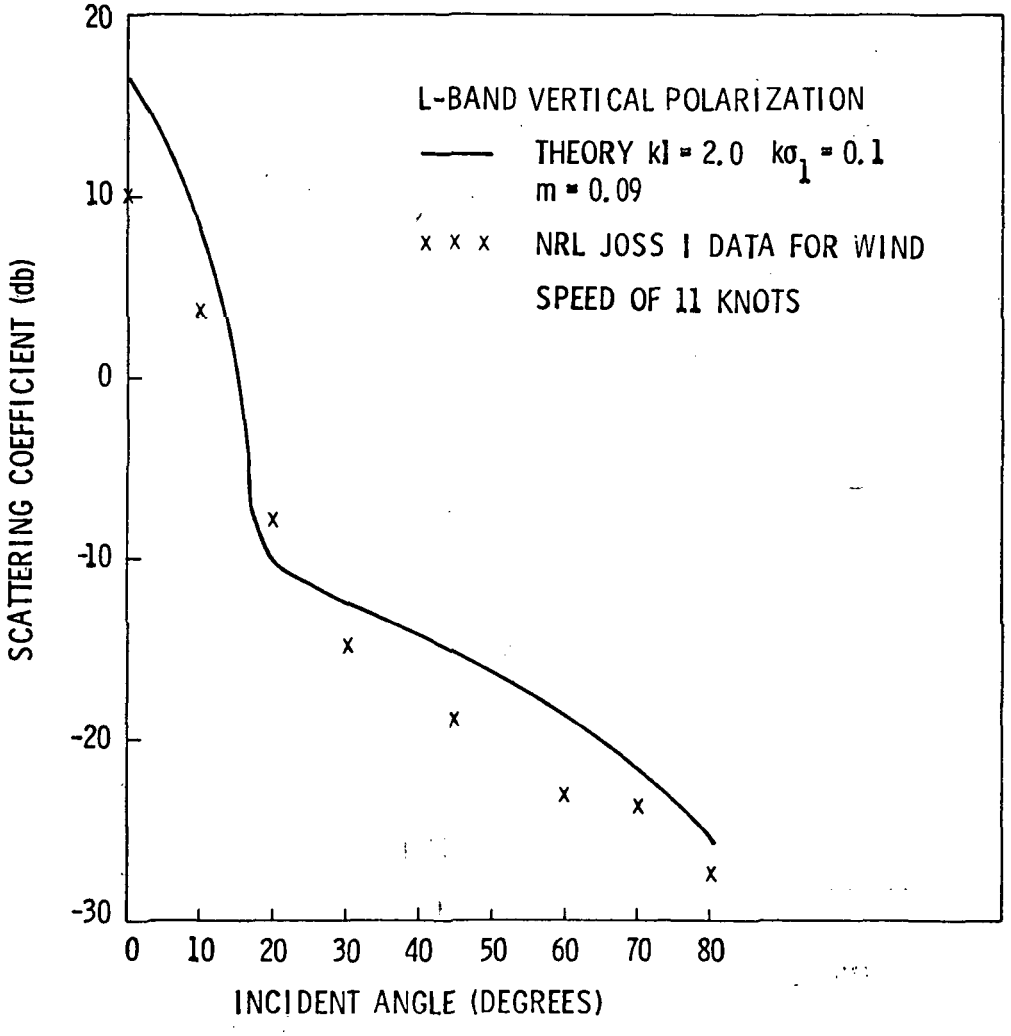

Figure 41. Comparison of Computed and Measured Backscatter Characteristics.

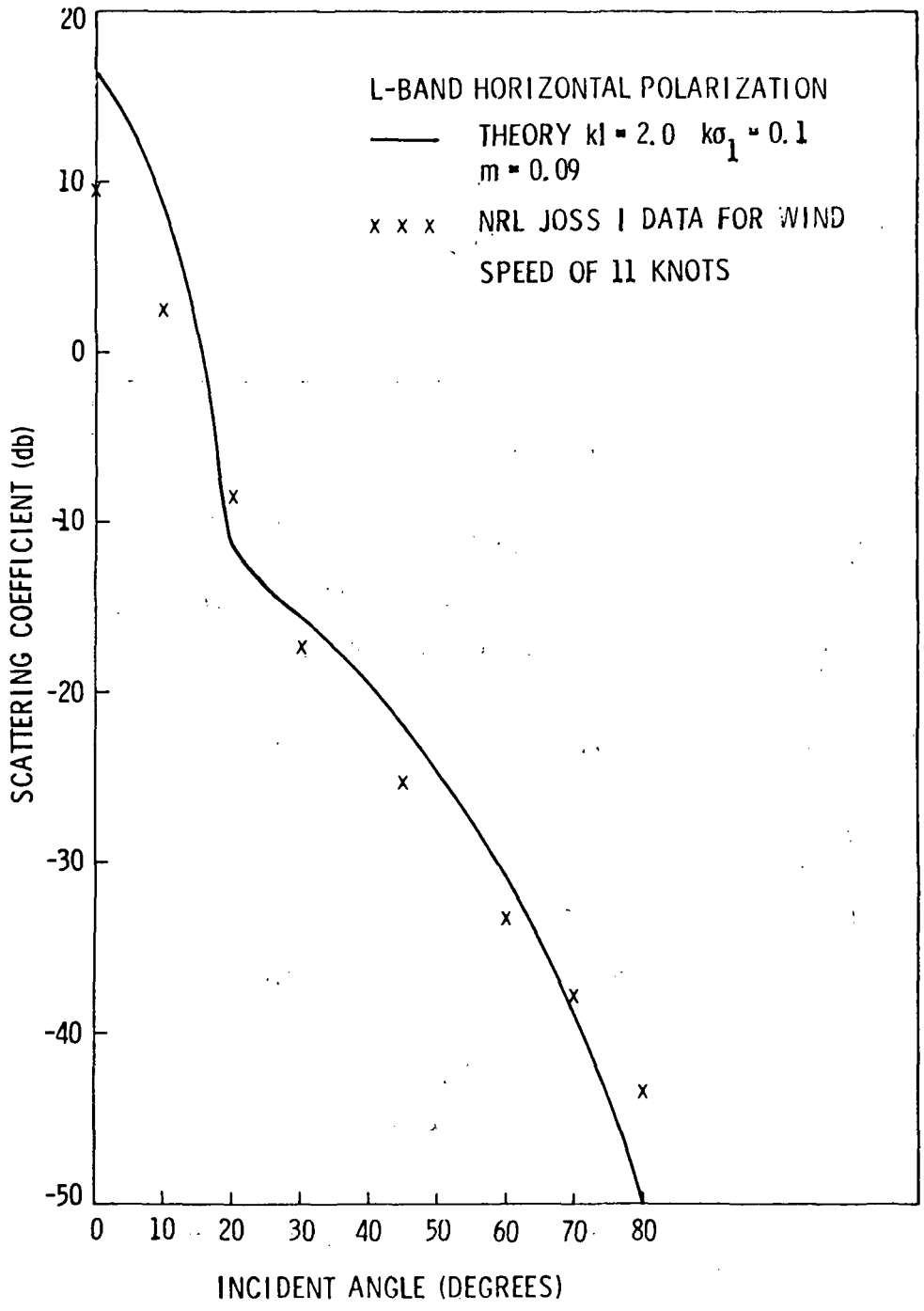

Figure 42. Comparison of Computed and Measured Backscatter Characteristics.

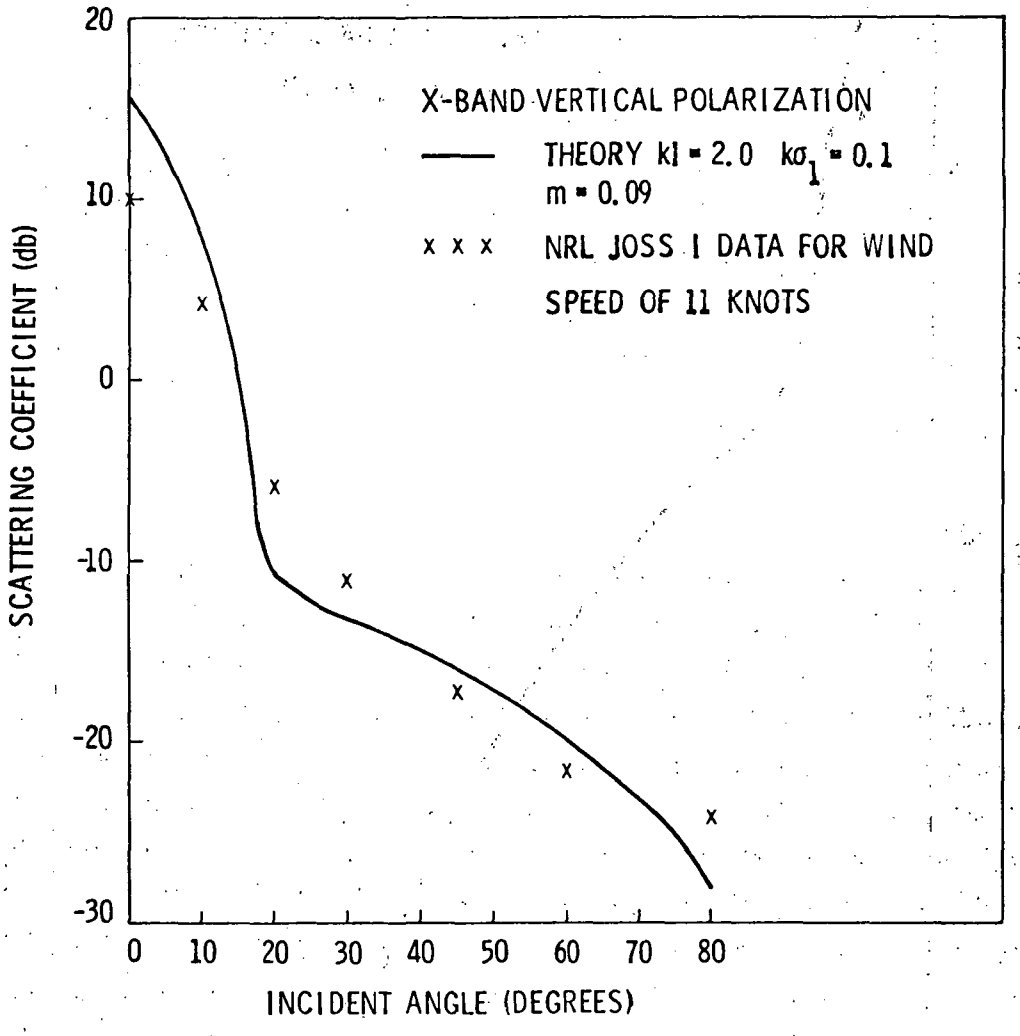

Figure 43. Comparison of Computed and Measured Backscatter Characteristics

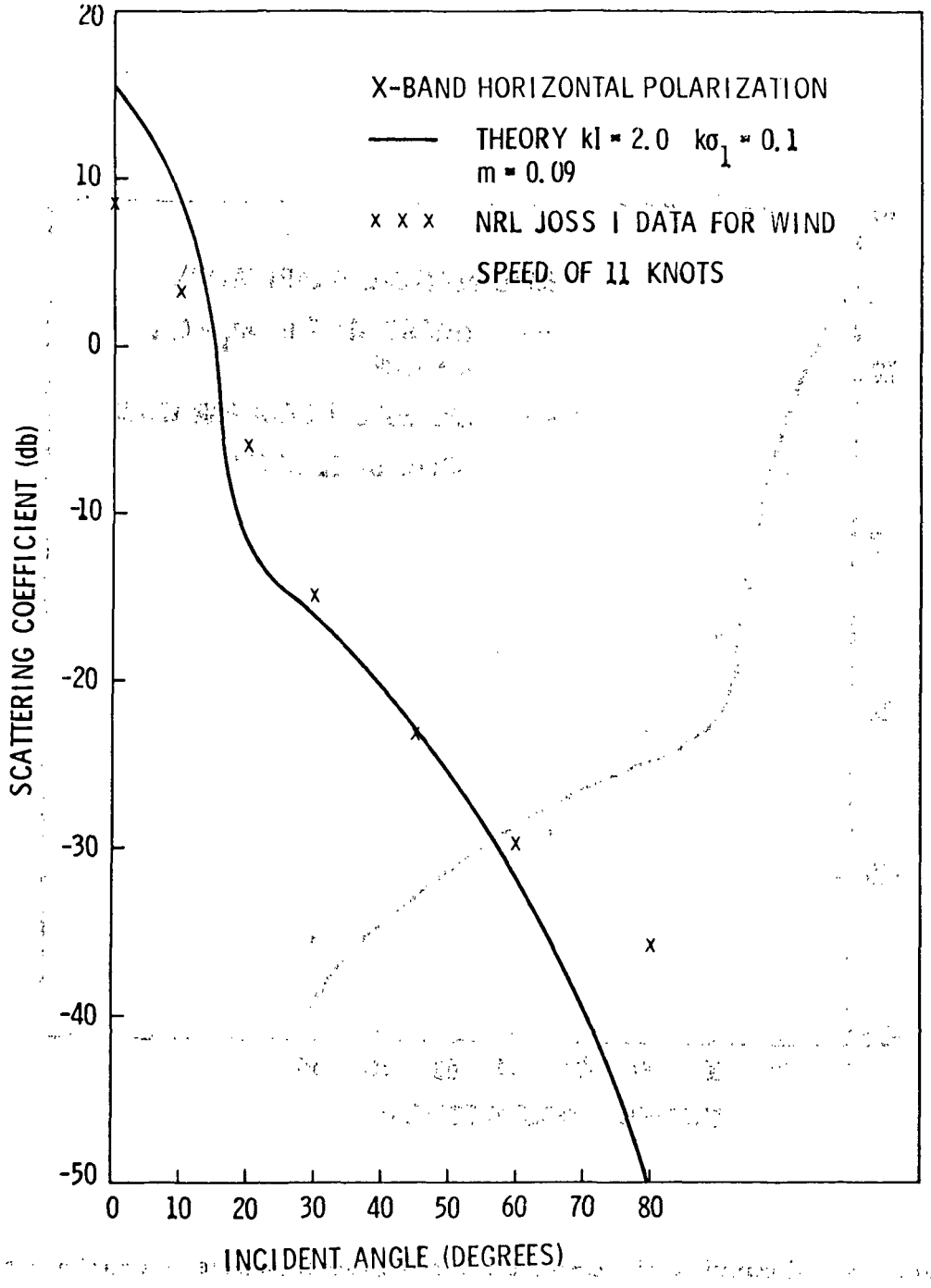

Figure 44. Comparison of Computed and Measured Backscatter Characteristics

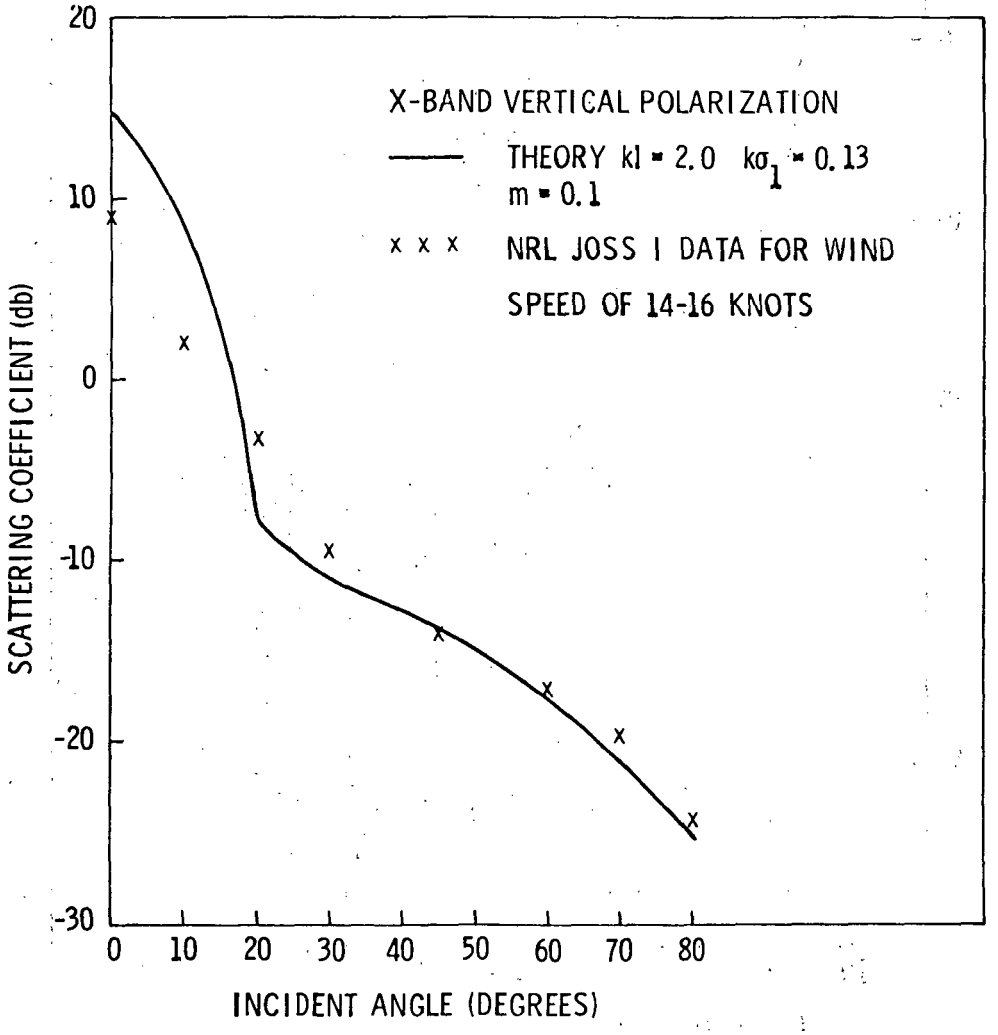

Figure 45. Comparison of Computed and Measured Backscatter Characteristics

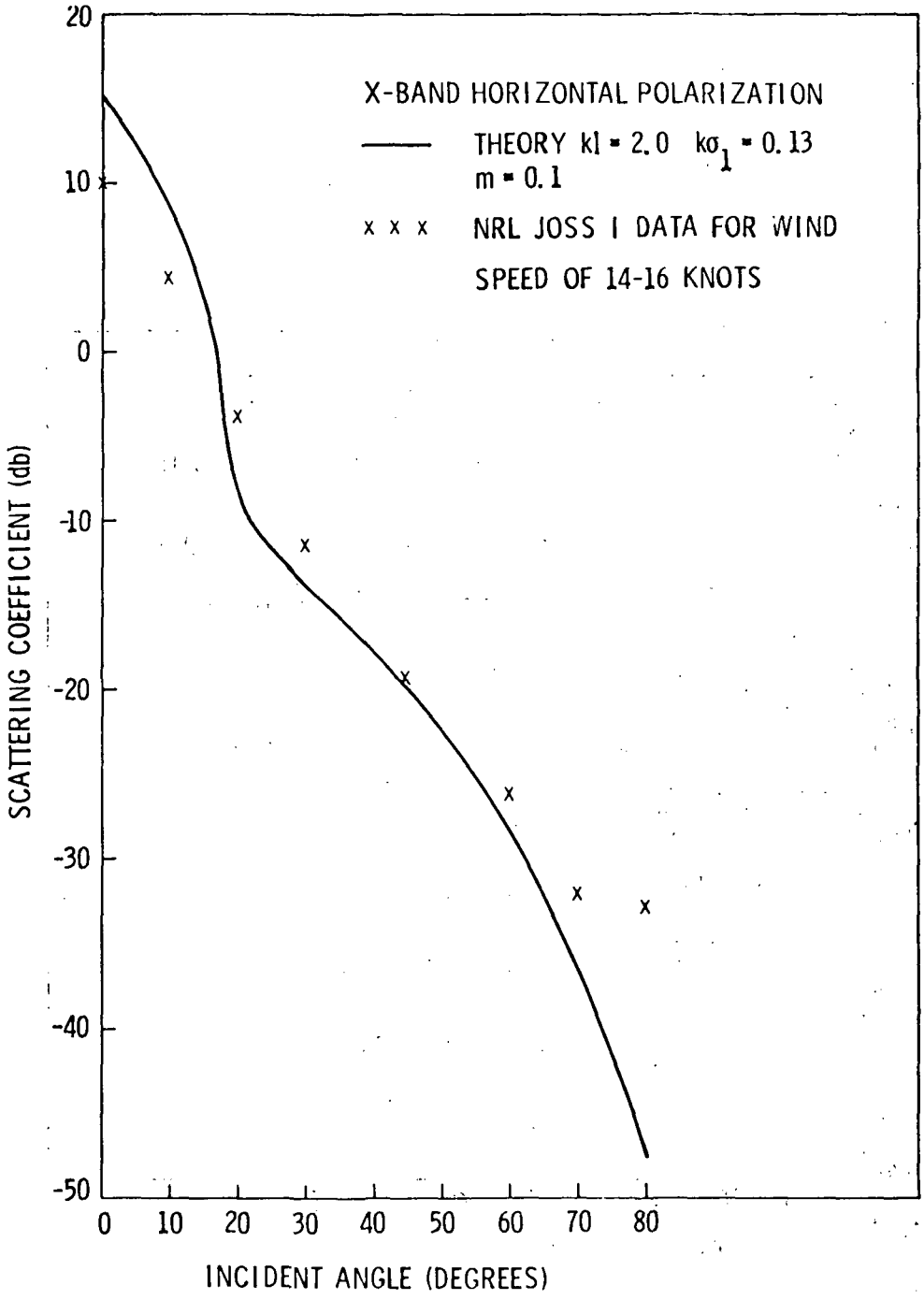

Figure 46. Comparison of Computed and Measured Backscatter Characteristics

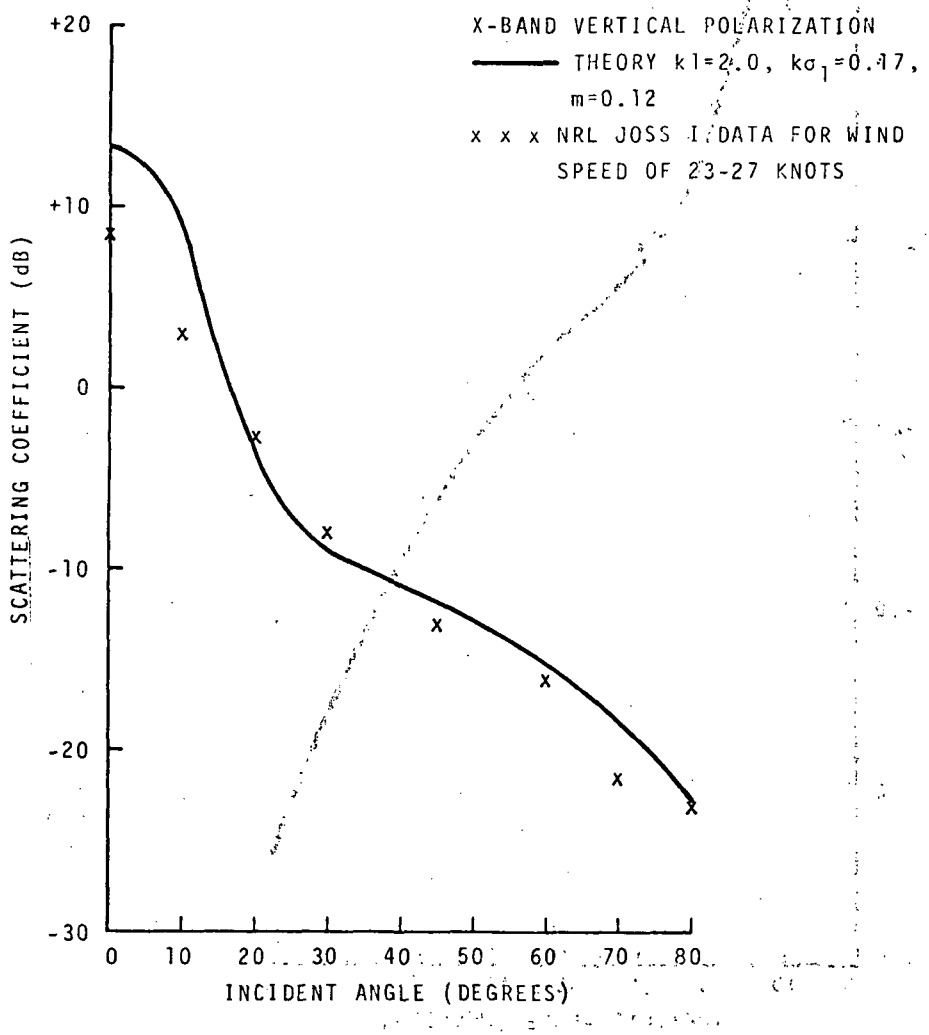

Figure 47. Comparison of Computed and Measured Backscatter Characteristics.

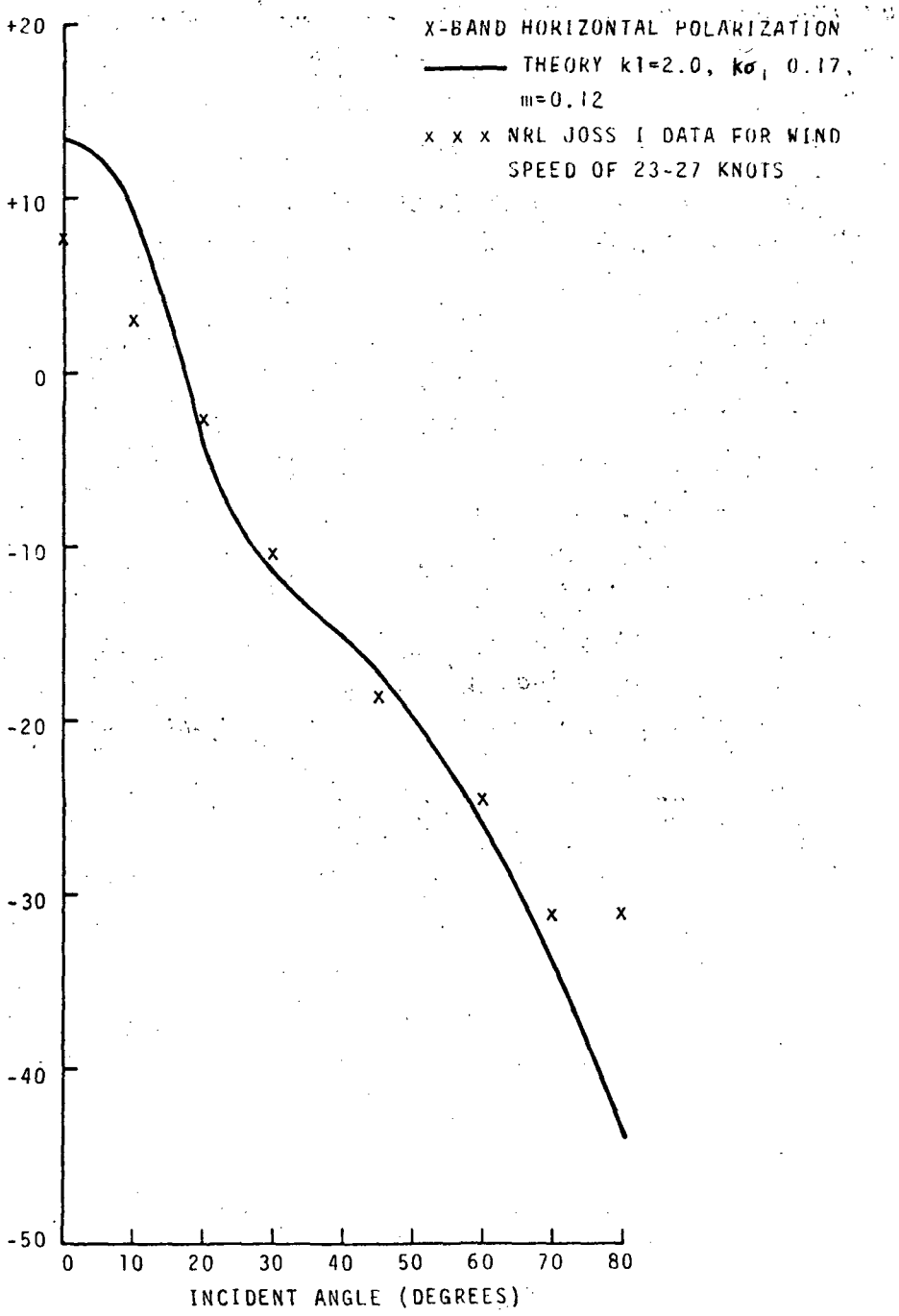

Figure 48. Comparison of Computed and Measured Backscatter Characteristics.

(2) Comparison with Other Theories

A comparison of this "coherent" backscatter theory with the "non-coherent" theory of Section V and the classical small perturbation theory[64] was made with a common set of surface parameters. The results are shown in Tables VIII through X for a domain of angles in which the theories may be compared. The cases shown in the tables reflect progressively rougher sea conditions. It is noted that the composite surface theories yield larger returns than the classical small perturbation theory which is a single surface model with the effect more significant for horizontal polarization. The "coherent" composite surface theory as one would expect, yields a slightly larger cross section than the "non-coherent" theory. The separation between the two composite surface theories becomes more significant as the sea surface becomes rougher and as the angle of incidence increases.

D. Recommendations

When enough scatterometric and radiometric data become available it will be possible to calibrate the surface parameters m, σ_1, and l and thus establish an experimentally calibrated sea scatter model. As indicated in Sections V.B and V.C radiometric data are important to estimating σ_1. If good scatterometric observations near the vertical become available it may also be possible to determine m. These observations should be considered in implementing the RADSCAT experiments. The value of composite sensor together with an adequate scattering theory may as a consequence also lie in its ability to assist the oceanographer in verifying the spectral characteristics of the sea and its wind dependence.

In view of the above results, it will now be advantageous to further examine and evaluate the general expressions for scattering from a non-isotropic two-dimensional composite surface from which these results were attained under certain simplifying assumptions. In future efforts means of incorporating the non-isotropic sea spectrum proposed by oceanographers should be considered.

TABLE VIII

COMPARISON OF COHERENT, NON-COHERENT, AND SMALL PERTURBATION THEORIES FOR $kl = 2$, $k\sigma = .15$ and $m = .09$

HORIZONTAL POLARIZATION		ANGLE	VERTICAL POLARIZATION	
$10\text{Log}\,\sigma^{\circ}_{COH}/\sigma^{\circ}_{NON}$	$10\text{Log}\,\sigma^{\circ}_{COH}/\sigma^{\circ}_{SP}$		$10\text{Log}\,\sigma^{\circ}_{COH}/\sigma^{\circ}_{NON}$	$10\text{Log}\,\sigma^{\circ}_{COH}/\sigma^{\circ}_{SP}$
dB	dB	DEGREES	dB	dB
-.024	-.075	20	-.34	-.40
.38	.48	30	- 34	-.36
.93	1.2	40	- 23	-.21
1.5	1.9	50	0.	.06
1.8	2.5	60	.21	.30
2.1	3.1	70	.28	.37
2.4	5.2	80	.53	.79

NOTE: σ°_{COH} = scattering coefficients for the coherent case,

σ°_{NON} = scattering coefficients for the non-coherent case,

σ°_{SP} = scattering coefficients for the simple small perturbation case.

TABLE IX

COMPARISON OF COHERENT, NON-COHERENT, AND SMALL PERTURBATION THEORIES
FOR $k\ell = 2$, $k\sigma = .17$ and $m = .12$

HORIZONTAL POLARIZATION		ANGLE	VERTICAL POLARIZATION	
$10\text{Log}\,\sigma^{\circ}_{COH}/\sigma^{\circ}_{NON}$	$10\text{Log}\,\sigma^{\circ}_{COH}/\sigma^{\circ}_{SP}$		$10\text{Log}\,\sigma^{\circ}_{COH}/\sigma^{\circ}_{NON}$	$10\text{Log}\,\sigma^{\circ}_{COH}/\sigma^{\circ}_{SP}$
dB	dB	DEGREES	dB	dB
.022	.12	20	-.63	-.74
.60	.77	30	-.67	-.72
1.4	1.9	40	-.47	-.43
2.2	3.0	50	.097	.20
2.7	3.8	60	.45	.60
2.9	4.7	70	.56	.72
3.0	7.1	80	.95	1.4

NOTE: σ°_{COH} = scattering coefficients for the coherent case,

σ°_{NON} = scattering coefficients for the non-coherent case,

σ°_{SP} = scattering coefficients for the simple small perturbation case.

TABLE X

COMPARISON OF COHERENT, NON-COHERENT, AND SMALL PERTURBATION THEORIES FOR $k\ell = 2$, $k\sigma = .2$ and $m = .15$

HORIZONTAL POLARIZATION		ANGLE	VERTICAL POLARIZATION	
$10\text{Log}\,\sigma^{\circ}_{COH}/\sigma^{\circ}_{NON}$	$10\text{Log}\,\sigma^{\circ}_{COH}/\sigma^{\circ}_{SP}$		$10\text{Log}\,\sigma^{\circ}_{COH}/\sigma^{\circ}_{NON}$	$10\text{Log}\,\sigma^{\circ}_{COH}/\sigma^{\circ}_{SP}$
dB	dB	DEGREES	dB	dB
-.002	-.15	30	-1.0	-1.2
.83	1.1	30	-1.1	-1.1
1.9	2.6	40	- .66	- .61
2.9	4.0	50	- .002	.16
3.5	5.1	60	.74	.97
3.7	6.2	70	.90	1.2
3.4	8.9	80	1.4	2.1

NOTE: σ°_{COH} = scattering coefficients for the coherent case,

σ°_{NON} = scattering coefficients for the non-coherent case,

σ°_{SP} = scattering coefficients for the simple small perturbation case.

VII. CONCLUSIONS

A. Introduction

The significant features of the various efforts are described below. The experiment designs are essential to the specification of the system requirements of a satellite oriented sea wind sensor. The theoretical efforts are essential to the proper interpretation of existing scatterometric and radiometric data and the near-simultaneous observations to be soon taken by the composite sensor at sub-orbital altitudes.

B. The Designs of the Radscat Experiments

Certain aspects of the experiment designs were treated in this report. Other details of the experiments may be found in reference [11]. It was specifically emphasized that well-instrumented, well-coordinated experiments are required to interpret the measurement by the composite microwave sensor (or a single sensor for that matter). In this respect the incorporation of calibrated recording anemometers into the sea truth documentation plan is shown to be essential. The anemometer(s) should be located near the observational cell for well coordinated measurements. An instrument mode sequence which accomplishes this objective is indicated. Other sea truth requirements and collection methods are also discussed.

Another approach to RADSCAT measurements over the sea emphasizes the random geometrical characteristics of the sea surface. This viewpoint dictates that for an average wind effect, microwave measurements should be performed over distances much larger than the largest scale of randomness.

Intensive studies were also performed to delineate meteorological and oceanographic situations which should form the bases for many of the experiments. It was shown that the extra-tropical cyclone offers many types of measurement situations.

C. Cloud and Rain Effects on the Apparent Microwave Temperature

Computer based techniques based on meteorological models and radiation transfer theory were developed to determine the cloud and rain emission contributions to the observed (apparent) temperature when looking downward over a quiet sea. At heavy rainfall rates the effects of scattering were incorporated into the radiation transfer model. It was shown that stratus, cumulus, overcasts, and rains all affect significant contributions to the observed temperature. Large sensitivities to clouds and rains were observed for horizontally polarized emissions at large nadir angles whereas relative insensitivity was observed for vertically polarized emissions at large nadir angles.

Under heavy rainfall rates the effect of rain scattering on the radiation transfer was observed. It was shown that scattering introduced a decrement in the observed temperature. The sky temperature (looking upward) was observed to be polarization dependent when scattering effects by heavy rains is accounted for. The separation is induced by multiple scattering between the rain and a surface having a polarization dependent reflectivity. This observation implies that the ratio of the polarized emissions where looking from above will be altered by the multiple scattering between the rain and the surface.

The meaning of these results as they apply to the interpretations of surface roughness and therefore windspeed, is that the radiometer loses contact with the surface brightness temperature through cloud and/or rain contributions. The ability to compensate the radiometric observations alone for cloud effects is problematic since in general cloud covers (as well as rains) are highly non-homogeneous. It is shown, however, that a potential exists in inferring atmospheric attenuation from (joint) observations by the composite sensor. This potential is based on numerical analyses which indicated that the excess temperature exhibited good correlation with attenuation. Extrapolation to (realistic) non-homogeneous cloud covers must await experimental verification. Nevertheless theoretical insight into the potential is evident.

D. Microwave Emissions from the Sea

A scattering theory developed by Semyonov[38] was extended to yield a bistatic scattering theory for a two-scale rough surface. Expressions were derived for polarized emissivities using a non-coherent assumption. The theory assumed Gaussian surface height distributions and Gaussian correlation functions for both scales of roughness. The scattering characteristic was shown to be dependent on the rms slope of the large undulations, m, the standard deviation of the small irregularities σ_1, and the correlation distance of the small irregularities ℓ. The wind dependence of the first two parameters was associated with m through slick sea measurements by Cox and Munk[37] and with σ_1 through the sea spectrum. The value of ℓ could be determined by the slope of the high frequency sea spectrum. The wind dependence of sea spectrum is not yet available; however, it was shown that ℓ could be reasonably chosen by fitting the sea spectrum BK^{-4} to the assumed Gaussian spectrum. It was then noted that the emission characteristic for horizontal polarization derived from the bistatic cross section in the standard way, was a very sensitive measure of σ_1. Thus, σ_1 was established by fitting the emission characteristics to measured characteristics for different wind speeds. The parameters chosen in this way were then used to compute the vertically polarized emission characteristic. Good agreement with measured characteristics and better agreement than a simple surface model were demonstrated.

The same set of surface parameters at each wind speed was then used to compute the backscatter characteristics. The results except for level were shown to agree reasonably over all angles with NRL backscatter data under similar wind conditions. Comparison of these characteristics with a single parameter surface model demonstrated better results.

These findings have proven that the validity of scattering theories is better demonstrated when both the predicted backscatter and the emission characteristics are compared with measurements. They have further shown that the measured emission and scattering characteristics with the aid of a reasonable composite surface theory may aid the oceanographer in identifying the wind dependence of the sea spectrum.

E. Microwave Backscatter from the Sea

A backscatter theory for a two-scale rough surface was developed without using a non-coherent assumption. The theory was based on a two-dimensional non-isotropic surface. Expressions for horizontally and vertically polarized cross sections were derived (they appear in reference [62]). To evaluate this new theory, the general results were reduced under certain simplifying assumptions and adapted for application to sea returns. In this simplified version the radar cross section was also shown to depend on the rms slope of the large undulations, the standard deviation of the small irregularities and the correlation distance of the small irregularities. The primary difference between this theory and that used in the microwave emission investigation is in the manner in which the large structures influence the scattering coefficient associated with the small irregularities. In applying this model to the sea the above parameters were chosen from the results of the microwave emission investigation.

It was shown that this composite surface scattering theory demonstrated reasonable agreement with measured backscatter characteristics reported by Daley et al.,[46] over all angles with poorer agreement at small incident angles. However, the accuracy of NRL data at these small angles is uncertain as indicated by Daley, et al. [46] Comparisons were made at L and X band. Better agreement was observed at X band. However, this may be attributable to the fact that a small structure parameter was based on X band emission characteristics. The composite surface scattering theory also demonstrated better agreement with measured characteristics over all angles than does the simple geometrics optics appraoch (a single surface model). Although not shown it is clear that the composite surface theory will show better agreement than any of the single parameter models known to the authors. Finally, it was shown that this "coherent" approach to scattering from composite surfaces yields a slightly larger cross section at large incident angles (nominally several dB) than the "non-coherent" approach adapted in Section V.

REFERENCES

[1] Pierson, W. J., Jr., "The Integration of Remote Sensing Data into Global Weather Prediction, Wave Forecasting, and Ocean Circulation Computer Based Systems," *New York University, Hydrology and Oceanography*, Third Annual Earth Resources Review, vol. 3, December 1970.

[2] Pierson, W. J., Jr., "On the Experimental Correlation of Radar Scatterometry Data with Sea Conditions," New York University, Radar Satellite Oceanography Project, Contract NGR-33-016-117, January 1968. (Available upon Request)

[3] Bradley, G. A., "Remote Sensing of Ocean Winds Using a Radar Scatterometer," Ph. D. Thesis, University of Kansas Center for Research, Inc., September 1971.

[4] Claassen, J. P. and M. Fung, "The Wind Response of Radar Sea Returns and its Implications on Wave Spectral Growth", University of Kansas Center for Research, Inc., Technical Report 186-5, September 1971. (Available upon Request)

[5] Hollinger, J. P., "Passive Microwave Measurements of the Sea Surface," Journal of Geophysical Research, vol. 75, no. 27, pp. 5209-5213, September 1970.

[6] Hollinger, J. P., "Passive Microwave Measurements of Sea Surface Roughness," IEEE Transactions, vol. GE-9 , no. 3 , pp.165-169, July 1971.

[7] Droppleman, J. D., "Apparent Microwave Emissivity of Sea Foam," Journal of Geophysical Research, vol. 75, no. 3, pp. 696-698, January 1970.

[8] Nordberg, W., J. Conaway and P. Thaddeus, "Microwave Observations of Sea State From Aircraft," Quarterly Journal of the Royal Meteorological Society, vol. 95, pp. 408-413, 1969.

[9] Nordberg, W., J. Conaway, D. B. Ross, T. Wilhert, "Measurement of Microwave Emission from a Foam Covered Wind Driven Sea," Goddard Space Flight Center, X-650-70-384, October 1970 (Submitted to Journal of Atmospheric Sciences).

[10] Cardone, V. J., "Specification of the Wind Distribution in the Marine Boundary Layer for Wave Forecasting," Ph. D. Thesis, New York University, Geophysical Science Laboratory, Technical Report 69-1, December 1969.

[11] Claassen, J. P., "The Design of the RADSCAT Experiments," University of Kansas Center for Research, Inc., Technical Report 186-2, Contract NAS 1-10048, February 1971. (Available upon Request)

[12] Ross, D. B., V. J. Cardone, J. W. Conaway, Jr., "Laser and Microwave Observation of Sea-Surface Condition for Fetch Limited 17-25 m/s Winds," IEEE Transactions, vol. GE-8, no. 4, pp. 326-336, October 1970.

[13] Pierson, W. J., Jr., L. J. Tick and L. Baer," Computer Based Procedures for Preparing Global Wave Forecasts and Wind Field Analyses Capable of Using Wave Data Obtained by a Spacecraft," Proceedings of the Sixth Naval Hydrodynamics Symposium, ONR Department of the Navy, ACR-136, 1966.

[14] Singer, S. F. and F. G. Williams, Jr., "Microwave Detection of Precipitation over the Surface of the Ocean," Journal of Geophysical Research, vol. 73, no. 11, pp. 3324-3327, May 1968.

[15] Conaway, J., "Microwave Radiometric Observations of Sea State in March 1966,"Microwave Observations of the Ocean Surface, Naval Oceanographic Office, SP-152, pp. 67-74, June 1969.

[16] Kreiss, W. T., "The Influence of Clouds on Microwave Brightness Temperature Viewing Downward over Open Seas," Proceedings of the IEEE, vol. 57, no. 4, pp. 440-446, April 1969.

[17] Stogryn, A., "Effect of Scattering by Precipitation on Apparent Sky Temperature in the Microwave Region," Space General Corporation, Rept SGC 613 TM-1, El Monte, California, 1964.

[18] Shifrin, K. S., "Transfer of Microwave Radiation in the Atmosphere," Transactions of the Main Geophysical Observatory (USSR), NASA, N69-31851-31868, July 1969.

[19] Haroules, G. G. and W. E. Browne III, "The Simultaneous Investigation of Attenuation and Emission by the Earth's Atmosphere at Wavelength from 4 Centimeters to 8 Millimeters," Journal of Geophysical Research, vol. 74, no. 18, pp. 4453-4471, August 1969.

[20] Strickland, J. I., "Attenuation, Emission, and Backscatter by Precipitation," USNC/URSI Meeting, Columbus, Ohio, September 15, 1970.

[21] Otsu , Yuichi, Measurement of Sky Noise Temperature at 16GHz and 35 GHz, Journal of the Radio Research Laboratories, Vol. 18, No 96, pp 87-111, March 1971.

[22] Crane, R. K., "Propagation Phenomena Affecting Satellite Communication Systems Operating in the Centimeter and Millimeter Wavelength Bands," Proceedings of IEEE, vol. 59, no. 2, pp. 173-188, February 1971.

[23] Ippolito, L. J., "Effects of Precipitation on 15.3 and 31.65 GHz Earth-Space Transmissions With the ATS-V Satellite," Proceedings of IEEE, vol. 59, no. 2, pp. 189-205, February 1971.

[24] Saxton, J. A. and J. A. Lane,"Electrical Properties of Sea Water,"Wireless Engr., vol. 29, p. 269, October 1952.

[25] Benoit, A., "Signal Attenuation Due to Neutral Oxygen and Water Vapour, Rain and Cloud," Microwave Journal, vol. 11, no. 11, pp. 73-80, November 1968.

[26] Gunn, K. L. S. and T. W. R. East, "The Microwave Properties of Precipitation Particles," Quarterly Journal of the Royal Meteorological Society, vol. 80, no. 346, pp. 522-545, October 1954.

[27] Wu, S., "The Meteorological Effects on Microwave Apparent Temperatures Looking Downward over a Smooth Sea," University of Kansas Center for Research, Inc., Technical Report 186-1, NASA Contract NASA 1-10048, October 1970.

[28] Chandrasekhar, S., "Radiative Transfer", Oxford Press, pp. 149-150, 1950.

[29] Chu, C. M. and S. W. Churchill, "Representation of the Angular Distribution of Radiation Scattered by a Spherical Particle," Journ. of Opt. Soc. of Am., vol. 45, no. 11, pp. 958-962, November 1955.

[30] Germogenova, T. A., "The Nature of the Solution of the Transfer Equation for a Plane Layer," USSR Computational Mathematics and Mathematical Physics, vol. 1, 3-4, pp. 1168-1186, 1962.

[31] Porter, R. A., "An Analytical Study of Measured Radiometric Data, Vol. 1," Radiometric Technology, Inc., JPL Contract 952397, NASA Accession No. N 70-20193, December 1969.

[32] Levine, J., "The Dynamics of Cumulus Connection in the Trade Winds - A Combined Observational and Theoretical Study," Woods Hole Oceanographic Institution, Ref. No. 65-43, August 1965.

[33] Neiburger, M., "Reflection, Absorption and Transmission of Insolation by Stratus Clouds," Journal of Meteorology, vol. 6, no. 2, pp. , April 1949.

[34] Valley, S. L., Handbook of Geophysics and Space Environment, McGraw-Hill Book Company, New York 1965.

[35] Moore, R. K. and F. T. Ulaby, "The Radar Radiometer," Proceedings of the IEEE, vol. 57, no. 4, pp. 587-590, April 1969.

[36] Moore, R. K. and W. J. Pierson, Jr., "Worldwide Oceanic Wind and Wave Predictions Using a Satellite Radar Radiometer," Journal of Hydronautics, vol. 5, no. 2, pp. 52-60, February 1971.

[37] Cox, C. and W. Munk, "Statistics of the Sea Surface Derived from Sun Glitter," Journal of Marine Research, vol. 13, no. 2, pp. 198-227, February 1954.

[38] Semyonov, B., "Approximate Computation of Scattering of Electromagnetic Waves by Rough Surface Contours," Radio Engineering and Electronic Phys., vol. 11, pp. 1179-1187, 1966.

[39] Hollinger, J. P., Private Communication.

[40] Sutherland, A. J., "Spectral Measurements and Growth Rates of Wind-Generated Water Waves," Stanford University, Dept. of Civil Engineering, Technical Report 84, August 1967.

[41] Peake, W. H., "Interaction of Electromagnetic Waves with Some Natural Surfaces," IRE Transaction, vol. AP-7, Special Supplement, pp. S324-S329, December 1959.

[42] Wu, S. and A. K. Fung, "A Non-Coherent Model for Microwave Emission and Backscattering from the Sea, " University of Kansas Center for Research, Inc., Technical Report 186-3, July 1971.

[43] Pierson, W. J.,Jr., "A Proposed Vector Wave Number Spectrum for a Study of Radar Sea Return,"Microwave Observations of the Sea, Naval Oceanographic Office, SP-152, pp. 251-282, June 1969.

[44] Phillips, O. M., "The Dynamics of the Upper Ocean," Cambridge University Press, London, p. 120, 1966.

[45] Pierson, W. J.,Jr., Private Communication.

[46] Daley, J. C.,J. T. Ransome,Jr., and J. A. Burkett, "Radar Sea Return - JOSS I," Naval Research Laboratory, Report No. 7268, May 1971.

[47] Valenzuela, G. R., M. B. Laing and J. C. Daley, "Ocean Spectra for High Frequency Waves from Airborne Radar Measurements," Journal of Marine Research, vol. 29, no. 2, May 1971.

[48] Parkins, B. E., "Scattering from the Time Varying Surface of the Ocean," Journ. of the Acoustic Soc. of Am., vol. 42, no. 6, pp. 1262-1267, December 1967.

[49] Valenzuela, G. R., "Depolarization of EM Waves by Slightly Rough Surfaces," IEEE Transactions, vol. AP-15, no. 4, pp. 552-557, July 1967.

[50] Wright, J. W., "Backscattering from Capillary Waves with Application to Sea Clutter," IEEE Transactions, vol. AP-14, no. 6, pp. 749-754, November 1966.

[51] Katzin, M., "On the Mechanism of Radar Sea Clutter," Proceedings of IRE, vol. 45, pp. 44-54, January 1957.

[52] Katzin, M., "Sea Clutter at High Depression Angles with Applications to the Ground Clutter Problem," 1959 Radar Return Symposium Part 1, U. S. Naval Ordnance Test Station and The University of New Mexico, AD No. 244 937, May 1959.

[53] Chia, R. C., "The Theory of Radar Scatter from the Ocean", Thesis, University of Kansas Center for Research, Inc., (CRES Technical Report 112-1), October 1968. (Available upon Request)

[54] Bass, F. G., I. M. Fuks, A. I. Kalmykov, I. E. Ostrovsky and A. D. Rosenberg, "Very High Frequency Radiowave Scattering by a Disturbed Sea Surface," IEEE Trans. Ant. Prop., vol. AP-16, no. 5, pp 560-568, September 1968.

[55] Valenzuela, G. R., "Backscattering of Electromagnetic Waves from a Tilted Slightly Rough Surface," Radio Science, vol. 3, no. 11, pp. 1057-1066, November 1968.

[56] Wright, J. W., "A New Model for Sea Clutter," IEEE Transactions, vol. AP-16, no. 2, pp. 217-223, March 1968.

[57] Fuks, I.M., "Theory of Radio Wave Scattering at a Rough Sea Surface," Soviet Radio Physics, vol. 9, no. 5, pp. 513-519, 1969.

[58] Chan, H. L. and A. K. Fung, "Backscattering from a Two-Scale Rough Surface with Application to Radar Sea Returns," University of Kansas Center for Research, Inc., Technical Report 186-4, August 1971.

[59] De Lorenzo, J. D. and E. S. Cassedy, "A Study of the Mechanism of Sea Surface Scattering," IEEE Transactions, vol. AP-14, no. 5, pp. 611-620, September 1966.

[60] Guinard, N. W. and J. C. Daley, "An Experimental Study of Sea Clutter Model," Proceedings of the IEEE, vol. 58, no. 4, pp. 543-550, April 1970.

[61] Fung, A. K. and H. L. Chan, "Backscattering of Waves Composite Rough Surfaces," IEEE Transactions, vol. AP-17, no. 5, pp. 550-597, September 1969.

[62] Fung, A. K. and H. L. Chan, "On Backscatter from Two-Scale Rough Surfaces," Propagation Limitations in Remote Sensing, AGARD Convention, Colorado Springs, June 1971.

[63] Pierson, W. J., Jr., Private Communication.

[64] Rice, S. O, "Reflection of Electromagnetic Waves from Slightly Rough Surfaces," Communications in Pure and Applied Mathematics, vol. 4, pp. 361-378, February 1951.

[65] Stilwell, D., Jr., "Directional Energy of Sea Waves from Photographs," Jour. Geophys. Res., vol. 79, no. 8, pp. 1974-1986, August 1969.

*U.S. GOVERNMENT PRINTING OFFICE: 1973-739-155/66

NATIONAL AERONAUTICS AND SPACE ADMINISTRATION
WASHINGTON, D.C. 20546

OFFICIAL BUSINESS
PENALTY FOR PRIVATE USE $300

SPECIAL FOURTH-CLASS RATE BOOK

POSTAGE AND FEES PAID
NATIONAL AERONAUTICS AND SPACE ADMINISTRATION
451

U.S.MAIL

POSTMASTER: If Undeliverable (Section 158 Postal Manual) Do Not Return

"The aeronautical and space activities of the United States shall be conducted so as to contribute . . . to the expansion of human knowledge of phenomena in the atmosphere and space. The Administration shall provide for the widest practicable and appropriate dissemination of information concerning its activities and the results thereof."

—NATIONAL AERONAUTICS AND SPACE ACT OF 1958

NASA SCIENTIFIC AND TECHNICAL PUBLICATIONS

TECHNICAL REPORTS: Scientific and technical information considered important, complete, and a lasting contribution to existing knowledge.

TECHNICAL NOTES: Information less broad in scope but nevertheless of importance as a contribution to existing knowledge.

TECHNICAL MEMORANDUMS: Information receiving limited distribution because of preliminary data, security classification, or other reasons. Also includes conference proceedings with either limited or unlimited distribution.

CONTRACTOR REPORTS: Scientific and technical information generated under a NASA contract or grant and considered an important contribution to existing knowledge.

TECHNICAL TRANSLATIONS: Information published in a foreign language considered to merit NASA distribution in English.

SPECIAL PUBLICATIONS: Information derived from or of value to NASA activities. Publications include final reports of major projects, monographs, data compilations, handbooks, sourcebooks, and special bibliographies.

TECHNOLOGY UTILIZATION PUBLICATIONS: Information on technology used by NASA that may be of particular interest in commercial and other non-aerospace applications. Publications include Tech Briefs, Technology Utilization Reports and Technology Surveys.

Details on the availability of these publications may be obtained from:

SCIENTIFIC AND TECHNICAL INFORMATION OFFICE

NATIONAL AERONAUTICS AND SPACE ADMINISTRATION

Washington, D.C. 20546